Tunable Decoupling and Matching Concepts for Compact Mobile Terminal Antennas

Von der Fakultät für Elektrotechnik und Informatik
der Gottfried Wilhelm Leibniz Universität Hannover
zur Erlangung des akademischen Grades

Doktor-Ingenieur
(abgekürzt: Dr.-Ing.)

genehmigte Dissertation

von

Dipl.-Ing. Yi Chen

geboren am 10.10.1982
in Ningbo, China

2017

1. Referee: Prof. Dr.-Ing. D. Manteuffel

     Leibniz University of Hannover, Germany

2. Referee: Prof. Dr.-Ing. H. Garbe

     Leibniz University of Hannover, Germany

3. Referee: Prof. Y. Vardaxoglou

     Loughborough University, United Kingdom

Date of the doctorate: December 14, 2017

Hiermit versichere ich, dass ich die Doktorarbeit

Tunable Decoupling and Matching Concepts for Compact Mobile Terminal Antennas

selbständig und ohne unzulässige fremde Hilfe angefertigt habe und dass ich alle von anderen Autoren wörtlich übernommenen Stellen, wie auch die sich an die Gedankengänge anderer Autoren eng anlehnenden Ausführungen meiner Arbeit, besonders gekennzeichnet und die entsprechenden Quellen angegeben habe. Weiterhin wurde die Arbeit ausschließlich der Leibniz Universität Hannover im Rahmen eines Prüfungsverfahrens vorgelegt, jedoch wurden Teile in Form von Beiträgen in Fachzeitschriften und Tagungsbänden veröffentlicht bzw. zur Veröffentlichung eingereicht (siehe Abschnitt zu Publikationen). Diese Arbeit ist unter Einhaltung der Regeln guter wissenschaftlicher Praxis der Deutschen Forschungsgemeinschaft entstanden.

Yi Chen

Abstract

In the last few decades, the need for modern wireless communications using compact mobile terminal antennas to support many standards has been rapidly increasing. However, limiting the antenna size typically precludes achieving a sufficiently broadband matching covering all the bands of operation, and utilizing compact multi-element antennas usually suffers from strong mutual coupling. Furthermore, the detuning of the antenna impedance as well as the mutual coupling caused by the user interaction is unpredictable. As a result, it is very challenging to mitigate these problems using the traditional common mobile terminal antennas as well as exploiting geometry-based techniques.

In this work, the antenna elements are designed to be generic, electrically small and placed close to each other and to the RF front-ends. The band of operation of the antenna elements on a small-sized terminal having a limited bandwidth is made reconfigurable over the frequencies of interest. The potential of reconfigurable tunability in usage scenarios is purely controlled by employing adaptive decoupling and matching techniques. As an important contribution to antenna adaptive systems, the design concepts of tunable decoupling and matching networks for compact mobile terminal antennas are investigated.

To simplify the process, the design of the tunable decoupling and of the tunable matching networks for closely-spaced multi-element antennas is separated, and an initial estimate regarding the possible network simplification of

decoupling networks is derived.

When using single-element or weakly-coupled multi-element antennas, for which the decoupling is unnecessary, a design concept for practical antenna matching systems containing compact antennas combined with tunable lumped-element matching networks is investigated. By exploiting this matching network, the suitable impedance behavior of small-sized antennas is investigated to maintain a good total efficiency of the frequency-reconfigurable operation band in typical usage scenarios. This matching concept is evaluated by calculation of transducer gain and efficiency measurements of a mock-up system.

For the cases in which the decoupling is necessary, the tunable matching concept is combined with a tunable decoupling approach. According to the initial estimate, a suitable decoupling structure based on several cascade-connected basic decoupling structures is investigated. The decoupling network is then connected to the matching networks, which compensate the impedance mismatch for each antenna element separately. The decoupling and matching concept is then evaluated.

Keywords — mobile terminal antennas, frequency reconfigurability, decoupling and matching networks

Zusammenfassung

Während der letzten Jahrzehnte ist der Bedarf an modernen Funkkommunikationssystemen unter Einsatz von kompakten Antennen, welche zugleich auf eine Vielzahl an Frequenzstandards abgestimmt sind, gestiegen. Allerdings führt die Reduktion der Antennengröße typischerweise zu einer Verschlechterung der Impedanzanpassung in Frequenzbändern und bei Mehrantennensystemen ggf. zu einer stärkeren Kopplung zwischen den RF Frontenden. Darüber hinaus können sich diese Effekte durch die Interaktion mit dem Nutzer verstärken und sind kaum deterministisch vorherzusagen. Als Konsequenz sind herkömmliche Lösungsmethoden, welche auf der traditionellen Antennentheorie oder der geometriebasierten Antennentechnik basieren unzureichend, um diese Probleme zu mildern.

In dieser Arbeit sind die Antennenelemente so konzipiert, dass sie generisch, elektrisch klein, nahe beieinander angeordnet sind, so wie nah an den RF Frontenden positioniert sind. Desweiteren wird das Betriebsband der Antennenelemente auf einem kleinen Chassis mit begrenzter Bandbreite im gesamten interessierenden Frequenzbereich rekonfigurierbar gestaltet. Die Fähigkeit, das Frequenzband für solche Einzel- und Multielementantennen in Nutzungsszenarien zu rekonfigurieren, wird allein mittels adaptiver Entkopplungs- und Anpassungsverfahren realisiert. Als ein Beitrag zu adaptiven Antennensystemen, werden Designkonzepte der abstimmbaren Entkopplungs- und Anpassnetzwerke für kompakte Antennen in mobilen Endgeräten untersucht.

Zur Vereinfachung des Prozesses werden das Design der abstimmbaren Entkopplungsnetzwerke und das der abstimmbaren Anpassnetzwerke für die dicht gepackte Multielementantennen voneinander getrennt. Eine initiale Schätzung bezüglich der möglichen Vereinfachung der Entkopplungsnetzwerke wird hergeleitet.

Bei der Verwendung von Einzelelement- oder schwach gekoppelten Multielement-Antennen wird ein Designkonzept für praktische Antennenanpasssysteme mit kompakten Antennen kombiniert. Dieses Konzept wird auf abstimmbaren konzentrierten Elementen basierenden Anpassnetzwerken untersucht. Durch die Implementierung wird ein geeignetes Impedanzverhalten kleiner Antennen untersucht, um eine gute Gesamteffizienz des frequenzrekonfigurierbaren Betriebsbandes in typischen Nutzungsszenarien beizubehalten. Das Anpassungskonzept wird durch die Berechnung des Übertragungsgewinns und Effizienzmessungen an einem Mock-Up-System evaluiert.

Für die Fälle in denen eine Entkopplung notwendig ist, wird dieses Anpassungskonzept mit einem abstimmbaren Entkoppelkonzept kombiniert. Aufbauend auf einer Startschätzung wird eine geeignete Entkopplungsstruktur auf der Basis mehrerer kaskadengebundener Entkopplungsstrukturen untersucht. Das Entkopplungsnetzwerk ist wiederum mit den Anpassnetzwerken verbunden, um die Impedanzfehlanpassung für jedes Antennenelement separat zu kompensieren. Das Entkopplungs- und Anpassungskonzept wird anschließend evaluiert.

Schlagworte — Antennen für mobile Endgeräte, Rekonfigurierbarkeit, Entkopplung- und Anpassnetzwerke

Acknowledgment

The work of this thesis has been carried as a research associate in the Institute of Wireless Communications at University of Kiel as well as in the Institute of Microwave and Wireless Systems at Leibniz University of Hannover.

First and foremost my warmest thanks go to my supervisor, Prof. Dirk Manteuffel, for providing me the opportunity to do the interesting doctoral research under his guidance and for the freedom to develop my own ideas. I really appreciate his contributions of time, constructive conversations and helpful comments on my work.

Besides my supervisor, I highly appreciate the contribution of the examiners, Prof. Heyno Garbe and Prof. Yiannis Vardaxoglou. Their insightful comments and valuable suggestions have certainly helped me a lot through the final phase of the dissertation process. I would also like to thank for the hard questions, which motivated me to widen the research from various perspectives.

I am very grateful to all my colleagues in Institute of Wireless Communications at Kiel University, Dr. Robert Ledig (born Martens), Markus Grimm, Dr. Eugen Safin, D. Sc. Risto Valkonen, Florian Marx and Thade Wunderlich (born Hademik) for great companionship and productive discussions at work during these years. My appreciation goes to Dr. Hector J. De Los Santos, who helped me through the final phase of the dissertation process. Also I would like to thank all my colleagues in Institute of Microwave and Wireless Systems at Leibniz University of Hannover for the assistance in completing

this dissertation.

Last but not the least, I owe many thanks to my wife and parents for their patience, encouragement and all kind of support throughout my long studies and my life in general.

Content

List of Author's Publications and Contributions

The dissertation contains textual materials and figures from the author's publications listed below. The relevant publications are cited in the text and in the captions of the respective figures. The use of those materials requires the permission of the *IEEE* and *EurAAP*.

I. **Y. Chen, R. Martens, R. Valkonen, and D. Manteuffel, "A Varactor-Based Tunable Matching Network for a Non-Resonant Mobile Terminal Antenna",** *European Conference on Antennas and Propagation (EUCAP)***, The Hague, pp. 2225-2229, April 2014.**

   The author developed and evaluated the antenna and its matching concept. Dr. Martens assisted in antenna design, measurements of the prototypes. Dr. Valkonen assisted in design and fabrication of the mock-up-system. Prof. Manteuffel supervised the work.

II. **R. Martens, Y. Chen, and D. Manteuffel, "Tunability Comparison of a Capacitive Coupling Element and a Planar Inverted-F Antenna",** *Loughborough Antennas and Propagation Conference (LAPC)***, Loughborough, pp. 667-668, November 2014.**

   The author was responsible of developing and calculations evaluating the matching concept. Dr. Martens made the antenna design

and had the main responsibility of the whole concept. Prof. Manteuffel supervised the work.

III.   **Y. Chen, R. Martens, R. Valkonen, and D. Manteuffel, "Evaluation of Adaptive Impedance Tuning for Reducing the Form Factor of Handset Antennas",** *IEEE Transactions on Antennas and Propagation*, **vol. 63, pp. 703-710, February 2015.**

The author had the main responsibility in developing the whole concept. Dr. Martens assisted in antenna design and measurements of the prototypes. Dr. Valkonen assisted in design and fabrication of the mock-up-system. Prof. Manteuffel supervised the work.

IV.   **Y. Chen and D. Manteuffel, "A Tunable Decoupling and Matching Concept for Compact Mobile Terminal Antennas",** *IEEE Transactions on Antennas and Propagation*, **vol. 65, pp. 1570-1578, April 2017.**

The author had the main responsibility in developing the idea and the concept of the paper. Prof. Manteuffel supervised the work.

Notation Remarks

Throughout the paper a clear notation is used to clarify the usage of the equations to the reader. All scalar values are denoted with italic letters. The vectors and matrices are denoted with bold and capital letters. Any italic subscript letter denotes a count index which is typically used within a summation. The regular subscript is used to specify the quantity.

List of Constants

c_0	3×10^8 [m/s]
ε_0	$8.8541878176 \times 10^{-12}$ [F/m]
μ_0	$4\pi \times 10^{-7}$ [H/m]
π	3.14159265 [1]
Z_{F0}	376.730 [Ω]

List of Latin Symbols

ABCD	ABCD-Matrix [1]
C	Capacitance [F]
E	Electric Field Strength [V/m]
f	Frequency [Hz]
G_T	Transducer Gain [1]
H	Magnetic Field Strength [A/m]
I	Current [A]
j	Imaginary Unit [1]
k_0	Scalar Wave Number of the Free Space [1/m]
L	Inductance [H]
P	Port [1]
P_{rad}	Radiated Power in Free Space [W]
Q	Quality factor [1]
R	Resistance [Ω]
S	Scattering (S)-Matrix [1]
T	Transmission (T)-Matrix [1]
T	Temperature [°]

U	Voltage [V]
X	Reactance [Ω]
Y	Admittance **(**Y)-Matrix [1]
Z	Impedance **(**Z)-Matrix [1]
Z	Impedance [Ω]
Z_0	Reference Impedance [Ω]
Z_A	Antenna Impedance [Ω]
Z_c	Characteristic Impedance [Ω]
Z_{in}	Input Impedance [Ω]

List of Greek Symbols

Γ	Reflection Coefficient [1]
$\tan(\delta)$	Loss Tangent [1]
ε_0	Permittivity of the Free Space [As/Vm]
ε_r	Relative Permittivity [1]
η_{tot}	Total Efficiency [1]
λ	Wavelength [m]
μ_0	Permeability of the Free Space [Vs/Am]
μ_r	Relative Permeability [1]
σ	Electric Conductivity [S/m]
φ	Phase of Signal [°]
ϕ_0	Build-In Potential [V]
ω	Angular Frequency [rad/s]

List of Mathematic Operations

$\mathbf{r} \cdot \mathbf{r}$ Scalar Multiplication between two Vectors

$\left|\mathbf{r}\right|$ Norm of a Vector

$\mathbf{A} \cdot \mathbf{r}$ Matrix Multiplication with a Vector

$\mathbf{A}^{-1}$ Matrix Inversion

$\mathbf{A}^{*}$ Matrix Complex Conjugation

$\mathbf{A}^{T}$ Transpose of a Vector or Matrix

$\det(\mathbf{A})$ Determinate

M_{mn} (m, n) Minor

List of Abbreviations

ADS	Advanced Design System
BST	Barium Strontium Titanate
CCE	Capacitive Coupling Element
CEA	Coupling Element Antenna
COMS	Complementary Metal Oxide Semiconductor
CPW	Coplanar Waveguide
CTIA	Cellular Telephone Industries Association
DET	Impedance Detector
DMN	Decoupling and Matching Network
DN	Decoupling Network
ESD	Electrostatic Discharge
FDTD	Finite Difference Time Domain
E-UTRA	Evolved UMTS Terrestrial Radio Access
FET	Field Effect Transistor
GaAs	Gallium Arsenide
GSM	Global System for Mobile Communications
IL	Insertion Loss

IP3	Third-Order Intercept Point
LTE	Long Term Evolution
MCU	Microcontroller
MIMO	Multiple Input Multiple Out
MIM	Metal–Insulator–Metal
MN	Matching Network
PCB	Printed Circuit Board
PIN Diode	Positive Intrinsic Negative Diode
PIFA	Planar Inverted-F Antennas
PSPICE	Personal Computer Simulation Program with Integrated Circuit Emphasis
PVC	Polyvinyl Chloride
PTD	Parameter Temperature Diode
RF	Radio Frequency
RF MEMS	Radio Frequency Microelectromechanical System
SMD	Surface Mounted Device
WLAN	Wireless Local Area Network

Chapter 1

Introduction

1.1 Background

Early mobile terminal devices were quite large and bulky. At that time, monopoles and helical antennas were normally implemented as mobile terminal antennas, which were located outside the casing and were only able to cover several narrow operating bands [Hua08]. Nowadays, advanced mobile terminals such as smartphones, aim at higher data rates in multiple standards. On the other hand, they are typically thinner and need to have large displays and batteries. This demand drives the need for mobile terminal antennas with limited size to support a wide frequency range of operation, which is very difficult to fulfill [Mcl96].

Traditionally, the design of many mobile terminal antennas only focuses on enabling operation in some predefined frequency bands in free space environment [Val07, Ela13, Xie14]. However, human tissue is usually in the near field of the antennas during their operation. Due to the fact that the antenna impedance shows high sensitivity to the usage environment, especially if the user approaches the antenna radiating element [Pol09], the original electro-

magnetic field of the antennas is distorted, and the antenna impedance is, consequently, detuned [Boy07, Li09]. The electromagnetic user interaction is not predictable, which complicates the antenna design for reducing its impact.

Moreover, to share the radio resources with respect to frequency and space efficiently, mobile devices need to have multiple closely-packed antenna elements for operation in so-called MIMO (Multiple Input Multiple Output) systems [Fos98]. In this context, it is advantageous to place these antenna elements next to each other and close to the RF front-ends. But on the other hand, the mutual couplings elicited by the electromagnetic interactions among the antenna elements distort the antenna characteristics such as radiation pattern and input impedance [Vau03, Lau06a]. This issue is made worse in compact mobile terminals, where the distance between elements within an antenna array on the limited size of the platform, is generally not sufficient to keep low mutual couplings. Furthermore, the mutual couplings would also be unpredictable caused by the user interaction. As a result, the impact of the mutual couplings on the unpredictable antenna impedance must be incorporated in the design.

To estimate the total losses of an antenna system, including those losses caused by the mutual coupling and the impedance mismatch, an important figure of merit called, total efficiency, can be used. It is defined as the ratio of the power radiated by one antenna element to the power delivered to it, when the other antenna elements are not excited and are terminated by the reference impedance.

Due to the size limitation and user interaction, the design of single- and multi-element antenna systems for achieving a good total efficiency over a

broadband frequency range is quite challenging [Mcl96, Kiv05, Lud76, Gup83, Lin08]. This dissertation, therefore, presents a number of contributions to address these challenges.

1.2   Objective of this Work

The purpose of this work is to mitigate the impedance mismatch as well as the mutual coupling and, consequently, to enhance the total efficiency of the band of operation in usage scenarios. To achieve this, the dissertation neither focuses on the design of small-sized inherently broadband decoupled and matched multi-element antennas on compact platform nor on the study of fixed decoupling and matching techniques for optimizing the antenna operation in some predefined bands. The idea presented in this work is to adaptively tune the band of operation of antenna elements having limited bandwidth on a compact mobile terminal, which are generic, small-sized, placed next to each other and close to RF front-ends, over the frequencies of interest. This is entirely achieved by employing adaptive decoupling and matching of adaptive antenna systems. In particular, tunable decoupling and matching networks (DMN) for compact mobile terminal antennas are studied. The main objective of this work, therefore, is to investigate network design concepts for compact mobile terminal antennas, which provide a frequency reconfigurable antenna operation band with a good total efficiency over a wide frequency range.

The main scientific merits of this thesis are:

- Demonstration of generic and compact single- and multi-element antennas having a limited bandwidth, yet operating in a band-reconfigurable fashion over a large frequency range by employing tunable DMNs.

- A separately designed tunable decoupling and matching concept, including an assessment of its simplifications and limitations for compact multi-element antennas.

- Developing a rational initial estimate for evaluating possible network simplifications for decoupling.

- Analysis of the antenna impedance characteristics of generic and compact antenna elements for effecting the reconfigurability of the band of operation under several usage scenarios.

- A concept for practical tunable matching circuits with high tunability including the influence of other components of adaptive matching systems for single-element and weakly-coupled multi-element antennas.

- According to the initial estimate, a simple design concept for decoupling networks based on the cascade connection of several basic decoupling structures of antenna arrays having any number of antenna elements.

1.3 Content and Organization of the Thesis

In this thesis, the theoretical investigations and practical evaluations of the tunable decoupling and matching concepts for generic and compact single- and multi-element mobile terminal antennas are the main focus of this work. The scientific contributions are based on the content of the author's publications [I-IV]. The organization of the work is as follows.

Chapter 2 reviews several problems to achieve communications over a large frequency range using compact mobile terminal antennas in various usage scenarios. As the traditional antennas and the geometry-based techniques are not able to mitigate them, an introduction of adaptive decoupling and match-

ing systems as a circuit-based technique is therefore presented. The design approach of tunable DMNs is based on implementing the decoupling and matching networks in different steps. For the purpose of simplifying the network complexity by omitting some or all the decoupling branches, an initial estimate based on the calculation of simultaneous conjugate complex matching for all the antenna elements in the lossless case is shown [IV].

For tunable DMNs, Chapter 3 introduces two different categories for building tunable capacitors suitable to implement the variable reactance value of some or all the network components. In the first one, the variation of the capacitance is realized by using a fixed capacitor bank controlled by RF switches such as PIN diodes, FET switches and RF MEMS switches. In the second one, several tunable RF components such as varactor diodes, BST varactors and RF MEMS varactors are presented. The advantages and disadvantages of using the different categories and RF components in the network design process are summarized.

According to the initial estimate obtained in Chapter 2, decoupling is unnecessary for weakly-coupled multi-element antennas. Chapters 4 and 5 [I, II and III] therefore present a matching design concept, containing a topology of tunable matching networks and suitable antenna elements that compensates the unpredictable impedance mismatch of the frequency reconfigurable operation band of compact single- and these weakly-coupled multi-element antennas in usage scenarios.

For the design of the matching networks providing a high tunability shown in Chapter 4 [I and III], the equivalent reactance of the *LC* configuration and the suitable component value over the investigated frequency range are studied. Based on this knowledge, the design of a Π-section tunable matching net-

work by taking into account the parasitic effects of some other components of adaptive systems is shown. This circuit is then utilized as a good representation of the matching topologies. As a practical evaluation, the matching circuit using varactor diodes as tunable capacitors is fabricated and its tunability is measured.

In Chapter 5, the in Chapter 4 studied tunable matching network with a high tunability is implemented to determine suitable antenna elements for achieving a reconfigurable band over a large frequency range [I, II and III]. As a reference, the total efficiency of an intrinsically broadband matched antenna with a large form factor is studied. For miniaturizing the antenna form factor, the tunability of a compact inherently multiband matched antenna combined with the matching circuit is studied. However, using such an inherently multiband matched antenna, the broadband tunability of the operation band cannot be realized. Hence, small-sized antennas having an appropriate antenna impedance behavior are investigated. The calculated transducer gain and the measured total efficiency of the operation band using such an antenna employing the proposed matching network are then compared to that of the above two antenna systems as an evaluation example.

Chapter 6 [IV] presents a tunable decoupling and matching concept. This is based on the antenna matching concept, which is suitable for multi-element antenna systems, where decoupling is needed. According to the initial estimate, a suitable decoupling network consisting of cascade connected basic decoupling structures is investigated. The concept is then evaluated with two classes of examples theoretically. First, several generic antenna matrices are discussed. A three-element antenna system on a mobile terminal is then investigated by numerical simulations for studying the achievable bandwidth of each tuning.

Chapter 7 presents, besides a theoretical study, an experimental investigation and evaluation of the concept through efficiency measurements for two-element antennas using realistic DMNs [IV].

Chapter 8 presents the conclusions and the discussions of the thesis.

Chapter 2

Tunable Decoupling and Matching Networks

[1]Since the mid-1990s, single-element antennas such as planar inverted-F antennas (PIFA) (e.g. in [Abu09]) and monopole antennas (e.g. in [Liu10]) have often been utilized as mobile terminal antennas [Fuj08]. Typically, these conventional antennas are compact in size but are designed to operate only in couple communication bands.

It is known that most of the current mobile terminal antennas operate within the application frequency range $0.69 \leq f\,[\text{GHz}] \leq 2.7$. For such a broadband communication, the usage of the CEA (coupling element antenna) becomes a promising approach [Vai02]. A CEA usually consists of a coupling element and a compact mobile handset chassis [Val13a]. The coupling element excites a set of characteristic modes of the metallic chassis, which radiate effectively near their modal resonances [Mar13, Fab07]. Several inherently broadband matched antennas based on this approach have been proposed [Kim12, Liu14]. However, a large antenna form factor (the space occupied by the

---

[1] The following chapter uses textual materials and figures from [Che17] ©
   2017 *IEEE*.

coupling element within the mobile devices) is usually required for these designs, and the antenna geometry becomes very complex. Moreover, the chassis also operates as a part of radiating elements at the frequencies below 1 GHz [Vai02, Val13a]. The size and the geometry of the chassis are commonly predefined and, therefore, are not allowed to be optimized. As a result, the bandwidth of operation is restricted by the limited size of the chassis and the coupling element in free space operation [Mcl96].

It is also known that the antenna impedance can be changed unpredictably due to user interaction. To reduce this impact, some investigations regarding parameters of mobile terminal antennas such as the size, position of the coupling element and the shielding have been presented [Val11, Ilv12]. Two common drawbacks of these geometry-based methods are the limitation of the antenna geometry and narrow bandwidth.

Besides the antenna impedance mismatch, closely-spaced multi-element antennas suffer from strong mutual coupling. For decreasing the mutual coupling, methods based on the modifications of the antenna geometry include ground plane modifications [Chi07, Zhu09a], the neutralization line technique [Dia08], and the use of parasitic scatterers [Lau12]. In the case of compact mobile terminals, however, the ground plane modifications are out of the question, because it is unbeneficial to place large slots on the circuit board of a small terminal. A common drawback related to all of the above-listed geometry-based methods is that the decoupling works only across a narrow bandwidth with fixed frequency bands in some predefined usage scenarios. As explained above, the optimization of the antenna geometry to mitigate these problems is quite challenging.

Another promising method is the usage of circuit-based techniques. In this

case, adaptive antenna decoupling and matching techniques are implemented, which are located between the RF front-ends and the antenna elements. By exploiting the decoupling and matching networks within the antenna systems, a reconfigurable antenna operation band of compact and generic mobile terminal antennas with a good total efficiency over a large frequency range in usage scenarios, can be achieved. To offer some insight, a brief introduction is presented in this chapter.

2.1 Adaptive Antenna Decoupling and Matching Systems

Because of user interaction, the mutual couplings as well as antenna impedance become unpredictable. Since, static antenna systems cannot handle all the possible cases, there is a need for adaptive decoupling and matching systems, which are amenable to automatically compensate the impedance mismatch and the mutual coupling and consequently enhance the total efficiency of compact mobile terminal antennas at the frequencies of operation in variable usage scenarios.

To study the adaptive decoupling and matching systems, adaptive antenna matching systems would be useful. To optimize the power transfer from RF front-end to the antenna elements, several tuning algorithms are shown in [Gu13, Smi13]. An adaptive antenna matching system, effected by minimizing the reflection coefficient at the RF front-end, is the traditional one to enhance the power transfer from RF_{IN} to RF_{OUT} see Fig. 2-1. Tunable matching network, microcontroller (MCU), impedance detector (DET), electrostatic discharge (ESD) protector and driver are usually included as the basic components in the adaptive antenna matching system.
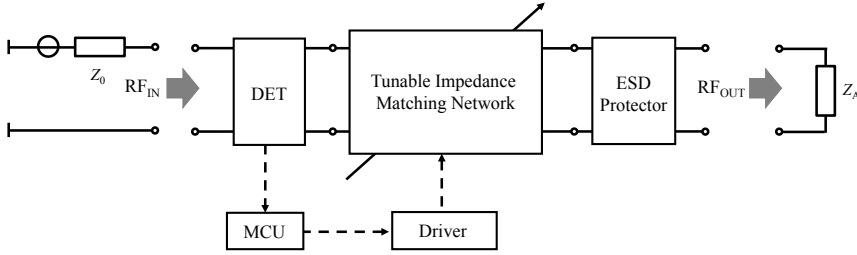
Fig. 2-1 Topology of an adaptive impedance matching system for minimizing the reflection coefficient.

In Fig. 2-1, the reference impedance Z_0 is set to $Z_0 = 50\ \Omega$, while Z_A is the antenna impedance. From the mathematical point of view, impedance matching networks transform a certain region of antenna impedances on the Smith-chart such that the predefined matching criterion $|S_{\mathrm{ma,thres}}|$ is reached. In this approach, broadband matched antennas are not be implemented for matching an entire band across the whole frequency of interest, which is presented in Fig. 2-2(a). Instead, only the band of operation for achieving $|S_{\mathrm{ma,thres}}|$ using this antenna adaptive matching system is typically realized at each tuning state of the adaptive matching system. Although its bandwidth is limited, and might only be able to cover an uplink or downlink or even a channel of a communication band, the band of operation can be made reconfigurable over the whole frequency range by modifying the tuning state, see Fig. 2-2(b). f_s and f_e are the starting and ending frequency point of the frequency range, respectively.

To compensate the antenna impedance mismatch and to enlarge the operating bandwidth [Val13a, Yar06, Li08], the matching networks as an important component of the adaptive matching system have been widely implemented for over 70 years [Dar39]. Based on analytical circuit theory, several broadband matching networks have been published [Bod45, You64, Che88]. Other commonly used matching techniques are the numerical optimization [Cut99],

12

real frequency techniques [Car83, Yar08] and H^{∞} approach [Sch04]. However, because of the unpredictable impedance behavior caused by user interaction, Z_A is arbitrary, and thus these fixed matching circuits may lead to increased losses, if some antenna impedance variations are not pre-estimated [Boy13]. Hence, the matching network needs to be tunable.
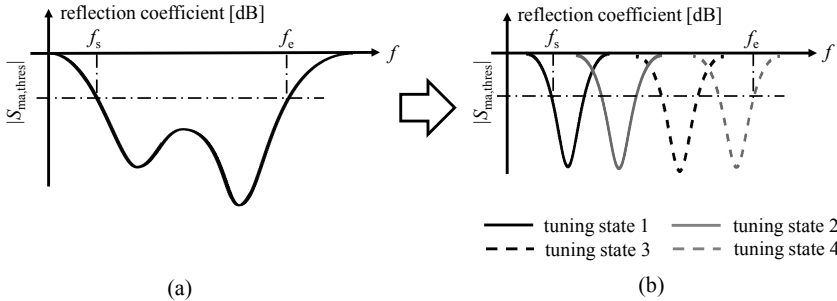

Fig. 2-2 Reflection coefficients over the frequencies of interest. (a) using broadband matched antennas. (b) with the help of antenna adaptive matching systems. f_s: starting frequency point. f_e: end frequency point.

Lumped-element and distributed-element networks are two main types of tunable impedance matching networks. Distributed-element networks based on transmission lines or stubs interconnected with tunable RF components or switches as tunable matching circuit have been published [Che12, Che13, Wha06, Smi13, Cas12]. However, a large network size is typically required for providing a satisfied matching region. Hence, tunable matching networks consisting of lumped-elements are exploited in this work.

By impedance modification, the microcontroller determines the optimal settings of the tunable impedance matching network based on the information provided by the impedance detector. Consequently, the driver adapts the state of tunable elements of the matching network, so that the reflection coefficient at the RF front-end is minimized. Hence, in addition to the matching network, some boundary conditions of a practical adaptive network electrically

influence the tunability of the antenna matching system and, therefore, need to be taken into account.

To detect the impedance mismatch, several methods such as voltage peak detection [Yok93, Qia05] and mixer-based quadrature detection [Bez08] are known. However, some drawbacks of these methods are extra parasitic capacitance, additional space requirement and additional lossy sensing element [Bez11]. To compensate these drawbacks, a generic impedance detector containing a quadrature detector combined with an amplitude detector as well as two dividers has been presented [Bez11]. The structure of this impedance sensing scheme is shown in Fig. 2-3 [Bez11].
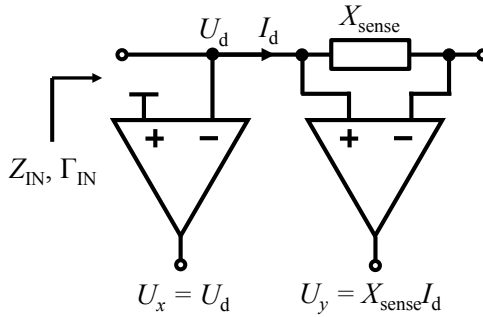

Fig. 2-3 A method of the impedance detection through sensing the voltage and current [Bez11]. Reproduced with permission from Springer Science and Bus Media B V.

In Fig. 2-3, U_d is the measured voltage, and I_d represents the current that flows through the sensing element with reactance value X_{sense}. According to the output voltages U_x and U_y, the detected input impedance Z_{IN} as well as the input reflection coefficient Γ_{IN} can be calculated as [Bez11]

$$Z_{IN} = \frac{1 + \Gamma_{IN}}{1 - \Gamma_{IN}} Z_0 = \frac{U_x}{U_y} X_{sense}.$$

(2.1)

It is seen from Fig. 2-3 that the parasitic effect of the sensing element can be

effectively represented by a fixed inductor or capacitor [Bez11]. Hence, an inductor L_{DET} is selected to mimic the influence of X_{sense} in this work.

In mobile terminal antennas, the electrostatic discharge generated by users is typically over 6 kV with a very short rising time of about 1 ns [Hil16, Lau03], and the electric components of the circuits are sensitive to it. Therefore, an ESD protection for the electronic components on the Printed Circuit Board (PCB) is required. The simplest ESD protector is an inductor to ground [Inf04], however, using only an inductor might not result a fast enough transient to reduce the ESD voltage to zero before damage is done. Because of the self-resonance frequency of realistic inductors, the implementation frequency range is limited as well [Inf04]. A solution for that would be adding two antiparallel diodes shunt-connected to the ESD inductor L_{ESD}, which is shown in Fig. 2-4 [Inf04]. These RF components also cause a parasitic effect on matching circuits. To briefly describe the parasitic effect of the ESD protection, L_{ESD} parallel to the antenna is sufficient [Hil16, Epc08].
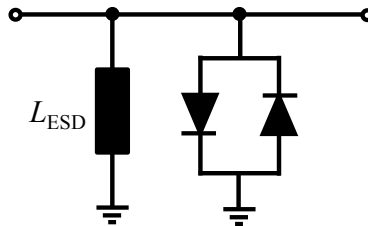

Fig. 2-4 A ESD protector containing an inductor shunt with antiparallel diodes. Reproduced with permission from Infineon Technologies AG [Inf04].

As a result, the structure of a simplified adaptive antenna matching system can be represented by a tunable matching structure by including a series as well as a shunt connected inductor embodying the parasitic effects of impedance detector and ESD protection see Fig. 2-5.

Adaptive antenna matching systems by minimizing the reflection coefficient

can be simply studied and implemented. Hence, this traditional tuning algorithm is the one used in this work for evaluating the tunability of the matching circuits. Practical RF components such as inductors and capacitors, however, contain losses, which limit the available reactance values and result in some power being dissipated during the power transfer. This fact may provide a low value of reflection at the RF front-end while reducing the power transferred to the antenna. Hence, by minimizing the reflection coefficients, the resultant power transfer in both the lossless and the realistic cases, will be investigated and measured in form of total efficiency in this work.
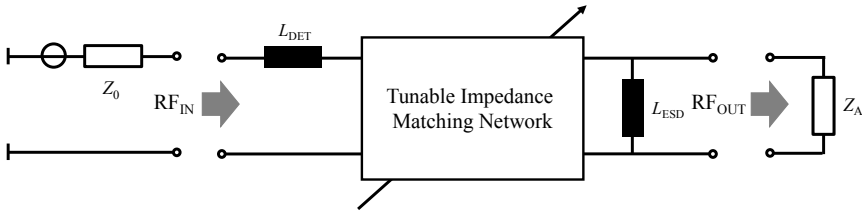

Fig. 2-5   Topology of a simplified adaptive impedance matching system.

As is known, inductors often have a substantially constant Q-factor (quality factor) value, while capacitors have typically a close-to-constant resistance value. To represent realistic RF components in SMD (surface-mounted device) packages, inductors having a $Q = 50$ and capacitors with a constant resistance of $0.3\ \Omega$ are used for the realistic case.

For multi-element antennas on a small-sized platform, a decoupling scheme should be included within the adaptive decoupling and matching systems. In particular, a multi-port conjugate matching method involves the utilization of decoupling and matching networks for simultaneous decoupling and matching of the antennas [Wal04, Lau06b]. Such a network derived from the antenna scattering parameters has been presented in [Dos04]. Similar approaches to compensate the mutual impedance between the antenna feeding ports

have been published as well, e.g. [Che08]. A closely related method is based on an eigenmode theory for implementation of a decoupling network using 180° directional couplers, which was introduced in [Vol08]. However, its direct application for small terminals is limited due to the size of the directional couplers. A common drawback related to all of the above-listed decoupling techniques is the limited bandwidth. Hence, the decoupling approach should also be set to be tunable, which by employing lumped-elements reduces the size.

Currently, no practical adaptive decoupling and matching systems are available. The work presented in this dissertation focuses on design concepts for tunable decoupling and matching networks that make a contribution to the field of adaptive decoupling and matching systems.

Although several reconfigurable multi-element antenna systems, that enable the tuning of the band of operation over a given frequency range have also been reported [Tan12, Cai11, Mur11], these employ antennas that are inherently matched, that have a large antenna form factor, and whose the number of the antenna elements is limited. By contrast, in the approach introduced in this work, the antenna elements are designed to be generic, small and placed closely to each other. The potential of reconfigurable decoupling and matching of such an antenna system should be purely controlled by tunable decoupling and matching networks consisting of lumped-elements, which can be designed following the proposed concepts.

2.2 Design of Antenna Decoupling and Matching Networks

An antenna system with N antenna elements can be treated as an N-port elec-

trical network. To describe the mutual coupling mathematically, several different expressions are presented [Hui07]. Two methods, however, are mainly used, namely: the impedance (Z)-parameter [Gup83] and the scattering (S)-parameter analyses [Wal04]. In these cases, the electrical behavior of the antenna systems can be characterized by an impedance (Z)-matrix or a scattering (S)-matrix. The investigation of the decoupling and matching network in this thesis is mainly based on the S-parameter analysis.

A general concept for an N-element antenna system is shown in Fig. 2-6 [Web06], where P_n denotes the nth port with $n = 1, \ldots, 2N$.
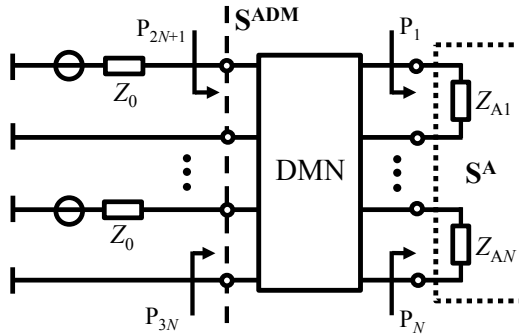

Fig. 2-6 Topology of an N-element antenna system containing DMNs. $\mathbf{S}^{\mathbf{A}}$ is the scattering matrix of a multi-element antenna surrounded by a dotted square. Z_{An} with $n = 1, \ldots, N$ is the antenna impedance of the nth antenna element. P_n denotes the nth port with $n = 1, \ldots, 3N$. Reproduced with permission from © 2006 *IEEE* [Web06].

The antenna impedance of an N-element antenna surrounded by a dotted square in Fig. 2-6, is defined as Z_{An}, with $n = 1, \ldots, N$, and $\mathbf{S}^{\mathbf{A}}$ represents the antenna S-matrix within this dotted square, which describes the electrical behavior at the antenna feeding points. $S_{A,mn}$, with $m, n = 1, \ldots, N$, are its (m, n) components. $S_{A,nn}$ is the reflection coefficient at the port P_n, while $S_{A,mn}$ with $m \neq n$ denotes the transmission coefficient from P_n to P_m. Due to the impedance mismatches and mutual couplings, some or all the parameters of $\mathbf{S}^{\mathbf{A}}$ are

18

nonzero in linear scale. Also shown in Fig. 2-6 is $\mathbf{S^{ADM}}$, the S-matrix used to quantify the effects of the DMNs, which represents the electrical behavior of the ports P_n, with $n = 2N+1, \ldots, 3N$ after performing decoupling and matching. $S_{ADM,mn}$ is the (m, n) component of $\mathbf{S^{ADM}}$. Lastly, $\mathbf{S^A}$ is assumed to be reciprocal, which makes the antenna mutual couplings between two arbitrary antenna elements identical ($S_{A,mn} = S_{A,nm}$). Due to the passivity of the networks, the couplings between every two ports are identical as well.

In the antenna system represented by Fig. 2-6, in addition to the radiated power, some of the power excited at the RF front-end of element n is either absorbed by the user or by reason of the material losses of the DMN, the plastic housing, the substrate, etc. To estimate these losses, the parameter denoted η_{cd} is used. The other parts of the dissipated power are reflected back due to the impedance mismatch or absorbed by the other RF front-ends because of the mutual coupling. The total efficiency then denoted η_{tot} is a figure of merit that includes all these losses for the excited element n can be expressed as

$$\eta_{tot} = \left(1 - \sum_{m=1}^{N} \left| S_{ADM,mn} \right|^2 \right) \eta_{cd}. \tag{2.2}$$

Although it is possible to increase η_{tot} by improving η_{cd}, the materials are typically fixed in consumer applications, and it is unrealistic to decrease the power absorbed by the user and the other objects in the usage scenario. Another method to enhance the total efficiency of all the elements by assuming a constant η_{cd} for each operation is to realize a perfect decoupling and matching, in which case $\mathbf{S^{ADM}}$ becomes a zero matrix in linear scale. The DMNs can then be considered as the multi-dimensional equivalent of single-element impedance matching circuits, which provide full power matching for all RF

front-ends [Vol10].

Typically, the general structure of DMNs, shown in Fig. 2-6 are quite complex, and the functions of decoupling and matching should be accomplished simultaneously [Web06]. In order to simplify the design, an approach based on the implementation of DMNs in different steps is used [Vol08]. In this case, the topology of a general separate designed DMN for an antenna array containing N elements is as shown in Fig. 2-7.
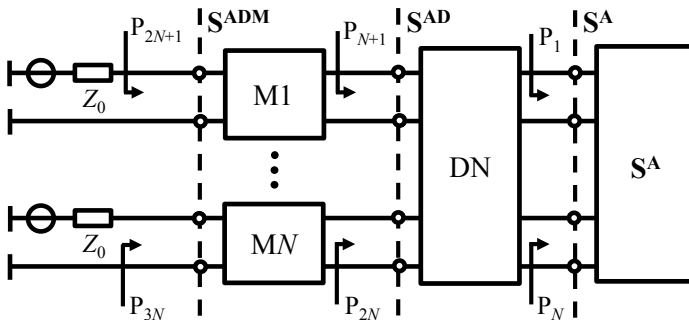

Fig. 2-7 Topology of an N-element antenna system with separate decoupling and matching networks [Vol08]. P_n denotes the nth port with $n = 1, \ldots, 3N$. DN represents the decoupling network, while M1 and MN are the matching networks. Reproduced with permission from © 2017 *IEEE* [Che17].

In this context, by utilizing the decoupling network (DN), the ports P_n, with $n = N+1, \ldots, 2N$, are no longer coupled to each other. The decoupling network is, in turn, connected to the matching networks, which are able to compensate the impedance mismatch at the corresponding RF front-ends (P_n with $n = 2N+1, \ldots, 3N$) individually. The matching network for element n is denoted by Mn.

In Fig. 2-7, the S-matrices $\mathbf{S^{AD}}$ are used to quantify the effects of the DN, which represent the electrical behavior of the decoupled ports. The (m, n) component of $\mathbf{S^{AD}}$ is $S_{AD,mn}$, with $m, n = 1, \ldots, N$. To realize the decoupling and matching using the DMN, $\mathbf{S^{AD}}$ and $\mathbf{S^{ADM}}$ should ideally become a diago-

nal and a zero matrix in linear scale, respectively.

In reality, decoupling and matching cannot be reduced to zero in linear scale. Therefore, a certain value $|S_{dc,thres}|$ will be set as the threshold for decoupling between the RF front-ends, while a value of $|S_{ma,thres}|$ will be set for matching at each RF front-end. The goal is then to keep the coupling coefficients of $\mathbf{S}^{ADM}$ ($S_{ADM,mn}$ with $m \neq n$) as well as the reflection coefficients of $\mathbf{S}^{ADM}$ ($S_{ADM,nn}$) below the corresponding thresholds. According to the results from simulations and measurements carried out to evaluate the concept, $|S_{dc,thres}|$ and $|S_{ma,thres}|$ are set to be -10 dB and -6 dB respectively, and the band of operation with a good total efficiency should be tunable over the frequency range $f_s\,[\mathrm{GHz}] = 0.69 \leq f\,[\mathrm{GHz}] \leq f_e\,[\mathrm{GHz}] = 2.7$, containing a low-band ($0.69 \leq f\,[\mathrm{GHz}] \leq 0.96$) and a high-band ($1.71 \leq f\,[\mathrm{GHz}] \leq 2.7$).

Using the DMNs, the threshold values ($|S_{dc,thres}|$ and $|S_{ma,thres}|$) should be reachable, which leads to the possibility that, if the thresholds are satisfied, the utilization of a complete DMN might not be necessary. In some cases, even on small terminals, certain antenna elements may only be weakly coupled to others. In this case, $|S_{ADM,mn}|$ with $m \neq n$ might still remain below $|S_{dc,thres}|$, even if the matching networks are implemented without decoupling, thus permitting the simplification of the DMN.

Assume that at least one coupling out of one of totally K antenna elements to the other $K - 1$ elements needs to be compensated, and only matching circuits are necessary for the other $N - K$ weakly coupled antenna elements. Then the topology of such an antenna system is as shown in Fig. 2-8, where the whole decoupling stage between P_n, with $n = N+1, \ldots, 2N$, and P_n, with $n = 3N+1, \ldots, 4N$, is surrounded by a dashed square.
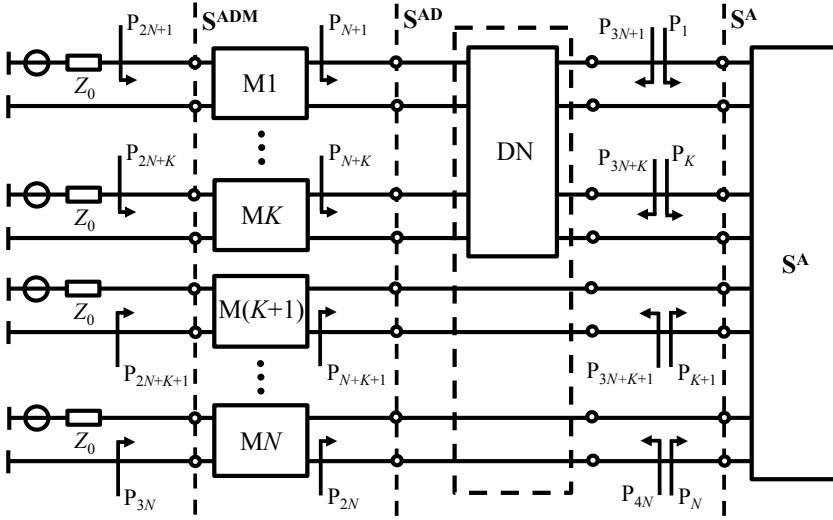
Fig. 2-8 Topology of an *N*-element antenna system. Some or all of the couplings between *K* antenna elements are needed to be compensated. Reproduced with permission from © 2017 *IEEE* [Che17].

If the possible simplifications by omitting some decoupling branches are known, the suitable decoupling stage surrounded by the dashed square can then be calculated. Let $\mathbf{a_c}$ and $\mathbf{b_c}$ be the vectors of the incident and reflected power waves at P_n, with $n = N+1, \ldots, 2N$, while $\mathbf{a_i}$ and $\mathbf{b_i}$ are the vectors of the incoming and outgoing power waves at P_n with $n = 3N+1, \ldots, 4N$. Then, a relationship between these waves is given by [Dob10]

$$\begin{bmatrix} \mathbf{b_c} \\ \mathbf{b_i} \end{bmatrix} = \mathbf{S}^{\mathbf{DN}} \begin{bmatrix} \mathbf{a_c} \\ \mathbf{a_i} \end{bmatrix} = \begin{bmatrix} \mathbf{T_{cc}} & \mathbf{T_{ci}} \\ \mathbf{T_{ic}} & \mathbf{T_{ii}} \end{bmatrix} \begin{bmatrix} \mathbf{a_c} \\ \mathbf{a_i} \end{bmatrix}. \tag{2.3}$$

where $\mathbf{T_{cc}}$, $\mathbf{T_{ci}}$, $\mathbf{T_{ic}}$ and $\mathbf{T_{ii}}$ are the submatrices of $\mathbf{S}^{\mathbf{DN}}$, which is the S-matrix between P_n with $n = N+1, \ldots, 2N$, and P_n, with $n = 3N+1, \ldots, 4N$. Once the suitable structure of the decoupling network is selected, these submatrices can be determined. Then the resultant S-matrix $\mathbf{S}^{\mathbf{AD}}$ as a function of the decoupling components can be expressed as [Dob10]

$$\mathbf{S}^{\mathbf{AD}} = \mathbf{T_{cc}} + \mathbf{T_{ci}} \left[\mathbf{I} - \mathbf{S}^{\mathbf{A}}\mathbf{T_{ii}} \right]^{-1} \mathbf{S}^{\mathbf{A}}\mathbf{T_{ic}} . \qquad (2.4)$$

where $\mathbf{I}$ is an $N \times N$ unit matrix. According to the reflection coefficients of $\mathbf{S}^{\mathbf{AD}}$, all the matching networks are designed and consequently $\mathbf{S}^{\mathbf{ADM}}$ can be calculated.

Based on the above remarks, a suitable antenna decoupling and matching system containing a compact N-element antenna and DMNs for achieving the threshold values ($|S_{dc,thres}|$ and $|S_{ma,thres}|$) can be designed according to the flowchart, shown in Fig. 2-9.
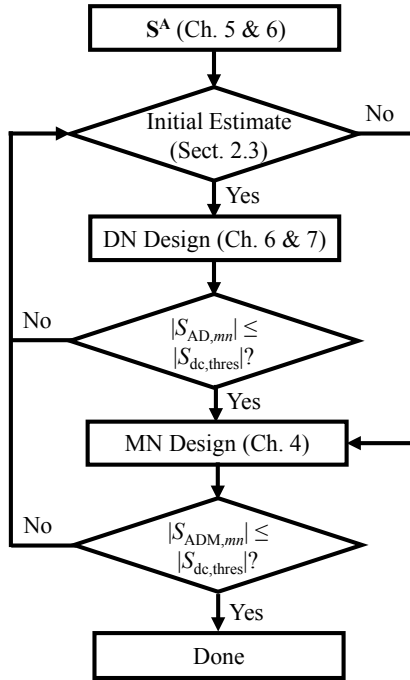
Fig. 2-9 Flowchart of the DMN design.

The presentation of the main scientific contributions for the design process in each step is organized as follows. Appropriate small-sized antennas for achieving a reconfigurable band with a sufficient bandwidth over a large fre-

23

quency range by utilizing DMNs are studied in Chapter 5 and Chapter 6. In order to evaluate possible simplifications by omitting some decoupling branches, an initial estimate, which determines which coupling existing in the antenna array should be compensated, is derived. With this, the value of K is calculated. This initial estimate will be discussed in Section 2.3. Then, if the decoupling is avoidable ($K = 0$), only the matching network for each antenna element is necessary. Its design concept will be presented in Chapter 4. Otherwise, a suitable decoupling network is required before implementing matching networks, which only needs that couplings be compensated according to the initial estimate. The design process of a suitable decoupling network can be found in Chapter 6 and Chapter 7. For cases where, even when using the decoupling network, not all the coupling coefficients of $\mathbf{S^{AD}}$ and $\mathbf{S^{ADM}}$ are below $|S_{dc,thres}|$, the decoupling network should be redesigned, and the value of these coupling coefficients need to be rechecked. The iteration is repeated until full decoupling is achieved.

2.3 Initial Estimate of the Implementing Decoupling Networks

It is known that in general the mutual couplings discussed above are modified through matching of the antenna elements. Therefore, it is important to find out whether effecting the decoupling for some of the multi-element antennas might be avoidable. In this context, the estimate for the necessity of decoupling is based on the calculation of simultaneous conjugate complex matching for all the antenna elements, using lossless RF components, at the same frequency point. The result of this analysis gives the worst case with respect to decoupling, since any power losses lead to decreasing the power transfer between the ports, the lossless case can be used as a reference. The analysis

can be repeated over the whole frequency range of interest. In this case, the antenna system presented in Fig. 2-7 can be simplified as shown in Fig. 2-10.
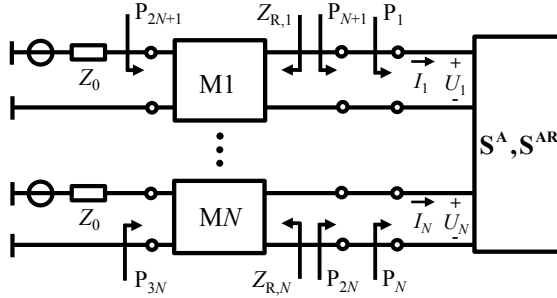

Fig. 2-10 Topology of a N-element antenna system only containing matching networks. $Z_{R,n}$ is the input impedance looking into the matching network for element n. $\mathbf{S^{AR}}$ denotes $\mathbf{S^A}$ with $Z_{R,n}$ as reference impedance assigned to P_n. Reproduced with permission from © 2017 *IEEE* [Che17].

In Fig. 2-10, U_n and I_n denote the total voltage at P_n and the total current flowing into P_n, with $n = 1, ..., N$. **U** and **I** are N-element column vectors, whose n^{th} component is U_n and I_n. $\mathbf{Z^A}$ represents the Z-matrix of the N-element antenna array, which can be converted from $\mathbf{S^A}$. In particular, **U** and **I** are related by $\mathbf{Z^A}$, according to [Poz11]

$$\mathbf{U} = \begin{bmatrix} U_1 \\ \vdots \\ U_N \end{bmatrix} = \mathbf{Z^A I} = \mathbf{Z^A} \begin{bmatrix} I_1 \\ \vdots \\ I_N \end{bmatrix}. \tag{2.5}$$

Also, $Z_{R,n}$ with $n = 1, ..., N$, is the input impedance looking into the matching network for element n, and $\mathbf{S^{AR}}$ denotes the renormalized antenna matrix with $Z_{R,n}$ as the reference impedance assigned to P_n. The incident and reflected power wave amplitudes a_n and b_n at P_n defined as linear transformations of U_n and I_n are given by [Poz11]

$$a_n = \frac{U_n + Z_{R,n} I_n}{2\sqrt{\operatorname{Re}\{Z_{R,n}\}}}, \tag{2.6}$$

and

$$b_n = \frac{U_n - Z_{R,n}^* I_n}{2\sqrt{\operatorname{Re}\{Z_{R,n}\}}}. \tag{2.7}$$

The asterisk in (2.7) denotes complex conjugation. These relationships can be transformed as functions of **U** and **I**, as follows [Poz11]

$$\mathbf{a} = \begin{bmatrix} a_1 \\ \vdots \\ a_N \end{bmatrix} = \mathbf{F_m}(\mathbf{U} + \mathbf{Z_R}\mathbf{I}), \tag{2.8}$$

and

$$\mathbf{b} = \begin{bmatrix} b_1 \\ \vdots \\ b_N \end{bmatrix} = \mathbf{F_m}(\mathbf{U} - \mathbf{Z_R^*}\mathbf{I}). \tag{2.9}$$

Here, **a** and **b** are N-element column vectors, whose n^{th} component is a_n and b_n with $n = 1, \ldots, N$, respectively, and $\mathbf{F_m}$ and $\mathbf{Z_R}$ are $N \times N$ diagonal matrices, which have $1/2\sqrt{\operatorname{Re}\{Z_{R,n}\}}$ and $Z_{R,n}$ as the nth entry respectively. Substituting (2.8) and (2.9) into (2.5) gives [Poz11]

$$\mathbf{b} = \mathbf{F_m}(\mathbf{Z^A} - \mathbf{Z_R^*})(\mathbf{Z^A} + \mathbf{Z_R})^{-1}\mathbf{F_m^{-1}}\mathbf{a}. \tag{2.10}$$

Due to the fact that $\mathbf{S^{AR}}$ relates **b** to **a**, it can be expressed as [Kur65, Poz11]

$$\mathbf{S^{AR}} = \mathbf{b}\mathbf{a}^{-1} = \mathbf{F_m}(\mathbf{Z^A} - \mathbf{Z_R^*})(\mathbf{Z^A} + \mathbf{Z_R})^{-1}\mathbf{F_m^{-1}}. \tag{2.11}$$

$S_{AR,mn}$ is the (m, n) element of $\mathbf{S^{AR}}$. According to (2.11), the element $S_{AR,mn}$ is

26

given by

$$
\mathbf{S}_{\mathrm{AR},mn} = \frac{1}{\det(\mathbf{Z}^{\mathbf{A}} + \mathbf{Z}_{\mathrm{R}})} \frac{\sqrt{\mathrm{Re}\{Z_{\mathrm{R},n}\}}}{\sqrt{\mathrm{Re}\{Z_{\mathrm{R},m}\}}} \cdot
$$

$$
\begin{pmatrix}
(-1)^{n+1} Z_{\mathrm{A},m1} M_{n1} + \ldots + (-1)^{n+(m-1)} Z_{\mathrm{A},m(m-1)} M_{n(m-1)} \\
+(-1)^{n+m} \left(Z_{\mathrm{A},mm} - Z_{\mathrm{R},m}^{*} \right) M_{nm} + (-1)^{n+(m+1)} Z_{\mathrm{A},m(m+1)} M_{n(m+1)} \\
+\ldots + (-1)^{n+N} Z_{\mathrm{A},nN} M_{nN}
\end{pmatrix}. \quad (2.12)
$$

where M_{mn} denotes the (m, n) minor of the resultant matrix of $\mathbf{Z}^{\mathbf{A}} + \mathbf{Z}_{\mathbf{R}}$.

By simultaneous matching, not only the reflections at the RF front-ends, but also $S_{\mathrm{AR},nn}$, with $n = 1, \ldots, N$, become zero in linear scale at the target frequency. Hence, N simultaneous equations can be derived from (2.11), and $Z_{\mathrm{R},n}$ is able to be computed [Rah07]. However, since some of the solutions cannot be realized using passive networks [Mav96], the value of $Z_{\mathrm{R},n}$ is optimized in order to minimize $|S_{\mathrm{AR},nn}|$. Substituting the calculated value of $Z_{\mathrm{R},n}$ into (2.11), then, gives the resulting $\mathbf{S}^{\mathbf{AR}}$. Due to the law of conservation of energy, the amplitude of coupling between the front-end for element m and that for element n is identical to $|S_{\mathrm{AR},mn}|$ in the lossless case [Rah07]. In this case, the amplitude value of the coupling coefficients ($|S_{\mathrm{AR},mn}|$ with $m \neq n$) is compared to $|S_{\mathrm{dc,thres}}|$, which provides an initial estimate regarding the necessity of decoupling. If a part of $|S_{\mathrm{AR},mn}|$ exceeds the threshold, although the decoupling network still has to be implemented, only their corresponding antenna couplings might have to be compensated. This result can then be used as a good starting point for the design of a suitable decoupling network, which is presented in Chapter 6. For the case, in which all $|S_{\mathrm{AR},mn}|$ are less than $|S_{\mathrm{dc,thres}}|$, the decoupling for the whole antenna system is unnecessary.

As an example of this procedure, three exemplary antenna matrices at one

single frequency are shown in Table 2-1, and the results corresponding to the initial estimate for the necessity of decoupling are presented in Table 2-2.

TABLE 2-1
EXEMPLARY ANTENNA MATRICES FOR INVESTIGATION REPRODUCED WITH PERMISSION FROM ©
2017 *IEEE* [CHE17].

example	$\mathbf{S^A}$
1	$\begin{bmatrix} 0.1 + j0.5 & -0.1 + j0.2 & -0.1 + j0.1 \\ -0.1 + j0.2 & 0.5 - j0.2 & 0.1 - j0.1 \\ -0.1 + j0.1 & 0.1 - j0.1 & 0.2 + j0.5 \end{bmatrix}$
2	$\begin{bmatrix} 0.42 - j0.29 & -0.08 - j0.23 & 0.11 + j0.24 \\ -0.08 - j0.23 & 0.05 + j0.51 & -0.21 + j0.15 \\ 0.11 + j0.24 & -0.21 + j0.15 & 0.39 + j0.43 \end{bmatrix}$
3	$\begin{bmatrix} 0.46 + j0.24 & 0.04 - j0.17 & -0.07 + j0.15 & 0.00 + j0.01 \\ 0.04 - j0.17 & 0.55 + j0.26 & -0.11 + j0.14 & -0.01 + j0.00 \\ -0.07 + j0.15 & -0.11 + j0.14 & 0.32 - j0.75 & -0.15 + j0.06 \\ 0.00 + j0.01 & -0.01 + j0.00 & -0.15 + j0.06 & -0.51 + j0.27 \end{bmatrix}$

TABLE 2-2
NECESSITY OF IMPLEMENTING DECOUPLING NETWORKS. REPRODUCED WITH PERMISSION FROM ©
2017 *IEEE* [CHE17].

example	$Z_{\mathrm{R},n}$ with $n = 1, \ldots, 4$ [Ω]	$\mathbf{S^{AR}}$ [dB]	initial estimate
1	$Z_{\mathrm{R},1} = 36 - j43$ $Z_{\mathrm{R},2} = 116 + j58$ $Z_{\mathrm{R},3} = 41 - j55$	$\begin{bmatrix} -53.7 & -10.6 & -13.5 \\ -10.6 & -54.9 & -15.3 \\ -13.5 & -15.3 & -52.6 \end{bmatrix}$	Decoupling is not necessary. $K = 0$
2	$Z_{\mathrm{R},1} = 111 + j68$ $Z_{\mathrm{R},2} = 30 - j39$ $Z_{\mathrm{R},3} = 52 - j67$	$\begin{bmatrix} -51.7 & -9.9 & -9.4 \\ -9.9 & -55.1 & -10.5 \\ -9.4 & -10.5 & -59.2 \end{bmatrix}$	Decoupling for $S_{\mathrm{A},23}$ might not be necessary. $K = 3$
3	$Z_{\mathrm{R},1} = 119 - j48$ $Z_{\mathrm{R},2} = 141 - j98$ $Z_{\mathrm{R},3} = 14 + j68$ $Z_{\mathrm{R},4} = 16 - j14$	$\begin{bmatrix} -44.4 & -8.9 & -9.1 & -20.3 \\ -8.9 & -42.9 & -8.5 & -20.3 \\ -9.1 & -8.5 & -40.1 & -9.2 \\ -20.3 & -20.3 & -9.2 & -52.0 \end{bmatrix}$	Decoupling for $S_{\mathrm{A},14}$ and $S_{\mathrm{A},24}$ might not be necessary. $K = 4$

For example 1, shown in Table 2-1, the antenna elements are weakly-coupled

to each other. Hence, only the impedance matching networks are needed. Although for the other two examples, decoupling networks are required before implementing the matching networks, some decoupling branches might be omitted according to the initial estimate.

Fixed DMNs are sufficient for decoupling and matching of these three exemplary antenna matrices at one single frequency. As discussed above, for providing a frequency reconfigurable antenna band over a wide frequency range in usage scenario for appropriate generic and small-sized antennas, which are presented in Chapter 5 and Chapter 6, tunable decoupling and matching networks are required. Hence, before presenting the network design concepts, tunable RF components within the networks are introduced first in the next chapter (Chapter 3).

Chapter 3

Tuning Approaches for RF Elements

As discussed in the last chapter, one popular solution for decreasing mutual coupling and impedance mismatch of the band of operation is to use antenna adaptive systems including tunable decoupling and matching networks. In this case, the value of some or all the RF components within the networks such as inductors and capacitors need to be controllable.

Although several inductors with variable reactance values have already been reported [Sal78, Kor98, Zin03], they suffer from several limitations, such as large area, limited tuning range and high fabrication costs [Nin06]. Therefore, up to now, no practical tunable inductors are available [Gu11]. Unlike tunable inductors, many different tunable capacitors have been widely studied and used over more than half a century. Hence, the tunability of the networks shown in this work is realized by using tunable capacitors.

In this chapter, two different approaches for building variable capacitors are presented. In the first one, a bank of fixed capacitors connected controlled by RF switches is implemented to control the total capacitance. In the second one, the capacitance value is varied mainly due to tunable RF components. To enlarge the tuning range, an approach for building a bank consisting of

tunable components can be used as well. To find the suitable one for implementation, the advantages and disadvantages of the tuning approaches are compared.

3.1 Switched Capacitor Arrays

To realize the tuning of the capacitance value, one possible method is to build a switched bank of fixed MIM (metal–insulator–metal) capacitors [Reb03a]. The required resultant capacitance of the whole array can be selected through varying the state of the switches. An example of arrays of capacitors is presented in Fig. 3-1 [Reb03a], where the fixed capacitances (C_n) connected to the switches in series is $C_n = 2^{n-1}C_1$, with $n = 1, …, 4$. C_1 is the lowest reactance value of the element capacitors, and C_0 is the capacitance value of the array if all the switches are in the off-state. Due to the different combination states of the switches, the total capacitance value in both configurations (C_t) is tunable. A capacitor array with N switches is able to provide 2^N different total capacitance values. Hence, the total capacitance can be controlled digitally, and the resolution of its value can be enhanced by increasing the number of the switches.
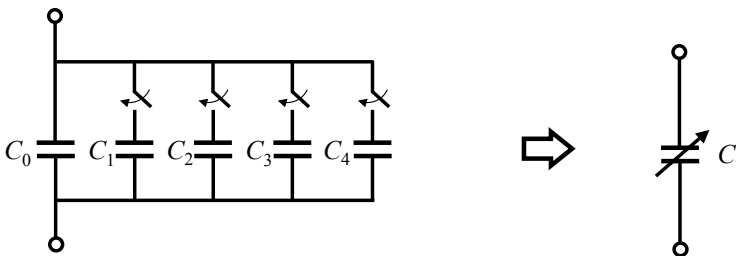
Fig. 3-1 Configuration of capacitor arrays with 4 switches. Reproduced with permission from John Wiley and Sons [Reb03a].

The switched capacitors have typically a high Q-factor, especially if RF MEMS (radio frequency microelectromechanical system) switches are used

for controlling. They have quite a large capacitance ratio especially for cases that $C_0 = 0$ and are also insensitive to bias [Reb03a]. However, these designs suffer from parasitic series inductance and a relative large size [Reb03a]. Based on this technology, several RF tunable capacitor arrays for wireless communications have been presented [Wha10, Hua10]. To modify the total capacitance value of the arrays, three RF switches, namely, PIN diodes, FET switches and RF MEMS switches are introduced in this section.

PIN (positive intrinsic negative) diodes are the most commonly used RF switches. They are quite fast, inexpensive as well as have a long lifetime. However, they suffer from high power consumption and need complex biasing networks. Some examples of capacitor arrays controlled by PIN diodes have been given in [Tan82, Wat08].

Besides PIN diodes, FET (field effect transistor) switches also belong to conventional semiconductor-based switches. FETs are three terminal RF components, whose electrical conductivity can be controlled by voltages. Similar as PIN diodes, they also provide a broad operation band, fast switching speed and have a small size. Compared to the PIN diodes, however, a much lower DC power consumption and a simpler bias network are needed [Rob01]. Several variable capacitor arrays controlled by FET switches have been presented such as in [Ima91] and [Wha10]. Using JPHEMT (junction pseudomorphic high electron mobility transistor) based on FET technology as the switches, the first commercial closed loop antenna tuner D7005 was introduced by Epcos [Epc].

RF MEMS switches exploit mechanical movements in micro- or nano-scale actuated structures by an electrostatic force. Unlike the traditional semiconductor switches, the RF MEMS switches provide near-zero power assump-

tion, very high isolation, low insertion losses and excellent linearity [Mal12]. However, while lifetimes of the order of more than one and a half trillion cycles have been achieved [Rad], their switching speed is quite low due to the inertia germane to mechanical movements [Reb03b]. They also suffer from high actuation voltage and great packaging requirements [Pat12]. Some RF MEMS switch-based capacitor arrays are shown in [Bra01, Riz02]. Moreover, one reconfigurable tuner utilizing this technique has been presented in [Pap03].

A detailed comparison of some important parameters of PIN diodes, FET switches and RF MEMS switches is shown in Table 3-1 [Reb03a, Reb09, Poi12, Luc10, Liu09, Obe04].

TABLE 3-1
PARAMETER COMPARISON OF PIN, FET AND RF MEMS. REPRODUCED WITH PERMISSION FROM JOHN WILEY AND SONS, © 2003 2009 *IEEE*, ARTECH HOUSE INC, CAMBRIDGE UNIVERSITY PRESS [REB03A, REB09, POI12, LUC10, LIU09, OBE04].

	PIN	FET	RF MEMS
actuation voltage [V]	$\pm 3 - 5$	$3 - 5$	$20 - 80$
power consumption* [mW]	$5 - 100$	$0.05 - 0.1$	$0.05 - 0.1$
bias power consumption [μW]	< 100	< 10	$\sim 10^{-6}$
switching time [μs]	$0.01 - 0.1$	$0.001 - 0.1$	< 35
series resistance [Ω]	$2 - 4$	$4 - 6$	$0.5 - 2$
RF isolation [dB] ($1\,\text{GHz} \leq f \leq 10\,\text{GHz}$)	> 35	$15 - 25$	> 40
loss [dB] ($1\,\text{GHz} \leq f \leq 100\,\text{GHz}$)	$0.3 - 1.2$	$0.4 - 2.5$	$0.05 - 0.2$
IP3 [dBm]	$27 - 45$	$27 - 45$	$66 - 80$
integration	COMS	COMS	hybrid
size [mm^2]	0.1	$1 - 5$	< 0.1

* Includes voltage upconverter or drive circuity

To gain some insight, the tuning algorithms and electrical behaviors of these three types of switches are presented below.

3.1.1   *PIN Diodes*

PIN diodes, whose structure and symbol are shown in Fig. 3-2 [Bah14], have a low doping concentration region (i-region) between a p- and an n-region.
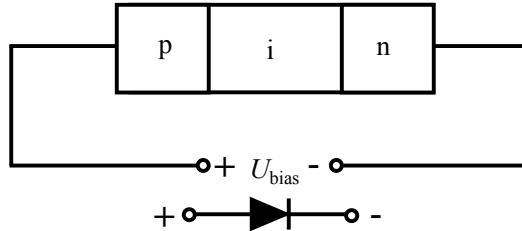

Fig. 3-2 A simplified structure of PIN diodes and the symbol. Reproduced with permission from Artech House Inc [Bah14].

The bias voltage (U_{bias}) can be positively and negatively operated. The current I as a function of U_{bias} is presented in Fig. 3-3 [Var03]. When the bias voltage is reversely applied, the diodes become highly resistive. In this case, the current I is almost blocked, and the diodes work in a so-called off-state. This reversed voltage should be less than a threshold voltage called U_b to prevent the breakdown. For the case that the diodes are forwardly biased and greater than a threshold voltage called U_{th}, the resistivity is reduced to an ohmic contact resistance value, which would allow the forward current to increase significantly [Bah14]. This case, in which the diode is almost short-circuited, is called the on-state. As a result, the PIN diodes are controlled by the bias voltage.

To characterize their electrical behavior, a simplified PIN diode equivalent circuit can be found in [Bah14], and a more precise one, including the influence of packaging, is shown in Fig. 3-4 [Mal12]. R_f and R_r represent the re-

35

sistance in the on- and off-state, while the junction capacitance is denoted by C_j. C_p and L_p are the capacitance and inductance representing the influence of the package.
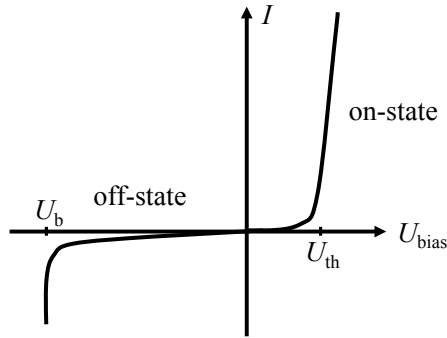
Fig. 3-3 Current I as a function of U_{bias}. Reproduced with permission from John Wiley and Sons [Var03].
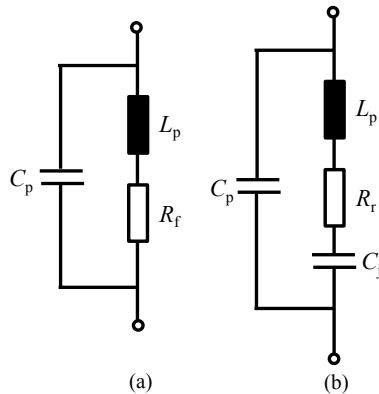

Fig. 3-4 An equivalent circuit of PIN diodes in the on-state (a) and off-state (b) including the influence of the package. Reproduced by permission from Artech House Inc [Mal12].

3.1.2 *FET switches*

The FETs invented in 1926 are unipolar transistors, which have three terminals, namely, drain (D), source (S) and gate (G). Typical structures of the FET switches are series and shunt configurations, which are shown in Fig. 3-

5 [Pet14]. Here, C_{DC} and R_F are the DC blocking and high-impedance resistor, respectively. They are controlled by the voltage of gate with respect to the source (U_{GS}) as the bias voltage [Rei04].

(a)   (b)
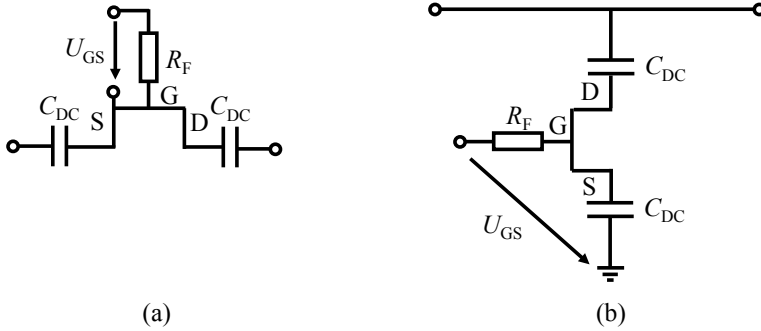
Fig. 3-5 Series (a) and shunt (b) configurations of FET switches. C_{DC} and R_F are the DC block and high impedance resistor. U_{GS} denotes the bias voltage of these switches. Reproduced with permission from John Wiley and Sons [Pet14].

JFET (junction field effect transistor) and MOSFET (metal oxide field effect transistor) are the two major types of FETs. Depending on the materials, two categories of each type (n-channel and p-channel) exist. The p-channel FETs are typically not utilized as RF switches because of their inherently lower carrier mobility and higher drain-source losses [Hil16]. Hence, only n-channel JFET and MOSFET are discussed below.

A schematic structure of n-channel JFETs is shown in Fig. 3-6(a) [Jai10]. By maintaining the value of the voltage between source and drain U_{DS}, the current I_D flowing from drain to source is dependent on the reversely operated gate source voltage U_{GS}. This dependence, which is called transconductance curve, is shown in Fig. 3-6(b) [Cox02].

For the case in which U_{GS} is set to be zero, I_D becomes the maximum value I_{DSS}. Increasing the negative U_{GS} would expand the depletion region and, consequently, reduce I_D. If U_{GS} reaches a certain threshold value called cut-

off voltage U_p, the current I_D becomes zero. Hence, JFETs can be used as switches by controlling the value of U_{GS}.

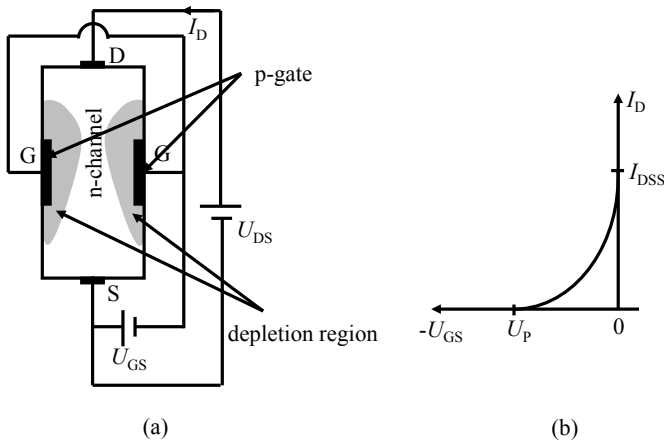(a)   (b)

Fig. 3-6 A schematic structure (a) and the transconductance curve (b) of n-channel JFETs. Fig. 3-6(a): Source – Jain: Modern Digital Electronics, 4th Edition. Reproduced with permission from McGraw Hill Education (India) Pvt. Ltd [Jai10]. Fig. 3-6(b): From Cox/Chartrand. Fundamentals of Linear Electronics Integrated and Discrete, 2E. © 2002 Delmar Learning, a part of Cengage, Inc. Reproduced by permission. www.cengage.com/permissions [Cox02].

MOSFETs can be classified into enhancement and depletion modes, whose structures are shown in Fig. 3-7 (a) and (b), respectively [Egg11]. In both modes, U_{GS} is used to control the drain source resistance. In the enhancement mode, the resistance is quite large unless U_{GS} is over a certain positive threshold voltage U_{th}. At this stage, no current from drain to source (I_D) flows and, therefore, this transistor is in the off-state. By increasing U_{GS}, the drain-source resistance drops and, as a consequence, the value of I_D increases and the transistor operates in the on-state. In the depletion mode, I_D already exists without applying the control voltage U_{GS}, which can be positively and nega-tively operated. By applying a negative U_{GS}, the resistance in the channel be-tween source and drain increases. As a consequence, I_D can be reduced to ze-ro, which represents the off-state. If U_{GS} is biased positive, I_D is enhanced. As

38

a result, similar as with JFETs, the state of the transistors is also switched according to the value of U_{GS}.
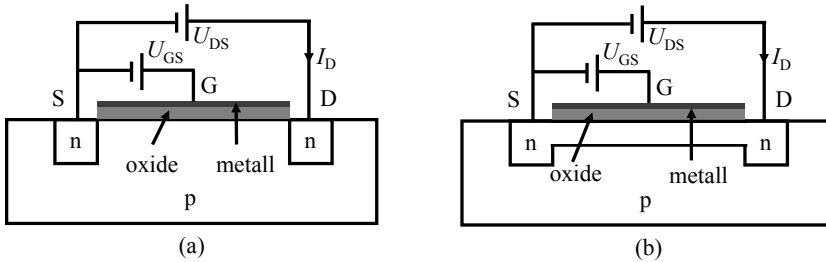

Fig. 3-7 A schematic structure of MOSFETs in enhancement mode (a) and in depletion mode (b). Fig. 3-7: Reproduced with permission from Cambridge University Press [Egg11].

3.1.3 *RF MEMS switches*

RF MEMS switches, containing small-sized and relatively fast moveable parts, which are a promising alternative to the conventional solid state devices, have been developed since 1970s. According to the controllable movement of the parts effected by an electrostatic force, certain RF capabilities can be achieved [Ian13, Liu06, Reb03a].

The RF MEMS switches can be basically classified as series and shunt types. An inline capacitive DC-contact RF MEMS series switch as an example of the series RF MEMS switches is shown in Fig. 3-8 [Reb03a].
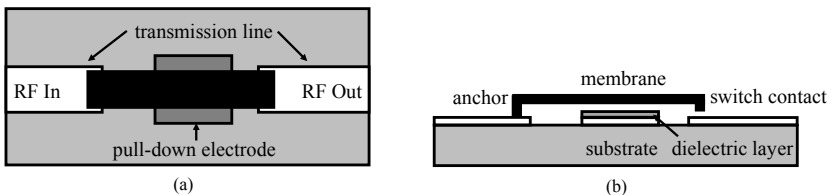
Fig. 3-8 General view of an inline capacitive DC-contact RF MEMS series switch. (a): Top view of the MEMS switch structure. (b): Cross section of the MEMS switch structure. Reproduced with permission from John Wiley and Sons [Reb03a].

A DC bias voltage (U_{bias}) is applied between the membrane and the pull-

down electrode to provide an electrostatic force. One end of the membrane is fixed while the other one is over the transmission line. By modifying the force, the RF MEMS switches operate basically in two states, up-state and down-state, which correspond to the off- and on-state of operation. In the down-state, this force drags the suspended membrane down, so that the RF transmission can be allowed. In the up-state, the voltage is removed and, hence, the membrane returns back to its original position, resulting in the transmission being interrupted. The dielectric layer prevents the short-circuit connection between the membrane and the pull-down electrode.

An inline MEMS capacitive shunt switch is used to realize the structure of RF MEMS shunt switches, whose top view and cross sections are shown Fig. 3-9.
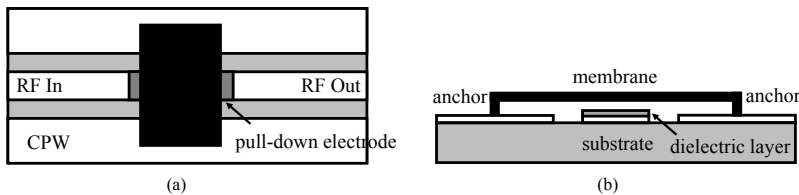
Fig. 3-9 General view of an inline RF MEMS capacitive shunt switch. (a): Top view of the MEMS switch structure. (b): cross section of the MEMS switch structure. Reproduced with permission from John Wiley and Sons [Reb03a].

The membrane, having two fixed anchors connected to the ground plane of the CPW (coplanar waveguide) line, is disposed over a CPW center/signal line. The height of the membrane over the dielectric layer is typically between 1.5 μm and 3 μm. In this switch, if no bias voltage (U_{bias}) is applied, the membrane is not deflected, and the state is called up-state, which is shown in Fig. 3-10(a) [Reb03a]. On the other hand, if the bias voltage exceeds a so called pull-down voltage, the membrane is dragged down directly on the dielectric surface. This down-state, which is presented in Fig. 3-10(b),

results an increase of the capacitance and, consequently, blocks the transmission through the CPW line [Reb03a]. The up-state and down-state in this type of the structure, therefore, correspond to the on- and off-state of the RF switches.
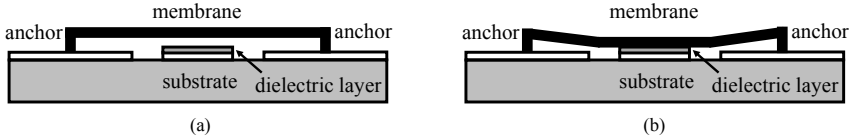

Fig. 3-10 Cross section of an inline MEMS capacitive shunt switch in up-state (a) and down-state (b). Reproduced with permission from John Wiley and Sons [Reb03a].

An equivalent *RLC* circuit model of RF MEMS capacitive switches is depicted in Fig 3-11 [Mul00]. Here, *S* denotes the length of RF MEMS structure, $Z_{c,CPW}$ is the characteristic impedance of the CPW transmission line, and C_b, L_b and R_b denote the electrical influence of the MEMS membrane. The capacitive value C_b is mainly dependent on the state of the switch as well as the type and the thickness of the dielectric [Luc10].
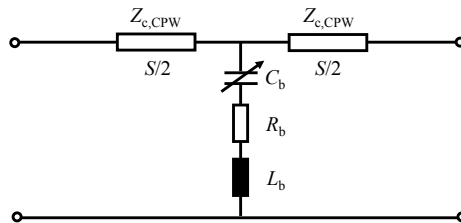
Fig. 3-11 An equivalent *RLC* circuit model of RF MEMS capacitive switches [Mul00]. $Z_{c,CPW}$ is the characteristic impedance of the CPW transmission line. C_b, L_b and R_b represent the electrical influence of the MEMS membrane. Reproduced with permission from © 2000 *IEEE* [Mul00].

3.2   Tunable RF Components

Besides the switch-controlled fixed capacitor arrays, tunable RF capacitors such as varactor diodes, BST varactors and RF MEMS varactors can also be

used as tunable elements. Unlike the discrete tuning using fixed capacitors combined with RF switches, the capacitance value in this case can be tuned continuously.

Varactor diodes are a type of p-n junction diodes, which are cheap, reliable and have a long lifetime. Because of these advantages, the use of traditional varactor diodes as RF tunable components is quite popular. However, these varactors suffer from low Q-factor, low linearity and poor power handling.

Abrupt and hyperabrupt are two basic types of varactor diodes. Typically, they are manufactured on Si (silicon) and GaAs (gallium arsenide) wafers. Many papers utilizing silicon hyperabrupt junction varactor diodes ([Pay13], [Lim10], [Elf12]) and silicon abrupt junction ([Beh06], [Khi15]) to modify and/or enlarge the bandwidth of their operating band have been published. In [Ngu08], [Oh07] and [Chi16], GaAs hyperabrupt junction varactor diodes are exploited as the tunable components to achieve the required capacitance value during operation.

To compensate some disadvantages of varactor diodes, BST (barium strontium titanate) varactors can be chosen as an alternative [Zhu09b]. The capacitance value of BST is variable due to its voltage dependent permittivity. Compared to the semiconductor varactor diodes, BST varactors don't suffer from junction noise and provide a much higher capacitance density. Moreover, they can be operated with positive or negative control voltage [Kab01]. Besides the relatively high losses at room temperature, the requirement of an external DC control voltage chip and AC coupling capacitors is one of their significant drawbacks [Ven99, Gu15].

BST varactors in parallel-plate form (such as [Car12] and [Ngu12]) and in interdigital form ([Ram16]) have been widely used as tunable components. For

mobile communications, the BST tunable technology was firstly commercially implemented by Samsung in 2010, and the first closed-loop antenna was published by BlackBerry in 2013 [Hil16].

Besides varactor diodes and BST varactors, RF MEMS varactors based on the electromechanical movements of membranes can also be used as tunable capacitors. Similar to the BST varactors, parallel-plate form and interdigital form are their two basic configurations as well. Several tunable circuits using MEMS varactors in the parallel-plate form as tunable capacitors can be found in [Mad07, Nat11, Pag15]. Examples of the tunable devices consisting of MEMS varactors in the interdigital form have been presented in [Bor03, Cha11, Ion02]. For the commercial implementation of RF MEMS varactors as tunable components, tuners for handsets have been published in [Wis, Mor11, Cav].

Some important parameters of varactor diodes, BST varactors and RF MEMS varactors are compared and summarized in Table 3-2 [Luc10, Sin11, Wan09, Nat06]. The structure, tuning principle and the equivalent circuits of the above listed tunable capacitors are briefly introduced in the next subsections.

3.2.1 *Varactor Diodes*

In 1961, varactor diodes were developed [Bar61], which are controlled by a forward bias voltage. They are commonly used as switches while the reversely-biased varactor diodes operate as tunable capacitors. The structure of the varactor diodes is shown in Fig. 3-12 [Sal16]. The depletion region, where only ionized donors and acceptors are present, can be considered as an insulating dielectric. Unlike that for the hyperabrupt ones, the doping concentration of the acceptors and donors is nearly constant for abrupt varactors [Mot73]. Due to the fact that p- and n-regions are conductive, the varactor

diodes are treated as capacitors where, by varying U_{bias}, the width of the depletion region is variable and, consequently, the capacitor value of the varactor diodes can be modified [Pat08].

TABLE 3-2
PARAMETER COMPARISON OF VARACTOR DIODES, BST AND RF MEMS VARACTORS. REPRODUCED WITH PERMISSION FROM CAMBRIDGE UNIVERSITY PRESS, JOHN WILEY AND SONS, [LUC10, SIN11, WAN09, NAT06].

	Varactor diode	BST varactor	RF MEMS varactor
typical tunability (high Q-factor)	$2 - 3 : 1$	$2 - 3 : 1$	$< 1.5 : 1$
control voltage [V]	< 10	$< 5 - 30$	< 60
tuning time	$1 - 5$ ns	< 30 ns	> 5 μs
Q-factor	< 60	< 100	$80 - 200$
IP3 [dBm]	$15 - 25$	$35 - 55$	> 65
power handling	$\sim$ mW	$\sim$ mW	$1 - 2$ W
% temperature stability of capacitance (-30 to +70°C)	< 1	10	10
integration	dies	monolithic / hybrid	hybrid
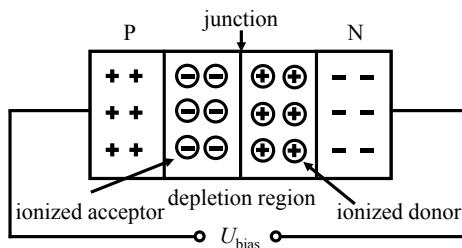
Fig. 3-12 Structure of a varactor diode [Sal16]. U_{bias}: bias voltage. Source – Salivahanan: Electronic Devices and Circuits, 4th Edition. Reproduced with permission from McGraw Hill Education (India) Pvt. Ltd.

The calculated value of the varactor capacitance C_j as a function of U_{bias} is

expressed as [Glo05]

$$C_j\left(U_{\text{bias}}\right) = \frac{C_{j0}}{\left(1 - \dfrac{U_{\text{bias}}}{\phi_0}\right)^{\gamma}} \, , \tag{3.1}$$

where C_{j0} is the capacitance for $U_{\text{bias}} = 0$. The value of build-in potential denoted by ϕ_0 is dependent on the semiconductor material, which is $\phi_0 = 0.7$ V for Si and $\phi_0 = 1.2$ V for GaAs [Pet14]. The value of γ is dependent on the type of the varactors. For an abrupt junction, the value of γ presented in (3.1) is $\gamma = 0.5$ while it is $1.15 \leq \gamma \leq 1.5$ for a hyperabrupt junction [Smi93]. According to (3.1), a brief comparison between capacitance variation of an abrupt and that of a hyperabrupt junction as a function of U_{bias} is shown in Fig. 3-13 [Swe07].
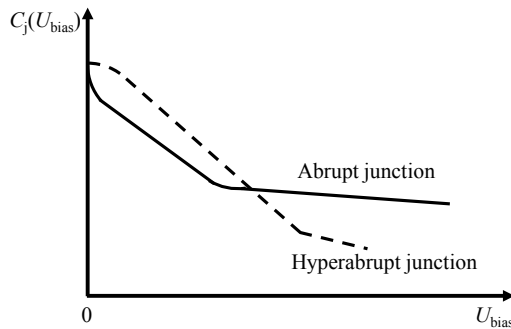
Fig. 3-13 A brief comparison between capacitance modification of an abrupt and that of a hyperabrupt junction as a function of U_{bias} [Swe07]. Reproduced by permission from Author Allen A. Sweet, *Designing Bipolar Transistor Radio Frequency Integrated Circuits*, Norwood, MA: Artech House, Inc., 2007. © 2007 by Artech House, Inc.

As can be seen in Fig. 3-13, the capacitance changes rapidly for the hyperabrupt junction, especially for the case when U_{bias} is low. As it is found that, hyperabrupt varactors are cheaper compared to abrupt ones, in mobile communications, where the control voltage is limited, the use of hyperabrupt

junction varactors is preferred.

Compared to silicon based varactor diodes, their GaAs counterparts have lower parasitic resistance and higher Q-factor [Wan09]. In addition to the cost, silicon varactor diodes show advantages over GaAs in other important parameters, such as PTD (parameter temperature diode), settling time, etc.

Fig. 3-14 shows capacitance-voltage curves for a number of silicon hyper-abrupt junction varactor diodes, namely, of type SMV123x with $x = 1, …, 7$, from the company Skyworks [Sky12]. These varactor diodes, which have a low resistance, are quite suitable for wireless communication requiring tunable capacitors controlled by a low DC voltage.
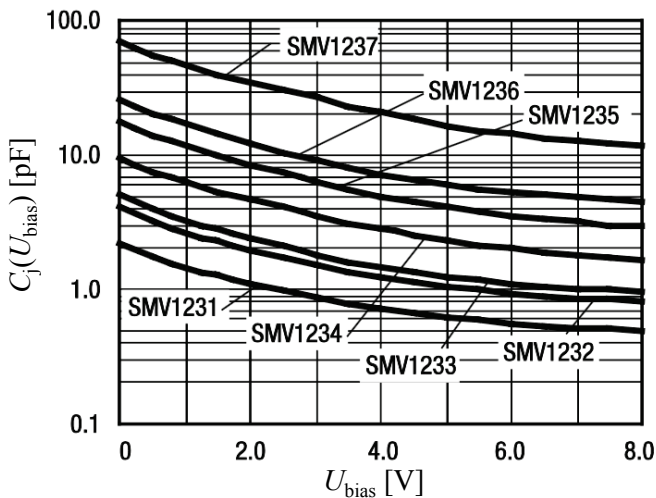
Fig. 3-14 Capacitance of SMV123x with $x = 1, …, 7$ as a function of U_{bias} [Sky12]. Reprinted by permission of ©2017 Skyworks Solutions, Inc. - All rights reserved.

Many equivalent circuits have been presented to model the electrical characteristics of varactor diodes [Rob01, Glo05, Ven05, Pet14]. One model of a packaged varactor diode is shown in Fig. 3-15(a) [Bah03, Pet14].
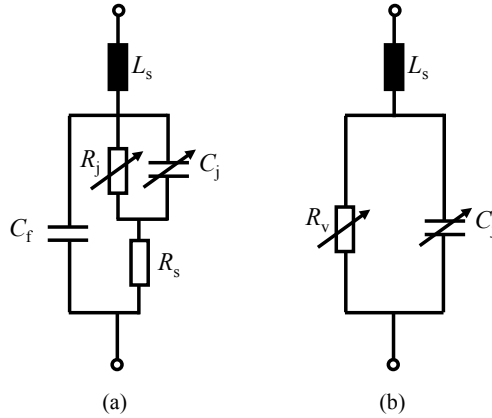
Fig. 3-15 An equivalent circuit model (a) and a simplified model (b) of varactor diodes. L_s, C_f and R_s: parasitic inductance, capacitance and ohmic losses. R_j: junction resistance. R_v: resistance of varactor model. Reproduced by permission from John Wiley and Sons and Artech House Inc [Bah03, Pet14].

R_j denotes the junction resistance, which is dependent on U_{bias}. L_s, C_f and R_s are the parasitic inductance, capacitance and ohmic losses associated with the packaging respectively. Since, for the investigated frequency range in this work, the parasitic effect can be neglected, the simplified equivalent circuit model presented in Fig. 3-15(b) is applicable [Bah03, Pet14], where R_v represents the U_{bias} dependent resistance in the simplified circuit model.

3.2.2   *BST varactors*

BST ($Ba_{1-x}Sr_xTiO_3$, where x varies from 0 to 1), invented in the 1950s, is also one of the most popular materials for RF varactors [Wan12]. It has a Perovskite atomic cell structure, which is shown in Fig. 3-16 [Sin11, Saa08, Wan12].

In this structure, Ti (titanium) is placed in the center, which is surrounded by Ba (barium) and Sr (strontium). By applying an external DC electric field, the relative position of Ti is displaced, which causes an electric polarization and

modifies the relative permittivity (ε_r) [Bau97, Tom02]. Using these properties, the capacitance of the BST varactors can be tuned [Gu15]. This displacement and the tunability are influenced by many factors, such as Ba/Sr ratio, temperature and residual strain in the BST film [Far07].
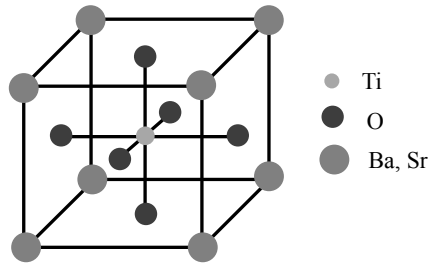

Fig. 3-16 Perovskite structure of BST. Reproduced by permission from John Wiley and Sons, Taylor & Francis Groups and Artech House Inc [Sin11, Saa08, Wan12].

Fig. 3-17 shows qualitatively the transition characteristics of BST material [Man05, Gev09]. According to the characteristics, BSTs can be either in the ferroelectric (polar) or in the paraelectric (non-polar) phase. They show ferroelectric properties, if the operation temperature (T) is below a certain transition temperature, which is called Curie temperature (T_c). Otherwise, they provide paraelectric properties.

In the ferroelectric phase, two equilibrium states of the spontaneous polarization ($+P_r$ and $-P_r$) are used to store binary information [Gev09], and the BSTs have a high tuning range of relative dielectric constant ε_r and, consequently, a large tuning range of the capacitance. However, since they suffer from large losses, for RF applications below 10 GHz, the BSTs in the paraelectric phase are mainly used [Gu15]. In order to achieve a sufficient tuning range in the paraelectric phase, the composite with Ba and Sr should be so optimized that T_c is below the temperature of operation where the BST still shows a relatively high ε_r [Wan12].
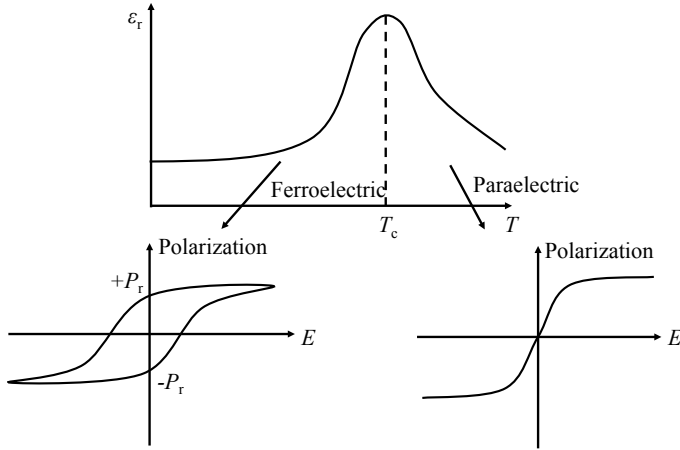
Fig. 3-17 Transition characteristics as tunable components. Reproduced by permission from Springer Science and Bus Media B V [Gev09].

Due to the field-dependent dielectric constant, the BST device capacitance C can be controlled by the bias voltage U_{bias}. A simple function to model the capacitance-voltage curve is expressed as [Wan12, Yor00]

$$C(U_{bias}) = C_{c,0} + C_{c,2}U_{bias}^2 , \qquad (3.2)$$

where $C_{c,0}$ and $C_{c,2}$ are the coefficients, whose values can be calculated by fitting (3.2) to the results of simulations or measurements. A more accurate empirical model is given by [Che04]

$$C(U_{bias}) = \frac{C_{c,1}}{\sqrt[3]{1 + \left(U_{bias} / U_{c,m} \right)^2}} . \qquad (3.3)$$

In this expression, $C_{c,1}$ and $U_{c,m}$ are the fitting parameters as well. In addition to the above two simple models, one including the influence of the geometry, film thickness and temperature is given in [Cha05].

If the thickness of the resultant BST film is less than 1 μm, it is considered as a BST thin film, which compared to the other BSTs, only requires a low tun-

ing voltage. This fact makes the BST thin film varactors quite suitable as tunable components for mobile communications [Nat06]. Interdigital form and parallel-plate form are two basic configurations of these thin-film varactors, see Fig. 3-18 [Gu15]. Compared to the parallel plate form, the interdigital form is easier to fabricate. However, the interdigital form exhibits two drawbacks, namely, low tunability due to the large fringing capacitance and relative high control voltage [Yor00].
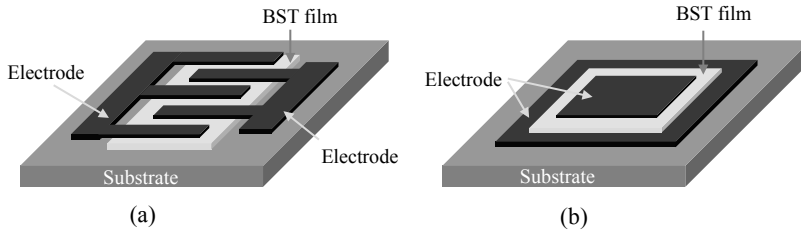

Fig. 3-18 Common configurations of BST thin-film varactors. (a) Interdigital form, (b) Parallel-plate form. Reproduced by permission from Springer Science and Bus Media B V [Gu15].

To model the electrical behavior of BST thin-film, equivalent circuits for the interdigital form and the parallel-plate form are presented in Fig. 3-19(a) and (b), respectively [Wan12, Jam04]. In Fig. 3-19(a), C_I and L_I are the voltage-dependent capacitance and the parasitic inductance of a typical BST in the interdigital form, while $R_{P,I}$ and $R_{ESR,I}$ denote the parasitic and equivalent series resistances. In Fig. 3-19(b), the series resistances ($R_{Top,P}$, $R_{Bot,P}$) and the inductances ($L_{Top,P}$, $L_{Bot,P}$) represent the influence of the top and the bottom plate in the parallel-plate form. C_p is the variable capacitance, which denotes the leakage current through the capacitor together with the conductance G_P.

3.2.3 *MEMS Tunable Capacitors*

RF MEMS varactors working at microwave frequencies have been demon-

strated since the 1990s [Lar91, Nat06]. Similar to BST varactors, two basic forms are used for building the MEMS varactors, which are parallel-plate and interdigital forms [Sha03]. The essential structure of the RF MEMS varactors in the parallel-plate form is shown in Fig. 3-9. They employ parallel plates, whose gap is changed by an induced electrostatic force. As a result, the variation of the capacitance value between the two parallel plates is effected by modifying the gap. Therefore, the DC control would be more complicated than that of the RF MEMS switches. The tuning range is defined as the ratio of capacitance with the minimum gap and that with the maximum gap [Gup13].
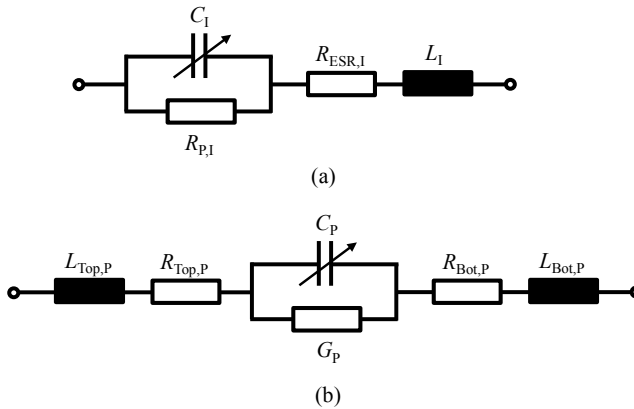
Fig. 3-19 Equivalent circuits of typical BST varactors. (a) Interdigital form, (b) Parallel-plate form. Fig. 3-19(a): Reproduced by permission from Artech House Inc [Wan12]. Fig. 3-19(b): Reproduced by permission from Taylor & Francis Groups [Jam04].

In the interdigital form, the capacitor plates (two combs) are placed in parallel horizontally, see Fig. 3-20 [Cor12]. In this device, one comb is stationary, and the other is horizontally moveable, thus, according to the electrostatic actuation, the overlapping area of both combs and, consequently, the capacitance value are variable. L_{RF} denotes an RF choke. The tuning range using this structure is limited by the length and the number of fingers of the combs.

In particular, the number of fingers, the actuation orientation, and the spring-constant of the movable structure can be freely chosen, which makes the design quite flexible [Reb03a].
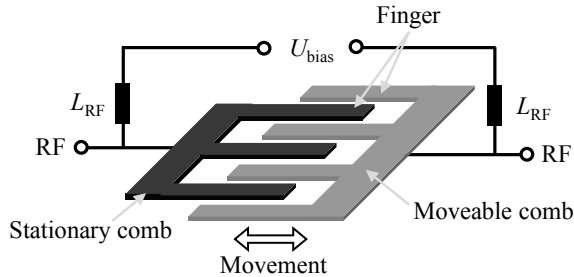

Fig. 3-20 Configuration of the RF MEMS varactors in the interdigital form. L_{RF} is the RF choke. Source: Baghelani, M., Ghavifekr, H. B., & Ebrahimi, A. (2012). RF-MEMS Components for Wireless Transceivers. In G. Cornetta, D. Santos, & J.Vazquez (Eds.), Wireless Radio-Frequency Standards and System Design: Advanced Techniques (p. 177). Hershey, PA: Copyright, IGI Global.Reprint by permission [Cor12].

Besides the above described three tunable capacitors, mechanical varactors and liquid crystal varactors would also be options. However, the large size and weight as well as the low tuning speed limit the applications of mechanical tuning [Gev09]. These mechanical varactors are, thus, amenable for applications such as trimmer capacitors [Vol] and are mostly used in tunable filter banks and frequency-agile devices [Nat06]. The liquid crystal varactors exploit the anisotropy of the molecules adjusted by applying an external DC voltage to tune their permittivity [Jak04]. Although their loss is low, some drawbacks such as very low speed (> 10 ms), narrow temperature range, necessity of proper sealing and high cost make them not favorite to be tunable elements of networks for mobile terminal antennas [Mar15, Gev09, Jak04].

In general, in order to achieve a large tuning range and a high tuning resolution, a bank of tunable RF components, instead of a series combination of switches to fixed capacitors, can also be used. Several commercial capacitor

arrays consisting of MEMS tunable capacitors haven been published. One digitally-controlled capacitor array presented by WiSpry, is able to provide a tunability 7 : 1 and a high Q-factor of 160 [Wis]. On the other hand, an antenna tuner presented by Cavendish Kinetics has a large tuning range and a high Q-factor over 200 [Cav]. Two disadvantages of this structure would be large chip area and complicated controlling systems.

According to the above discussion, no approach for tunable RF capacitance is optimal as tunable RF components for wireless communications. The suitable tuning components should be, therefore, chosen according to the concrete application. Due to the fact that the investigation of tunable decoupling and matching concepts for compact multi-element antennas is the main focus of this work, silicon hyperabrupt junction varactor diodes SMV123x with $x = 1, \ldots, 7$, which can be simply implemented with a low control voltage, are exploited in the next chapters as a representation of commonly used tunable components of DMNs for studying and evaluating the design concepts.

Chapter 4

Investigation of Tunable Matching Networks

[2]As discussed in Chapter 2, the predefined threshold values for decoupling and matching should be achieved by using DMNs. If the couplings between all the antenna elements of some arrays in the context of simultaneous matching are still less than the coupling threshold, then, according to the initial estimate, they need not be necessarily compensated. Therefore, for the single-element and such weakly-coupled multi-element antennas, only tunable matching circuits need to be designed.

The matching criterion used in this work is to keep the input reflection coefficient Γ_{IN} at the RF front-end below $|S_{ma,thres}|$ in the usage scenarios. Based on this matching approach, the tunable impedance matching network including the parasitic effects of impedance detector and ESD protection is as seen in Fig. 4-1, where Γ_S and Γ_L represent the source and load reflection coefficients, respectively, with respect to Z_0. L_{DET} and L_{ESD} are coils taking into account the effect of the detector and the ESD protection. In this topology, the trans-

---

[2] The following chapter uses textual materials and figures from [Che14] and [Che15] © 2017 *IEEE* and copyright *EurAAP*; used with permission.

ceiver front-end is assumed to have an input impedance equal to $50\ \Omega$, i.e. $\Gamma_S = 0$ and, because the antenna impedance Z_A under the effects of user interaction is uncertain, Γ_L cannot be pre-estimated.
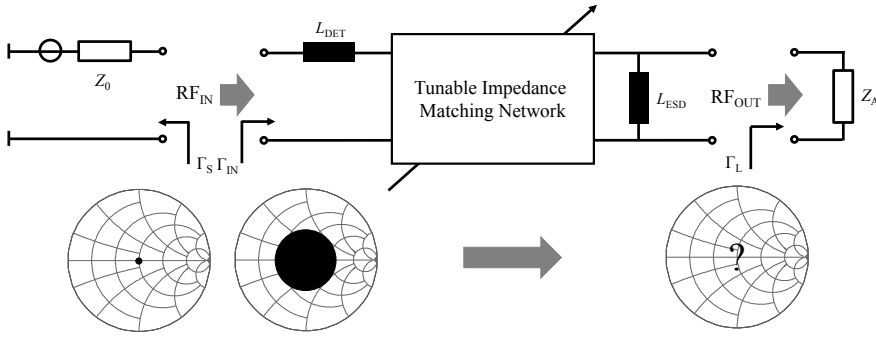

Fig. 4-1 Visualization of the proposed impedance matching networks. L_{DET} and L_{ESD} are coils taking into account the effect of the detector and the ESD protection.

Several tunable matching networks within adaptive matching systems have been designed and published in the last few years (e.g. [Ida04, Ram12]), nevertheless, the frequency reconfigurability of these matching networks is limited. In order to compensate the unpredictable antenna impedance mismatch, it is important to design a tunable matching network maintaining a good tunability in the usage scenarios and providing the frequency reconfigurability of the antenna operation band over the frequency range of application.

This chapter consists of three main parts for presenting the design concept of a suitable tunable matching network. First, it starts with the investigation of possible *LC* configurations of matching components over the frequency range. Second, it engages in optimizing the network structure to achieve a good tunability, which can be implemented as an example to study the effect on the compensation of the antenna impedance mismatch. And third, the implementation and evaluation of such a tunable matching network are presented. Based on this knowledge, suitable compact antennas for a good antenna

matching system to mitigate the impact of the impedance mismatch in the usage scenarios can be determined, which is discussed in the next chapter.

4.1 Equivalent Reactance for *LC* Configurations

To realize the tunability of matching networks, it is important to find out the suitable tunable components for the pertinent frequencies within the application range. Theoretically, a lumped-element tunable matching network can be realized using inductors or/and capacitors having adaptive reactance values. Due to the fact that no practical tunable inductors are available, the variation of the inductance is usually realized through a parallel or series connection of a fixed inductor and a tunable capacitor [Gu11]. For describing the reactance variation of such combinations, either an equivalent inductance or an equivalent capacitance can be used. For the case of an inductor L and a tunable capacitor C in parallel, the equivalent inductance L_{ep} and the equivalent capacitance C_{ep} at the angular frequency ω are given by

$$L_{\mathrm{ep}} = \frac{L}{1-\omega^2 LC} \ \ (\text{if } 1-\omega^2 LC > 0) , \tag{4.1}$$

and

$$C_{\mathrm{ep}} = \frac{\omega^2 LC - 1}{\omega^2 L} \ \ (\text{if } 1-\omega^2 LC < 0) . \tag{4.2}$$

The equivalent inductance L_{es} and the equivalent capacitance C_{es} for representing L and C in series at the angular frequency ω are given by

$$L_{es} = \frac{\omega^2 LC - 1}{\omega^2 C} \ \ (\text{if } 1-\omega^2 LC < 0) , \tag{4.3}$$

and

$$C_{es} = \frac{C}{1 - \omega^2 LC} \quad (\text{if } 1 - \omega^2 LC > 0). \tag{4.4}$$

It is observed from (4.1) that, because of the $0 < \omega^2 LC < 1$ condition, the value of L_{ep} is larger than that of the fixed inductor L. On the other hand, according to (4.3), the reactance value of L_{es} cannot exceed that of L. Similarly, the tuning range of the equivalent capacitance in both topologies (C_{es} and C_{ep}) can also be determined. These observations suggest that variation range of the equivalent inductance and the equivalent capacitance may be realized by exploiting a suitable tunable LC topology.

Suppose now that C_{min} and C_{max} are set to be the minimum and maximum tuning value of a tunable capacitor, and assume that the tuning range of its capacitance is $C_{min} = 0.5 \leq C \, [\text{pF}] \leq 5 = C_{max}$, and the possible fixed value of the inductor L is set to $L = 5$ nH. Then, the equivalent inductance and capacitance for L and C in parallel and series settings as a function of the frequency of operation f is calculated and depicted in Fig. 4-2.

As shown in Fig. 4-2, the equivalent inductance and the equivalent capacitance of the LC configuration can be modified by varying the tunable capacitor C combined with the fixed inductor L. Furthermore, within a certain frequency range, not only the equivalent inductance but also the equivalent capacitance can be realized at the same operating frequency through the capacitor tuning. This duality increases the tunability of the matching. To maintain the duality, the range of the operating frequency f is given by

$$\frac{1}{2\pi\sqrt{LC_{max}}} \leq f \leq \frac{1}{2\pi\sqrt{LC_{min}}}. \tag{4.5}$$
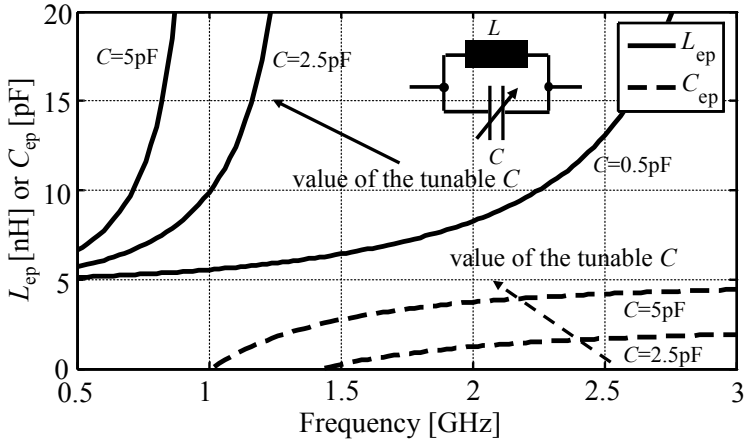
(a)
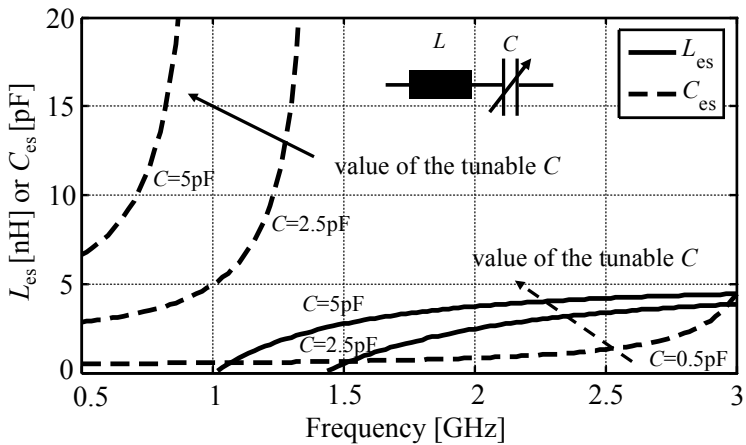
(b)

Fig. 4-2 The frequency dependent variation of the equivalent inductance and the equivalent capacitance for representing $L = 5$ nH and $0.5 \leq C$ [pF] ≤ 5 in parallel (a) and in series (b). Reproduced with permission from © 2015 *IEEE* [Che15].

For the case in which $L = 5$ nH and $0.5 \leq C$ [pF] ≤ 5, the frequency range of the duality is $1.00 \leq f$ [GHz] ≤ 3.18, which coincides with the results shown in Fig. 4-2. Increasing the value of the fixed inductor L from 1 nH to 9 nH

59

and maintaining the tuning range of C, the frequency range of the duality is varied from $2.25 \leq f\,[\text{GHz}] \leq 7.12$ to $0.75 \leq f\,[\text{GHz}] \leq 2.27$. Therefore, the equivalent reactance can be quite flexibly selected for a broad bandwidth, which covers most of the investigated frequency range $0.69 \leq f\,[\text{GHz}] \leq 2.7$. Moreover, the losses of realistic inductors within this range of values are limited by requiring a high Q-factor of the components. Usually, the Q-factor is reduced as the reactance value of realistic inductors increases. As a result, the fixed inductor value is set to be within the value range of $1 \leq L[\text{nH}] \leq 9$, and the tunable capacitor with the value range $0.5 \leq C\,[\text{pF}] \leq 5$ is used for calculation.

4.2 Design of a Π-section based Tunable Matching Network

Each matching circuit can transform a certain area of antenna impedances on the Smith-chart to compensate the mismatch to the reference impedance. It is known that at least a suitable two-element matching network can compensate a finite antenna impedance mismatch having a nonzero realistic part at a single frequency point. Compared to the two-element matching networks, the matching networks with three elements such as T and Π structures provide a broader matchable impedance region. Therefore, in this investigation, an antenna matching network with the Π structure is chosen.

When the electrical influence of the ESD protection and impedance detector shown in Fig. 4-1 is added, the general topology of a tunable impedance matching network with Π structure is depicted in Fig. 4-3.

The capacitor C_3 having the tunable range $0.5 \leq C_3\,[\text{pF}] \leq 5$, which is placed parallel to L_{ESD}, works as a tuning component. The values of L_{DET} and

L_{ESD} are $L_{DET} = 2.7$ nH and $L_{ESD} = 15$ nH, respectively. The topology of each of the tunable blocks Z_1 and Z_2 can be a single tunable capacitor C or can be composed of the tunable capacitor C in parallel/series to a fixed inductor L. To restrict the losses present in realistic inductors, the possible values of fixed inductors in series (L_s) and in parallel to the capacitor (L_p) are respectively limited to $1 \leq L_s \, [\text{nH}] \leq 5$ and $5 \leq L_p \, [\text{nH}] \leq 9$ in the design phase. Based on these preconditions, the optimal topology of Z_1 and Z_2 is determined.
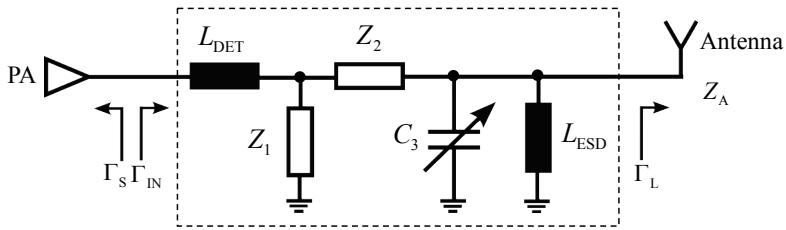
Fig. 4-3 General schematic of a tunable matching network with Π structure containing Z_1 and Z_2 blocks (dashed line surrounded structure). Reproduced with permission from © 2015 *IEEE* [Che15].

For performing an accurate evaluation of the tunablilty, the whole variety of antenna impedances Z_A in usage scenarios must be considered. Due to the unpredictable impedance behavior resulting from user interaction, the antenna impedance can be located arbitrarily on the Smith-chart. Therefore, these possible Z_A are assumed to be uniformly distributed across the whole Smith-chart. For investigation, which is done by a Monte Carlo simulation, the number of the whole possible Z_A is set to be 1500. Because of the predefined antenna impedance matching criterion $|S_{ma,thres}| = -6$ dB, the matching network should be able to reach $|\Gamma_{IN}| \leq -6$ dB for the maximum possible amount N_m of antenna impedances from these 1500 impedances. The ratio of N_m to the whole 1500 investigated antenna impedances is defined as the success rate of the impedance matching.

In a typical case, the impedance mismatch would, on average, be better compensated when located within a frequency band than when located at the boundary frequencies. Hence, for searching the optimal topology of Z_1 and Z_2 in the worst case, the tunability of the matching networks at the four boundary frequencies of the low-band and high-band is studied. At this stage, the individual reactive components are considered to be ideal, and the values of the tunable capacitors are optimized for each one of the 1500 impedances at a time. Fig. 4-4 lists the average success rate using the presented Π-section containing lossless RF components with the different settings of Z_1 and Z_2 at the boundary frequencies of the low-band and the high-band. The settings highlighted with the thick black line provide at least 80% probability of success for an arbitrary antenna impedance to achieve the matching criterion in both bands. These include the settings with Z_1 being an inductor L_{p1} parallel to a tunable capacitor and the Z_2 comprising an inductor L_{s2} in series to a tunable capacitor. The possible values of the fixed inductors L_{p1} and L_{s2} are limited to $7 \leq L_{p1}$ [nH] ≤ 9 and $2.5 \leq L_{s2}$ [nH] ≤ 5.

In addition to the lossless case, the average success rate using the Π-section network having realistic RF components (inductors having a $Q = 50$ and capacitors with a constant resistance of 0.3 Ω) with the different settings of Z_1 and Z_2 at the boundary frequencies of both bands is investigated as well, see Fig. 4-5. Due to the losses of the RF components, some power is dissipated in the network, which reduces the amplitude of the input reflection coefficient $|\Gamma_{IN}|$. Hence, the threshold value of the high success rate in the realistic case should increase compared to the lossless case, which is set to 85%. Although the investigation includes the influence of component losses for the realistic case, the highlighted settings are quite similar to those in the lossless case shown in Fig. 4-4.

Moreover, due to the resonance behavior, *LC*-series configurations at Z_1 and/or *LC*-parallel configuration at Z_2 would create stopband frequencies, which limit the tunability of matching circuits. Hence, some topologies such as with Z_1 and Z_2 in *LC*-series configurations are not chosen, although they would also provide a quite acceptable average success rate according to Fig. 4-4 and Fig. 4-5.
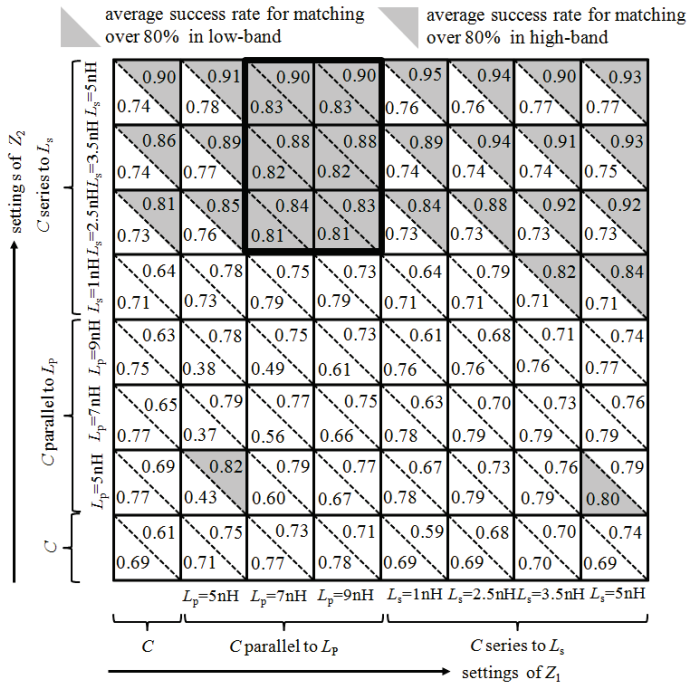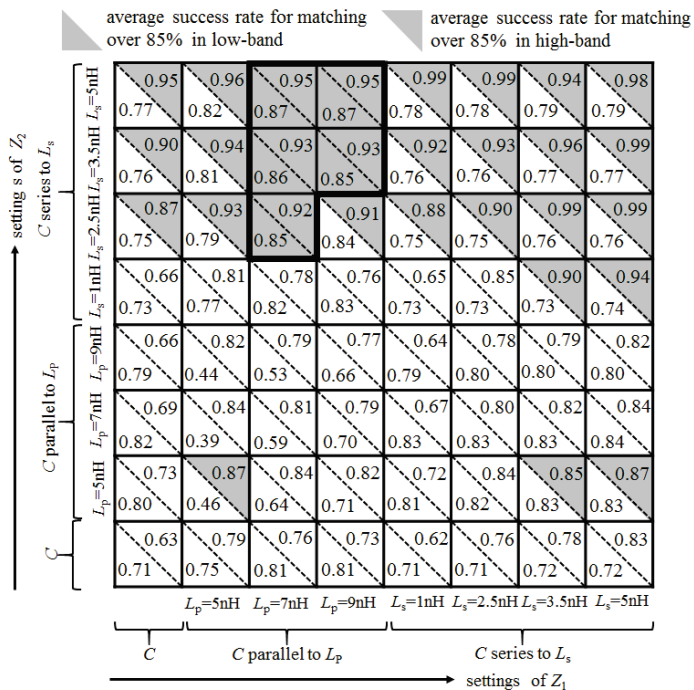

Fig. 4-4 Average success rate using different settings of Z_1 and Z_2 for fulfilling the matching criterion in low- and high-band with the matching topology shown in Fig. 4-3 using lossless RF components. Thick black line surrounded settings: the average success rate is at least 80% in both bands. Reproduced with permission from © 2015 *IEEE* [Che15].

Due to the fact that the effective value of a real inductor normally increases with the operating frequency, the fixed inductor values are selected from the lower end of the recommended ranges. Thus, an inductor with $L_{p1} = 7$ nH parallel to a tunable capacitor and an inductor with $L_{s2} = 2.5$ nH in series to a

tunable capacitor are chosen as the combinations for the tunable topology of Z_1 and Z_2. The corresponding tunable impedance matching network is shown in Fig. 4-6. In this topology, C_1, C_2 and C_3 are the tunable capacitors.

Fig. 4-5 Average success rate using different settings of Z_1 and Z_2 for fulfilling the matching criterion in low- and high-band with the matching topology shown in Fig. 4-3 in the realistic case. Thick black line surrounded settings: the average success rate is at least 85% in both bands.
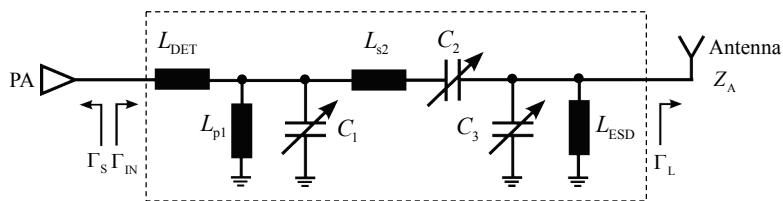
Fig. 4-6 Topology of the tunable antenna matching network (dashed line surrounded structure) for a good tunability. L_{DET} and L_{ESD} represent the inductance of the impedance detector and the ESD calculation. Reproduced with permission from © 2015 *IEEE* [Che15]. Taken from [Che14]; copyright *EurAAP*; used with permission.

Using the final topology of the tunable antenna matching network as shown in Fig. 4-6, the magnitude of the achievable input reflection coefficient $|\Gamma_{IN}|$ using lossless components is calculated as a function of the arbitrary antenna impedance Z_A at the low-band and high-band boundary frequencies. The average values of $|\Gamma_{IN}|$ for each antenna impedance at the boundary frequencies of each band are then presented on the Smith-chart in Fig. 4-7. Each point on the Smith-chart represents a possible antenna impedance, normalized to Z_0. The inside of the white dash-dot circles denote the antenna impedances, which would fulfill the -6 dB matching criterion without implementing a matching network. The areas inside the white contours represent impedances, which could be matched to $|\Gamma_{IN}|$ = -6 dB or better on average using the presented impedance matching network, are defined as highly matchable areas.
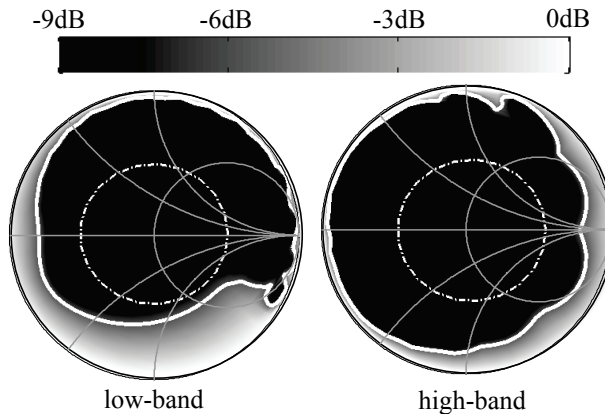

Fig. 4-7 Average achievable input reflection coefficient at the boundary frequencies of the low-band ($0.69 \leq f$ [GHz] ≤ 0.96, left) and high-band ($1.71 \leq f$ [GHz] ≤ 2.7, right), represented on the Smith-chart for different Z_A. White solid line surrounded area: average reflection coefficient better than $|\Gamma_{IN}|$ = -6 dB at the boundary frequencies of each band using the presented matching network. White dash-dot circle: $|\Gamma_{IN}|$ = -6 dB without matching. Reproduced with permission from © 2015 *IEEE* [Che15].

To investigate the power transfer from RF front-end to the antenna by minimizing $|\Gamma_{IN}|$ using commercial RF components, this matching network pre-

sented in Fig. 4-6 can be considered as a two-port network terminated by Z_0 as the source and the antenna impedance as the load termination (or vice versa). The whole antenna matching system as a hybrid system consists of three calculation- or measurement-based blocks (RF frond-end, with/without matching network and the mobile terminal antenna), as shown in Fig. 4-8. This hybrid system is analyzed with or without the tuning of the matching circuit.
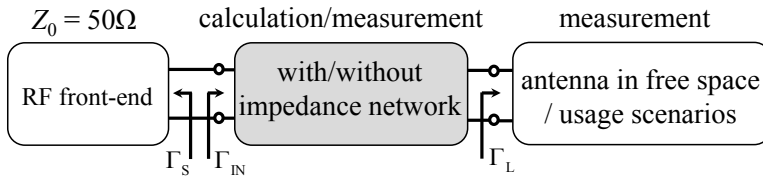

Fig. 4-8 Structure of the hybrid system for evaluating the antenna matching system. Taken from [Che14]; copyright *EurAAP*; used with permission.

In this case, the varactor diodes SMV1233, SMV1234 and SMV1233 are used for representing the tunable capacitors C_1, C_2 and C_3 shown in Fig. 4-6, respectively. The values of the fixed inductors L_{p1} and L_{s2} are chosen from Murata's chip inductor selection LQW15AN and LQW18AN [Mur]. Their values are $L_{p1} = 7.5$ nH and $L_{s2} = 2.7$ nH, respectively, which are the closest values available corresponding the recommended values (7 nH and 2.5 nH) showing in Fig. 4-4 and Fig. 4-5. The values of the other inductors $L_{DET} = 2.7$ nH and $L_{ESD} = 15$ nH are also modeled with Murata inductors. The PSPICE (personal computer simulation program with integrated circuit emphasis) of these RF components including the realistic losses is employed for simulating the realistic tunability of the matching network, so that the power dissipation of the tuning circuit can be included in the calculation. In this case, the tunability of the chosen matching network can be studied through calculating the transducer gain (G_T), which is defined as [Gil03]

$$G_{\mathrm{T}} = \frac{\text{power delivered to the load}}{\text{power avaiable from matched source}}$$

$$= \frac{(1 - |\Gamma_{\mathrm{S}}|^2) |S_{\mathrm{M},21}|^2 (1 - |\Gamma_{\mathrm{L}}|^2)}{\left| (1 - S_{\mathrm{M},11}\Gamma_{\mathrm{S}})(1 - S_{\mathrm{M},22}\Gamma_{\mathrm{L}}) - S_{\mathrm{M},12}S_{\mathrm{M},21}\Gamma_{\mathrm{S}}\Gamma_{\mathrm{L}} \right|^2}. \tag{4.6}$$

$S_{\mathrm{M},mn}$ with m, $n = 1$, 2, are the S-parameters of the matching network normalized to Z_0 in one operation state. The transducer gain G_{T} of each tuning is calculated by varying the values of these three tunable varactors to minimize $|\Gamma_{\mathrm{IN}}|$ for the antenna impedance. According to (4.6), $G_{\mathrm{T}} = $ -1.25 dB corresponds to 6 dB return loss in the lossless case. To study the realistic matching capability on the antenna impedances at the boundary frequencies of the low- and high-bands using the realistic tunable Π-section matching network, G_{T} of the hybrid system is calculated as a function of the arbitrary antenna imped-ance Z_{A} and is presented on the Smith-chart in Fig. 4-9. It is seen that the matching network is also able to provide a large matchable area ($G_{\mathrm{T}} \geq$ -1.25 dB) using realistic RF components.

As described above, the design of presented matching network is based on the assumption that the unpredictable antenna impedances in usage scenarios are uniformly distributed across the whole Smith-chart. To compensate the impact caused by the realistic user interaction, a more accurate network de-sign would be based on the experimental study [All11, Hua07].
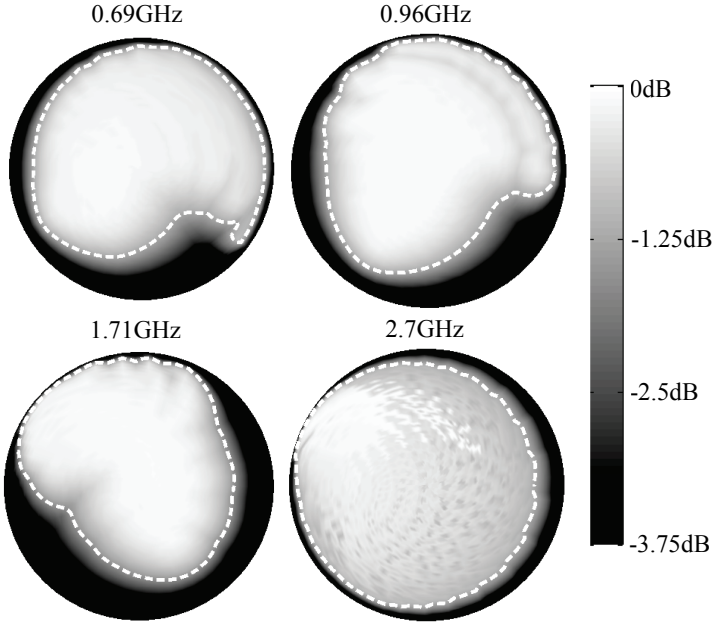
Fig. 4-9 Transducer gain (G_T) at the boundary frequencies of the low- and high-bands. White dashed line surrounded areas: $G_T \geq$ -1.25 dB using the tunable matching network.

4.3 Experimental Evaluation of the Π-section based Matching Network Circuit

In order to confirm the capability of the tunable matching network, the tunability of the matching network shown in Fig. 4-6 is evaluated. The layout of the matching circuit, depicted in Fig. 4-10, is designed.

In Fig. 4-10, C_{DC1} and C_{DC2} are DC blocking capacitors. L_{RF} denotes a RF choke related to the biasing circuit of the varactors. The capacitances of the varactors can be modified by changing the three DC control voltages U_{DC1}, U_{DC2} and U_{DC3}. The DC voltages applied across these three varactors (U_{C1}, U_{C2} and U_{C3}) are: $U_{C1} = U_{DC1}$, $U_{C2} = U_{DC1} - U_{DC2}$, $U_{C3} = U_{DC3}$. In this case,

68

U_{DC2} could be negative and should not be larger than U_{DC1}. Hence, the sign of the U_{DC2} is designed to be switched in this feeding system, which is supplied by 12 V batteries. As a result, the tunable ranges of the voltage applied across the varactors are $0V \leq U_{DC1}$, $U_{DC3} \leq 12$ V, 0 V $\leq U_{DC2} \leq 15$ V.
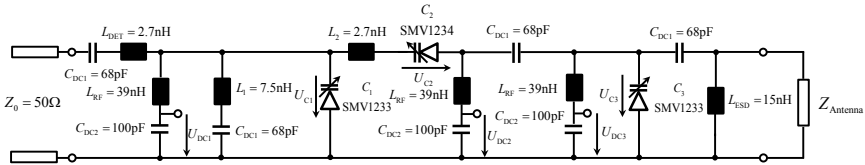

Fig. 4-10 Layout of the antenna matching circuit. C_{DC1}, C_{DC2} are DC blocking capacitors and L_{RF} denotes a RF choke related to the biasing circuit of the varactors. Reproduced with permission from © 2015 *IEEE* [Che15]. Taken from [Che14]; copyright *Eur-AAP*; used with permission.

A prototype of the tunable matching circuit based on the exemplary circuit model presented in Fig. 4-10 is fabricated, and is shown in Fig. 4-11.
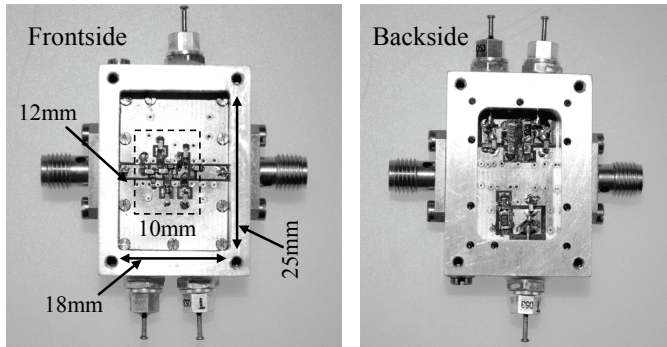

Fig. 4-11 A picture of the Π-section based tunable antenna matching circuit based on the commercial RF-components.

In addition to measuring it, the matching circuit is simulated in the ADS simulator [Ads]. The simulation results should represent the measurements accurately in order to allow a precise study of the effect of the antenna matching networks on the antenna impedance via simulations. To prove this accuracy,

the evaluation is performed through a comparison between the simulated and the measured S-parameters of the matching network connected with Z_0 at both sides in different tuning states. The fabricated matching network as well as the simulated one is tuned with identical DC control voltage in order to check the agreement.

Two comparisons as examples are selected. The combination of the three control voltages in the first comparison is $U_{DC1} = U_{DC2} = U_{DC3} = 0$ V, and that in the second one is $U_{DC1} = U_{DC3} = 5$ V, $U_{DC2} = 1$ V. The capacitance-voltage curve for the used varactors can be found in Fig. 3-14. The results of these two biasing states, which are shown in Fig. 4-12 and Fig. 4-13 respectively, are matched quite well in the low-band.

The differences between the measurement and the simulation in the high-band are mainly caused by the discrete (non-integrated) matching circuit, in particular, the non-embedded matching circuit itself. Furthermore, the losses of the RF-components (especially the Murata inductors) are drastically increased at higher frequencies and change the tunability as well.

In the next chapter, the presented tunable impedance matching network is exploited for founding out suitable compact mobile terminal antennas in usage scenarios to provide the reconfigurability of the operation band over the investigated frequency range.
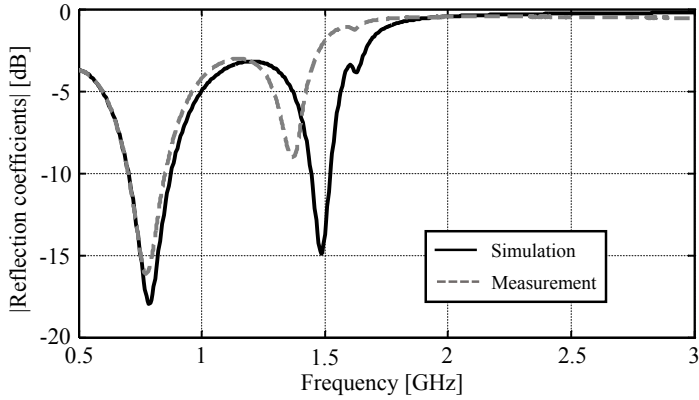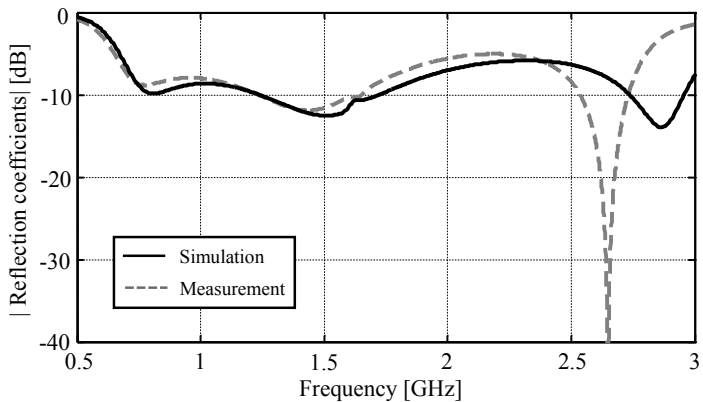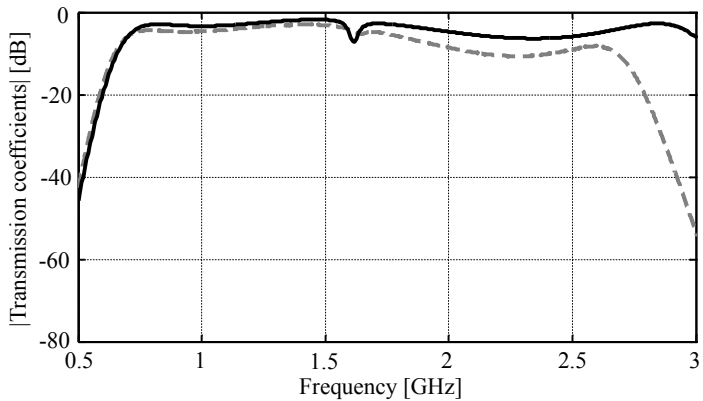
(a)
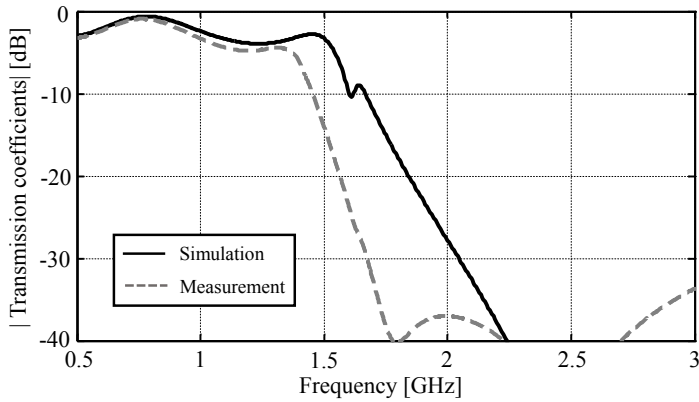
(b)

Fig. 4-12 S-parameter comparison between the simulation and measurement results for $U_{DC1} = U_{DC2} = U_{DC3} = 0$ V. (a): reflection coefficients. (b): transmission coefficients.

(a)

(b)

Fig. 4-13 S-parameter comparison between the simulation and measurement results for $U_{DC1} = U_{DC3} = 5$ V and $U_{DC2} = 1$ V. (a): reflection coefficients. (b): transmission coefficients.

Chapter 5

Appropriate Generic and Compact Mobile Terminal Antennas in Usage Scenarios

[3]Tunable impedance matching networks for compensating the impedance mismatch of compact mobile terminal antennas in usage scenarios are one of the focuses of this work. In Chapter 4, a design concept of tunable matching networks with a good tunability has already been studied. By implementing the presented matching network as a good representation to study the matching effect on the antenna impedances over the investigated frequency range, appropriate generic and small-sized antennas need to be studied.

In this chapter, a concept for compact antennas having appropriate impedance behavior combined with a tunable matching network is presented to achieve an antenna having a reconfigurable band of operation with a good total efficiency over a broad frequency range in typical usage scenarios. In Section 5.1, the total efficiency of an intrinsically broadband matched mobile terminal antenna is measured as a benchmark. Then, to shrink the antenna form factor,

---

[3] The following chapter uses textual materials and figures from [Che14], [Mar14] and [Che15] © 2017 *IEEE* and copyright EurAAP; used with permission.

the tunability of an antenna matching system containing a compact multi-band matched antenna is evaluated in Section 5.2. Such an antenna matching system is not able to provide sufficient frequency tunability of the operation band. Hence, in Section 5.3, antennas with a small-sized antenna form factor having a suitable impedance behavior are studied. The tunability of such an antenna combined with tunable matching networks in the common usage scenarios is then evaluated and compared to that of the other mock-up systems.

5.1 Applicability Evaluation of Intrinsically Matched Antennas

Traditional mobile terminal antennas are usually self-resonant at their operating frequencies. These resonances are created due to the geometry and dimensions of antenna element and chassis, which provide sufficient impedance match without additional matching circuits [Val13b]. In order to achieve a broadband matching and, consequently, a good total efficiency over a large frequency range, these intrinsically matched antennas are usually implemented. A dual-broadband monopole type antenna is chosen as an example. The entire prototype of the dual-broadband antenna is depicted in Fig. 5-1(a). The exploded view of its excitation part (structure demarcated by the dashed line in Fig. 5-1(a)) is presented in Fig. 5-1(b). The prototype of the antenna is realized using a 1.5 mm thick FR4 PCB enclosed by a plastic housing with 1 mm thickness. The material of the housing is PVC (polyvinyl chloride) ($\varepsilon_r = 2.91$, $\tan(\delta) = 0.025$) with the outer dimensions $133 \times 68 \times 8$ mm^3.

The measured magnitude of the load reflection coefficient Γ_L due impedance mismatch of the antenna in free space is illustrated in Fig. 5-2. Using the in-

herently matched antenna, the matching criterion is satisfied in almost the whole frequency band containing the low-band and the high-band. Hence, this antenna can be considered as an inherently broadband matched mobile terminal antenna. However, in order to achieve the broadband matching, the form factor of this antenna is quite large [Mcl96, Row12], which is shown in the Fig. 5-1(b).
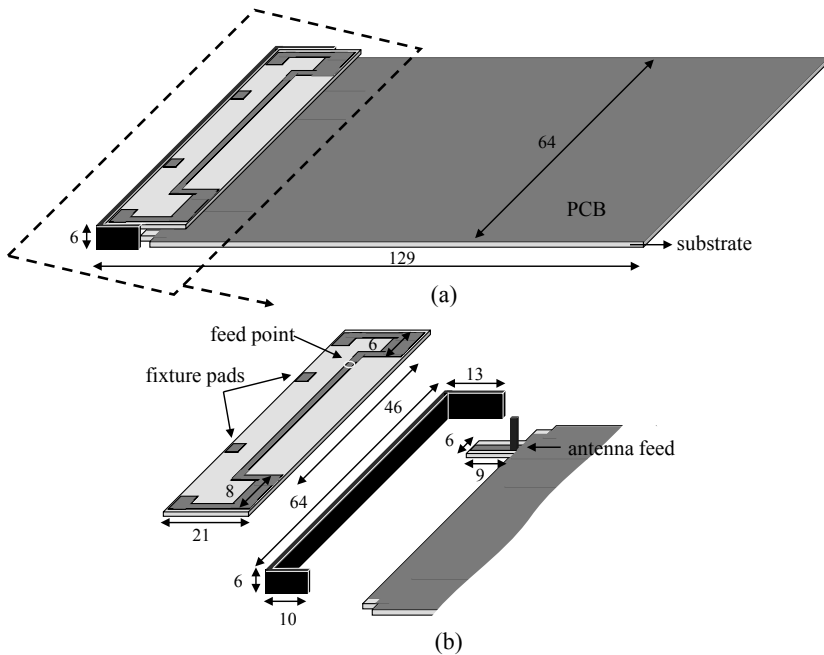

Fig. 5-1 The entire prototype (a) and the exploded excitation part (b) of the dual-broadband monopole type antenna. Dimensions are in mm. Reproduced with permission from © 2015 *IEEE* [Che15].

It is known that the user interaction conditions during operation commonly modify the electromagnetic near fields of handset antennas. Hence, the antenna impedance is also measured in the presence of head and hand (right) phantoms from the company SPEAG [Spe]. The test configurations include the data mode (hand only) and the talking mode (head + hand) according to

the CTIA (cellular telephone industries association) standard [Cti]. The variation of the antenna impedance due to the user effect is presented in Fig. 5-2. It is seen that the antenna impedance is detuned under the influence of user proximity, and therefore the matching criterion cannot be kept for the broadband matched antenna in the whole low-band.
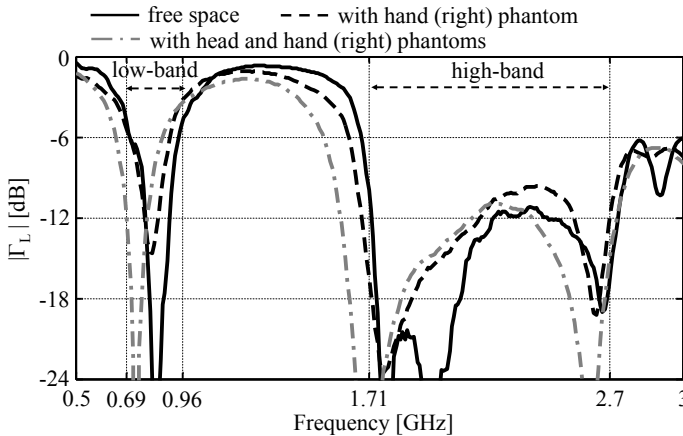

Fig. 5-2 The measured load reflection coefficient ($|\Gamma_L|$) of the broadband matched antenna in usage scenarios. Reproduced with permission from © 2015 *IEEE* [Che15].

The measurements of the total efficiency η_{tot} are carried out in free space and with the predefined user interaction, whose results are shown in Fig. 5-3. This antenna prototype provides a good total efficiency, without the user, especially in the high-band. The results including the user interaction are significantly lower, but are quite well comparable with other results reported in the literature [Guo13, Gar13, Zha13]. In the low-band, the efficiency is additionally degraded because of the impedance detuning mentioned above.

Although the presented intrinsically broadband matched antenna shows good results, one should aim for a smaller form factor. Also the degradation of the total efficiency due to impedance mismatch caused by the user is undesired.

The investigation as to what extent both of these issues can be compensated by an adaptive antenna system containing a small-sized radiating element while maintaining comparable total efficiency over the band of operation in usage scenarios is in order.
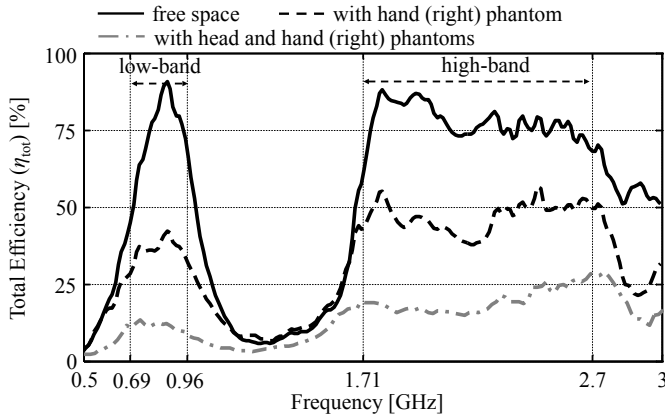

Fig. 5-3 Measured total efficiency (η_{tot}) of the broadband matched antenna in usage scenarios in linear scale. Reproduced with permission from © 2015 *IEEE* [Che15].

5.2 Applicability Evaluation of Antenna Matching System Containing Compact Multi-Resonant Antennas

When shrinking the size of the coupling element, the matching created by the antenna geometry cannot cover the whole frequency range [Mcl96, Row12]. Therefore, one possible method is to combine external tunable matching networks for adapting a band of operation over a wide frequency range. For achieving this purpose, several requirements on the impedance of the compact antennas should be fulfilled. Firstly, to compensate the antenna impedance mismatch as a result of user interaction, the whole impedance trace of the antennas should be kept within the highly matchable area of the tunable matching network. And secondly, the reconfigurability over the whole inves-

tigated frequency range should be realized in a simple way.

Compared to the inherently broadband matched antenna, the initial matching of the antennas with a reduced antenna form factor created by their geometry might cover at most several bands of operation, each with limited bandwidth. To evaluate the tunability under user interaction of such inherently multi-band matched antennas, a PIFA, which is inherently matched in the E-UTRA (evolved UMTS terrestrial radio access) band 20, 2 and 40 in free space, is designed. In order to make a fair comparison, the platform (PCB, housing) of the PIFA has the same terminal size and predefined location as those of the broadband matched one, except for the excitation part. The drawing of the PIFA is presented in Fig. 5-4. Its antenna form factor is only about one-fourth that of the inherently broadband matched antenna shown in Fig. 5-1.
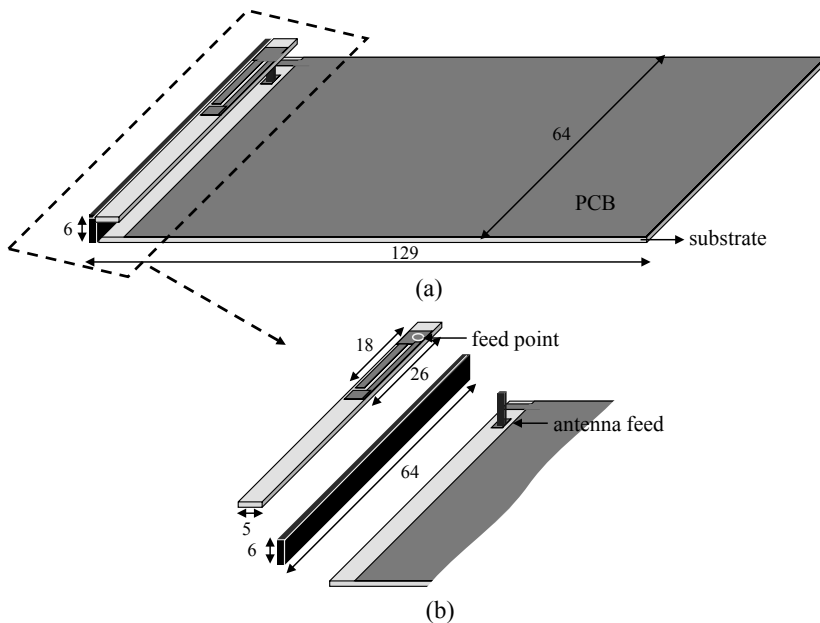
Fig. 5-4 The entire prototype (a) and exploded excitation part (b) of the PIFA. Dimensions are in mm.

5.2.1 *Study of the Impedance Matching under the Influence of User Interaction*

The measured impedance behavior of the PIFA in free space in the low- and the high-band is shown on the Smith-chart in Fig. 5-5. Except for some in the low-band, most of the input impedances in free space are located within the highly matchable area of the tunable network presented in Fig. 4-6, which is beneficial for compensating the impedance mismatch at each single frequency point of interest.
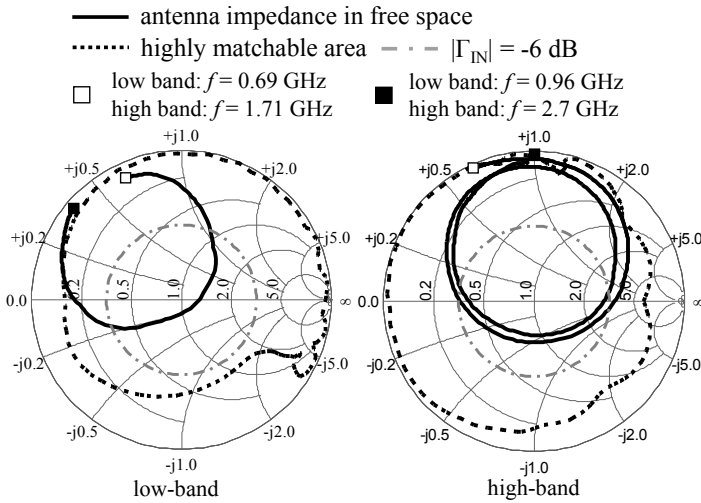

Fig. 5-5 The free-space antenna impedances of the PIFA in the low-band $(0.69 \leq f\,[\text{GHz}] \leq 0.96$, left) and the high-band $(1.71 \leq f\,[\text{GHz}] \leq 2.7$, right).

To study the impedance variation in usage scenarios, the antenna impedance is also measured with the CTIA hand and head phantoms, see results in Fig. 5-6. Although the antenna impedance is detuned, due to user interaction, the antenna impedance at most of the frequencies still is remained within the highly matchable region, which ensures a high success rate of impedance matching using the tunable matching network.

5.2.2 *Investigation of the Frequency Reconfigurability of the Antenna Band*

In addition to a high ability for compensating the impedance mismatch at each single frequency within the frequency range in the usage scenario, the capability of adapting the band of operation of the antenna over the whole investigated frequency range is expected as well.
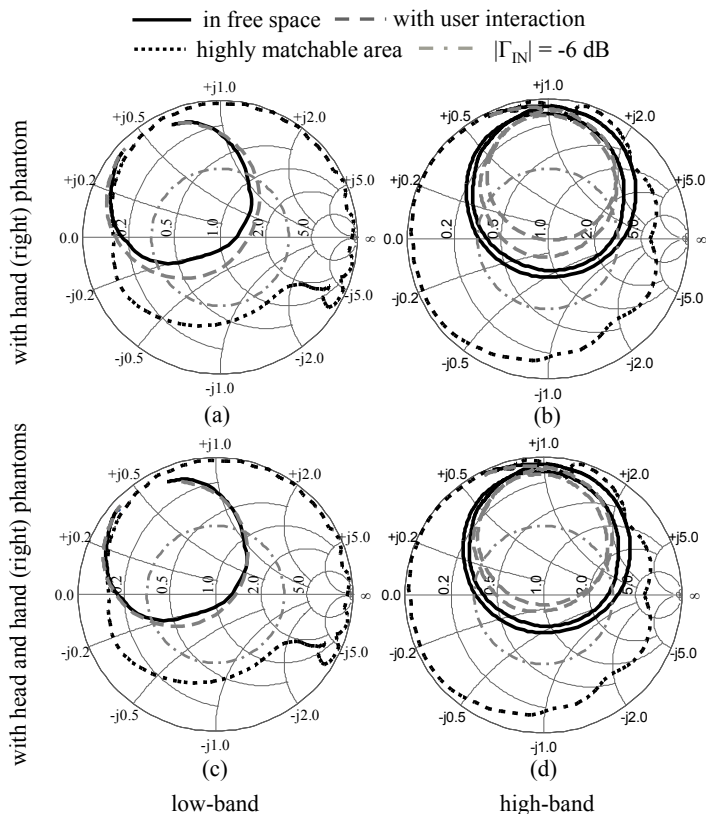

Fig. 5-6 Measured impedance of the PIFA in the predefined usage scenarios in low-band (a, c) and in high-band (b, d). (a, b) with hand (right) phantom, (c, d) with head and hand (right) phantoms.

To evaluate the antenna matching system within the frequency range, 9 an-

tenna operation bands containing 8 E-UTRA bands and the 2.45 GHz WLAN (wireless local area network) band, which cover most of the low- and high-band, are selected as bands of operation. The target of the proposed PIFA combined with the tuning circuit is to provide $G_T \geq$ -1.25 dB for each selected antenna band of operation in the realistic case. Based on the optimized capacitance of the varactors for each communication band, the calculated transducer gains for the PIFA in free space are shown in Fig. 5-7.

Fig. 5-7   Calculated transducer gain (G_T) for the PIFA without (grey dashed lines) and with (black solid lines) the proposed matching network in free space. n = 1, 2, 3, …: E-UTRA operating band n. WL: WLAN.

Except in the inherently matched operation bands (E-UTRA band 20, 2 and 40), the transducer gain of the PIFA combined with the matching network is higher than that provided by just the antenna itself. However, the threshold value G_T = - 1.25 dB can still not be reached across the whole band. One reason for that is the dissipated power absorbed by the network due to component losses, and another is the high variation of the antenna impedance Z_A over the investigated frequency range, which is shown in Fig. 5-8.
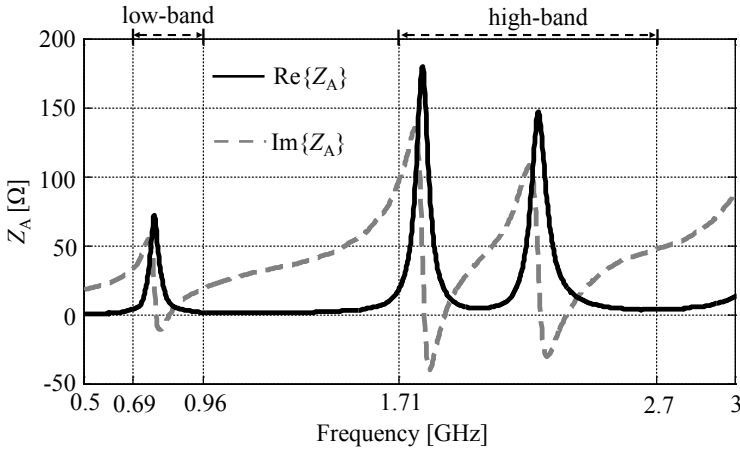
Fig. 5-8 Antenna impedance Z_A of the PIFA in free space.

Due to the fact that the required value of the tunable components is a function of the antenna impedance, the impedance mismatch can be compensated perfectly only at one single frequency point. If the antenna impedance is sensitive to the frequency variation over the whole frequency range, then these required component values for matching at frequency points within each band of operation would also have a strong frequency-dependence. As a result, the bandwidth maintaining a good impedance matching of each tuning is limited for such antennas. Moreover, due to the limited tuning range of realistic tunable elements, a low frequency variation of the required component values would be beneficial for their utilization over a broad frequency range.

To study the tunability of the antenna matching system including the PIFA under user interaction, the transducer gain is calculated in this case as well, see Fig. 5-9
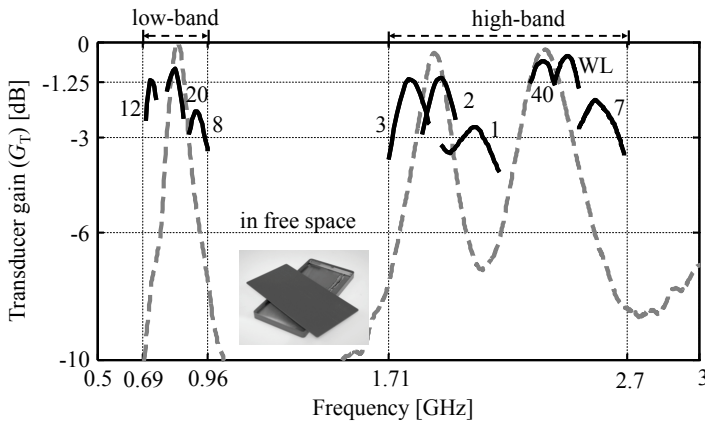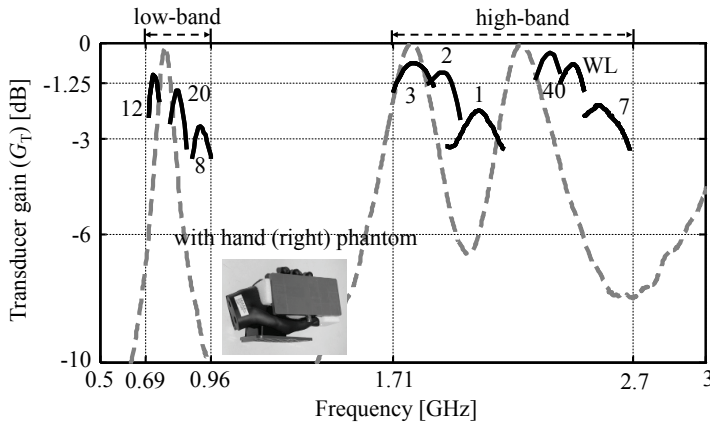
(a)
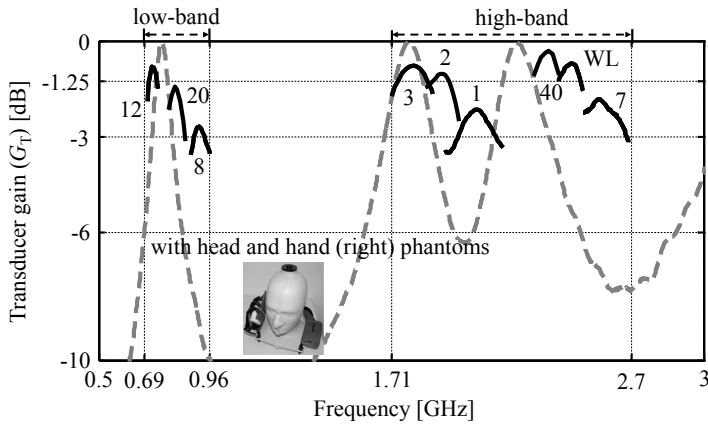
(b)

Fig. 5-9 The calculated transducer gain (G_T) of the PIFA without (grey dashed lines) and with (black solid lines) the proposed matching network. $n = 1, 2, 3, …$: E-UTRA operating band n. (a) with hand (right) phantom, (b) with head and hand (right) phantom.

As presented in Fig. 5-6, the antenna impedance under the effect of usage scenarios still shows a quite strong frequency variation. Hence, similar to the results in free space, although the antenna system is able to enhance the
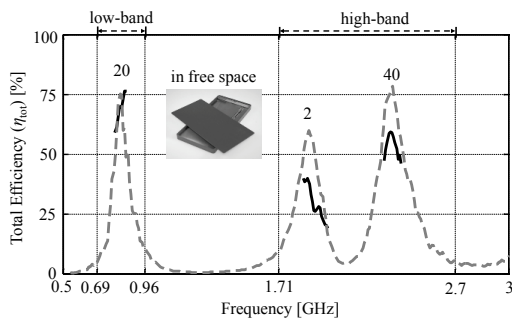
transducer gain compared to the case without employing the matching network, the threshold $G_T \geq$ - 1.25 dB cannot be reached in most cases across the whole band of operation because of the high frequency-dependent antenna impedance behavior. Thus, it is desired that the antenna impedance can be always located within the highly matchable area of the tunable matching network and shows a low frequency-dependence for keeping a good tunability over the whole frequency range.

Due to the fact that the transducer gain in the inherently matched bands of the PIFA (E-UTRA band 20, 2 and 40) is better than that in most of the other operating bands, the total efficiency of the mock-up system with the tunable matching circuit in these inherently matched bands is measured as some of the best cases. First, the varactors of the network are tuned to implement the impedance matching across each desired E-UTRA band in a separate measurement. Then, the full 3D radiation pattern of the antenna is measured in an anechoic chamber, and the total radiated power is normalized against a known reference antenna. The measurement results are shown in Fig. 5-10.

Although the multi-resonant antennas occupy a smaller antenna form factor, the mock-up system is not able to provide a similar total efficiency even in these inherently matched bands as that of the inherently broadband matched one. Therefore, suitable antennas with a small antenna form factor still have to be found out, so that a frequency reconfigurable band with a good total efficiency can be provided by employing tunable matching networks in both bands.

(a)

(b)

(c)

Fig. 5-10 Measured total efficiency (η_{tot}) of the mock-up-system containing PIFA without
(gray dashed lines) and with (black solid lines) the matching network in linear
scale. $n = 1, 2, 3, \ldots$: E-UTRA operating band n. (a) in free space, (b) with hand
(right) phantom, (c) with head and hand (right) phantoms.

5.3 Applicability Evaluation of Antenna Matching System Containing Compact Inherently Unmatched Antennas

Besides the inherently multi-band matched antennas, another compact mobile terminal antenna candidate to achieve the frequency reconfigurable matching over the whole frequency range is CCE (capacitive coupling element). It is a type of coupling element antenna due to its capacitive excitation [Vil06, Val10, Hol10a]. Unlike that of the inherently matched antennas, the geometry structure of these coupling elements is typically quite small, simple and generic, which by itself is not able to create impedance matching at the operating frequencies. Hence, for such an inherently unmatched antenna, an external impedance matching network is necessary [Val12, Val13b]. Except for the capacitive reactance part of the antenna impedance at frequencies, whose corresponding wavelength is much greater than the antenna size, the variation of the impedance of these antennas over the whole frequency range is typically quite low [Val13b]. This impedance behaviour is called low frequency-dependent.

Moreover, the body of the user, when closes to the antenna radiating element, has a greater impact on the antenna detuning than that closes to the antenna chassis [Boy07, Hua07, Hol10b]. It would be beneficial, therefore, to mitigate the user interaction by having a small antenna form factor and placing the antenna radiating element in a location infrequently approached during operation [Boy07]. Compared to the common inherently matched mobile terminal antennas, the simple structure of the inherently unmatched antennas would provide more degrees of freedom for the antenna design to reduce the

impact of the user interaction.

To evaluate the tunability of such an antenna combined with the tunable matching network shown in Fig. 4-6 over the whole frequency range, an inherently broadband unmatched coupling element antenna having low frequency-dependent impedance behavior is designed as an example. Its structure is identical to that of the PIFA presented in Fig. 5-4, except in the geometry of the excitation part. The drawing of its structure is shown in Fig. 5-11.
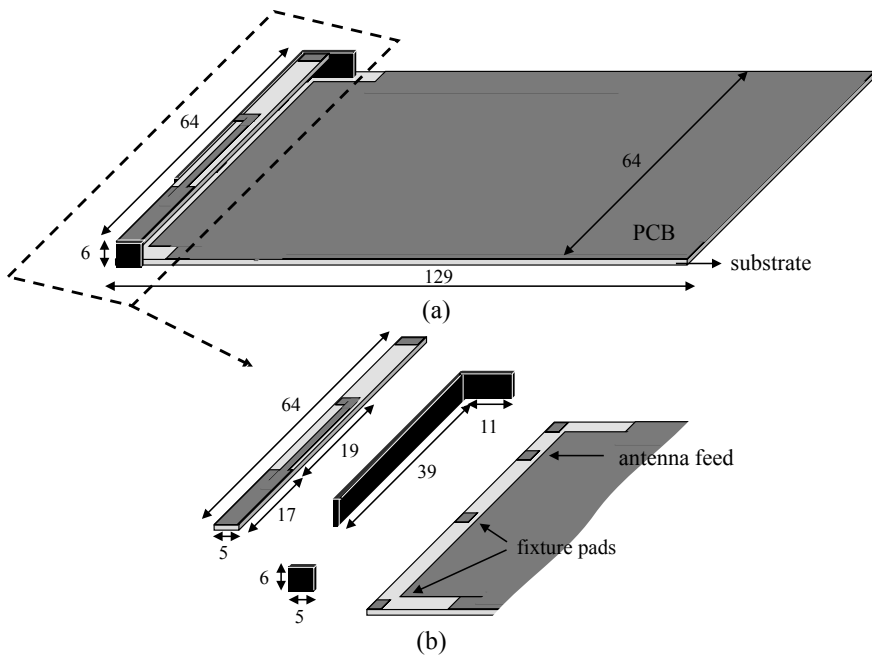
Fig. 5-11 The entire prototype (a) and exploded excitation part (b) of the designed inherently unmatched antenna. Dimensions are in mm. Reproduced with permission from © 2015 *IEEE* [Che15].

5.3.1   *Study of the Impedance Matching under the Influence of User Interaction*

Most of the antenna impedances of the designed inherently broadband un-

matched antenna in free-space in the low- and high-band, which is presented in Fig. 5-12, are within in the highly matchable area of the matching network. This fact guarantees the success rate of impedance matching.
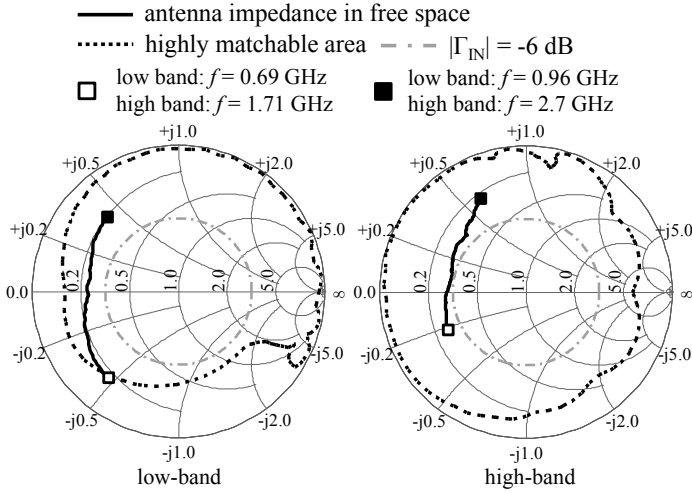
Fig. 5-12 The free-space antenna impedances of the intrinsically broadband unmatched antenna in the low-band $(0.69 \leq f \, [\mathrm{GHz}] \leq 0.96$, left) and the high-band $(1.71 \leq f \, [\mathrm{GHz}] \leq 2.7$, right). Reproduced with permission from © 2015 *IEEE* [Che15].

The antenna impedance is also measured with the CTIA hand and head phantoms to study the impedance modification under user interaction. The measurement results depicted in Fig. 5-13 show that this antenna impedance is very robust against user interaction, so that the impedance of the antenna still remains within the matchable region of the matching network. This relatively good stability against the impact of the user has also been reported in other publications [Ilv11, Ilv14a, Val11, Val12].
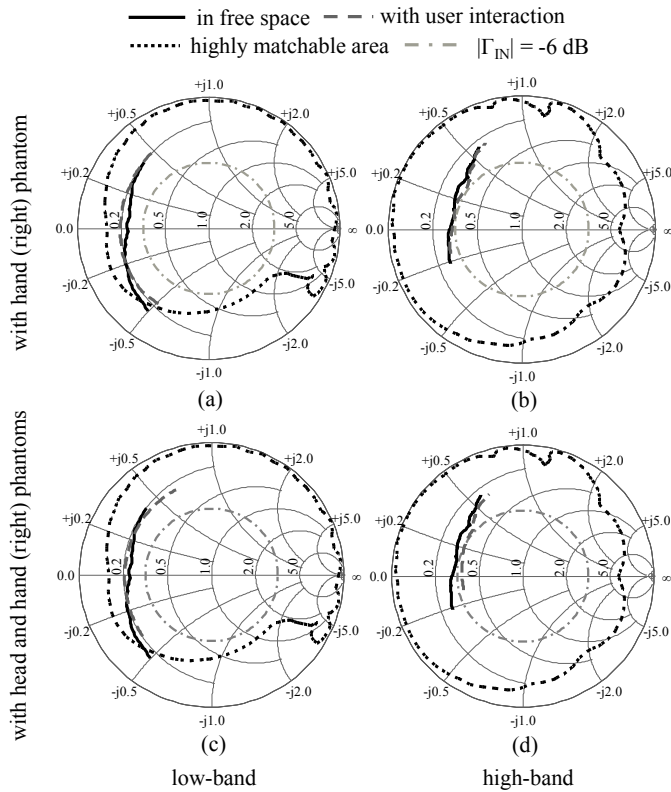
Fig. 5-13   The measured impedance of the inherently broadband unmatched antenna in the predefined usage scenarios in low-band (a,c) and in high-band (b,d). (a,b) with hand (right) phantom, (c,d) with head and hand (right) phantoms. Reproduced with permission from © 2015 *IEEE* [Che15].

5.3.2   *Investigation of the Frequency Reconfigurability of the Antenna Band*

It is shown in Fig. 5-12 and Fig. 5-13 that the impedance of the inherently broadband unmatched antenna is insensitive to frequency variation and user interaction. Hence, the required tunable component values at the frequencies within a band of operation typically don't have a large deviation. This property would be quite advantageous to keep a good impedance matching across

the whole frequency reconfigurable band.

As an evaluation, the transducer gain for the inherently unmatched antenna presented in Fig. 5-11 with and without employing the matching network in free space and under user interaction in the realistic case is calculated using (4.6), and the results are shown in Fig. 5-14 and Fig. 5-15, respectively. Compared to the case without the matching network, the transducer gain of the antenna combined with the matching circuit is strongly improved. In particular, the threshold value $G_T = -1.25$ dB can be reached for the whole bands in almost all of the matching cases.
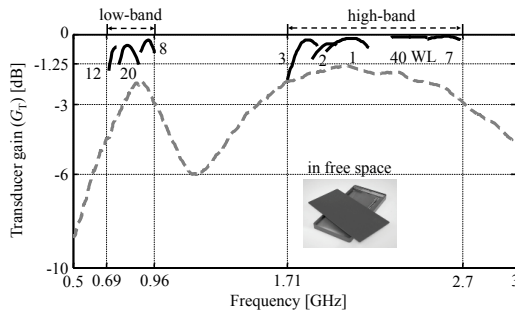
Fig. 5-14 The calculated transducer gain (G_T) for the inherently broadband unmatched antenna without (grey dashed lines) and with (black solid lines) the proposed matching network in free space. n = 1, 2, 3, …: E-UTRA operating band n. WL: WLAN. Reproduced with permission from © 2015 *IEEE* [Che15]. Taken from [Che14]; copyright *EurAAP*; used with permission.

In addition to the calculation of the transducer gain, the total efficiency of the fabricated mock-up-system containing the inherently broadband unmatched antenna and the tunable matching circuit, which is shown in Fig. 5-16, is also measured in each band of operation in the predefined usage scenarios, see Fig. 5-17.
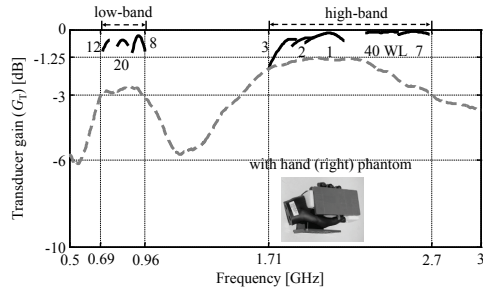
(a)
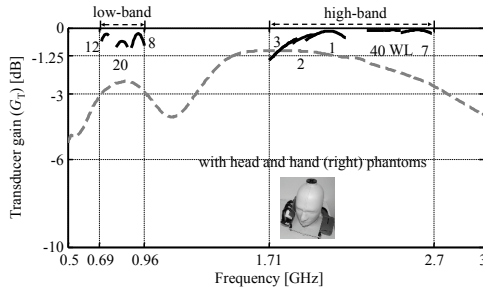
(b)

Fig. 5-15 The calculated transducer gain (G_T) for the inherently broadband unmatched antenna without (grey dashed lines) and with (black solid lines) the proposed matching network. $n = 1, 2, 3, \ldots$: E-UTRA operating band n. WL: WLAN. (a) with hand (right) phantom, (b) with head and hand (right) phantom. Reproduced with permission from © 2015 *IEEE* [Che15]. Taken from [Che14]; copyright *EurAAP*; used with permission.
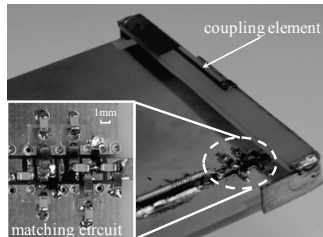
Fig. 5-16 A picture of the fabricated mock-up-system containing the inherently broadband unmatched antenna and the tunable matching circuit. Reproduced with permission from © 2015 *IEEE* [Che15]. Taken from [Che14]; copyright *EurAAP*; used with permission.
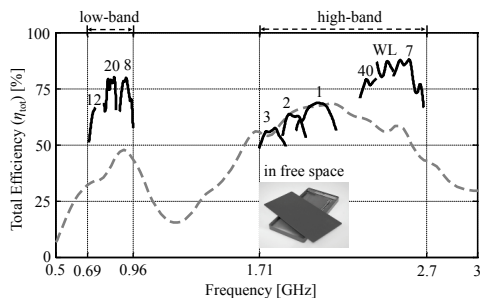
(a)
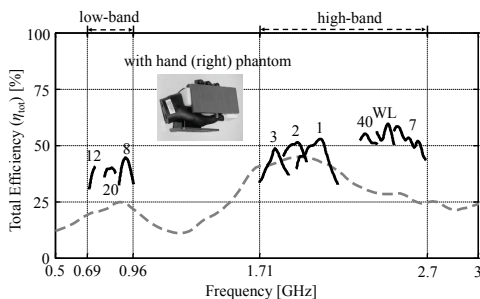
(b)
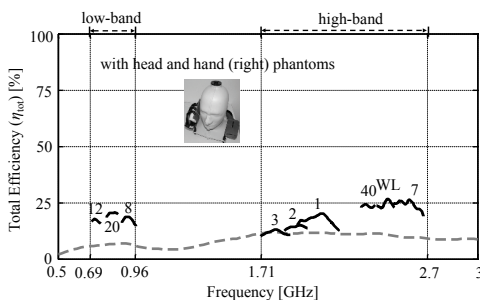
(c)

Fig. 5-17 Measured total efficiency (η_{tot}) of the mock-up-system containing the inherently broadband unmatched antenna without (gray dashed lines) and with (black solid lines) the presented matching network in linear scale. $n = 1, 2, 3, \ldots$: E-UTRA operating band n. WL: WLAN. (a) in free space, (b) with hand (right) phantom, (c) with head and hand (right) phantoms. Reproduced with permission from © 2015 *IEEE* [Che15]. Taken from [Che14]; copyright *EurAAP*; used with permission.

The measurement results show that a frequency-reconfigurable band with a good total efficiency over the investigated frequency range can be achieved using the inherently broadband unmatched coupling element combined with the tunable matching circuit. The broadband matched antenna without matching network provides a similar value, on average in usage scenarios shown in Fig. 5-3. However, this antenna suffers from impedance mismatch especially in the low-band and the large antenna form factor, which is about four times larger than that of the inherently broadband unmatched one.

Although a multi-band matched antenna has the same compact antenna form factor, a strong impedance deviation over the investigated frequency range is typically unavoidable. Hence, the band of operation of an antenna matching system containing such an antenna cannot be tuned to enable sufficient power transfer, as characterized by total efficiency and transducer gain over a wide frequency range. As a result, the combination of tunable matching networks and inherently broadband unmatched coupling element antenna having a weak frequency-dependent impedance behavior supports the broadband flexibility of the impedance control.

To have a deeper understanding of the antenna matching system containing the inherently broadband unmatched antenna, the power dissipation distribution is analyzed. In particular, the power dissipation over the E-UTRA operating band 20 in the presence of the head and hand (right) phantoms is calculated as an example. The radiated power of the whole mock-up system is estimated through the measurement of the total efficiency. The other parts of the dissipated power are either reflected due to the impedance mismatch or absorbed by the phantoms (head and hand) and by reason of the material losses of the plastic housing, the tunable matching network, etc. The mis-

match losses are calculated through the measurement of the input reflection coefficient, whereas the analysis of the other losses is based on the difference between the power accepted by the antenna and the radiated power. The proportions between dissipative losses are based on measurements in the predefined scenarios, under the assumption that the current distribution of the antenna is not remarkably altered. The ratio of the calculated dissipated power to the input power in percentage form is shown in Table 5-1.

TABLE 5-1

THE POWER DISSIPATION OF THE MOCK-UP-SYSTEM WITH AND WITHOUT THE MATCHING NETWORK IN THE BAND E-UTRA 20 IN THE PRESENCE OF THE HEAD AND HAND (RIGHT) PHANTOMS REPRODUCED WITH PERMISSION FROM 2015 © *IEEE* [CHE15].

power dissipation	without matching network	with matching network
radiated power	6% - 7%	18% - 20%
mismatch losses	45% - 47%	3% - 9%
material losses	11% - 20%	15% - 23%
hand losses	14% - 17%	27% - 35%
head losses	14% - 18%	23% - 30%

As expected, using the matching network results in low mismatch losses and consequently enhances the power transfer to the antenna, and therefore the total efficiency is improved. On the other hand, the improvement of the radiation results in increased power absorption in the head and hand phantoms. The increment of the power dissipation due to the material losses is mainly caused by the matching network. Hence, one possible method to reduce this part of the losses calls for some other tuning components having lower losses such as RF-MEMS-based devices instead of varactor diodes, which would consequently enhance the total efficiency according to (2.2).

If the decoupling of multi-element antennas is unavoidable, suitable decoupling and matching networks are necessary. In this case, the presented matching concept combined with a suitable decoupling approach based on the initial estimate, which is shown in the next chapter, could be employed.

5. Appropriate Generic and Compact Mobile Terminal Antennas in Usage Scenarios

Chapter 6

Investigation of Decoupling and Matching Networks for Multi-Element Antennas

[4]If some or all the mutual couplings between the multi-element antennas are not negligible, a decoupling approach should be included as an extension of the tunable matching concept presented. According to the flowchart shown in Fig. 2-8, the design of DMN is proceed as follows.

For all the antenna couplings ($S_{\text{A},mn}$ with $m \neq n$), which should be compensated according to the initial estimate, the values of their corresponding coupling coefficients of $\mathbf{S^{AD}}$ ($S_{\text{AD},mn}$ with $m \neq n$) in (2.4) need to become zero in linear scale at the target frequencies with the help of a suitable decoupling network. The values of the network components can be computed from these simultaneous equations at each frequency point. By substituting these component values into (2.4), the other uncompensated coupling coefficients of $\mathbf{S^{AD}}$ are calculated. If not all of them can reach $|S_{\text{dc,thres}}|$, the decoupling network should be redesigned to eliminate more antenna couplings, and the value of all the $|S_{\text{AD},mn}|$ with $m \neq n$ is also necessarily to be rechecked. This itera-

---

[4] The following chapter uses textual materials and figures from [Che17] © 2017 *IEEE*.

tion should be repeated until the compensation of all the couplings is achieved.

After implementing the DN, the consequent matching stage is based on $\mathbf{S}^{AD}$. The matching circuits can be designed either based on the reflection coefficients individually, or according to the simultaneous conjugate complex matching through the renormalization of $\mathbf{S}^{AD}$. To mimic the couplings between the RF front-ends in the worst case after the matching stage, the latter is selected. For renormalization, the reference impedances assigned to P_{N+n} ($Z_{R,n}$), with $n = 1, \ldots, N$, are so optimized that the reflection coefficients of the renormalized $\mathbf{S}^{AD}$ are minimized. In the lossless case, the amplitude of the elements of $\mathbf{S}^{ADM}$ is identical to that of the renormalized $\mathbf{S}^{AD}$. Hence, if the amplitude values of coupling coefficients of the renormalized $\mathbf{S}^{AD}$ are not all below the decoupling threshold, the compensation of some antenna couplings, which might be unnecessary according to the initial estimate, should be considered. In this case, the iteration needs also to be repeated until the off-diagonal elements of $|\mathbf{S}^{ADM}|$ are all less than $|S_{dc,thres}|$.

As a result, according to the initial estimate introduced in Section 2.3, some branches of the decoupling network might be omitted to simplify its structure. Such a structure of the DN needs to be designed. Moreover, due to the frequency-dependent S-matrix $\mathbf{S}^A$ of the antenna, some components of DMNs are made tunable to enable the operation over a wide frequency range. Since DMNs in each tuned state only provide a limited bandwidth at a time, and the value of realistic tunable components has a limited tuning range, the achievable bandwidth of each state should be discussed as well. Therefore, this chapter is organized as follows. In Section 6.1, a design concept for decoupling structures based on the initial estimate is illustrated. This is then evaluated by

decoupling and matching for several generic antenna matrices. In Section 6.2, the achievable bandwidth in each tuned state is explored based on simulations of tunable decoupling and matching for a generic three-element antenna system on a mobile terminal as an example.

6.1 Investigation of a Suitable Decoupling Network

To simplify the network complexity for an antenna with a total of N antenna elements, the decoupling network (demarcated by the dashed square shown in Fig. 2-7) is firstly designed, before implementing matching networks, to compensate only the antenna couplings, which need to be decoupled according to the initial estimate. If these couplings only exist between two out of N antenna elements i.e. $K = 2$, a suitable decoupling network is shown in Fig. 6-1(a). For $K = 3$, two decoupling networks are available. If not all the couplings between the three elements should be counteracted such as example 2 shown in Table 2-1, a structure for this case is presented in Fig. 6-1(b). Otherwise, its pertinent structure is illustrated in Fig. 6-1(c). These three decoupling structures are denoted by DN1, DN2 and DN3 respectively. Besides these networks, there are also other possible decoupling structures available. In order to preserve a reasonable simplicity in the network design, only DN1, DN2 and DN3 as basic decoupling networks are utilized.

In Fig. 6-1, $Z_{p,\mathrm{DN}q}$ with $p = 1, \ldots, 6$, whose values are $Z_{p,\mathrm{DN}q} = (R_{p,\mathrm{DN}q} + jX_{p,\mathrm{DN}q})\,\Omega$ are the passive decoupling components of DNq with $q = 1, 2, 3$, and $R_{p,\mathrm{DN}q}$ and $X_{p,\mathrm{DN}q}$ are their respective resistive and reactance parts. It is noticed that, with the three different decoupling components of DN1, the number of solutions might be infinite. The excess degree of freedom is exploited by setting $Z_{1,\mathrm{DN}1} = Z_{2,\mathrm{DN}1}$ in order to limit the number of solutions. This approach of setting the two decoupling components equal

proved to be better than omitting one of the two. For the same reason, the
value of $Z_{2,DN2}$ and $Z_{3,DN2}$ can also be set to be identical.

(a)   (b)   (c)
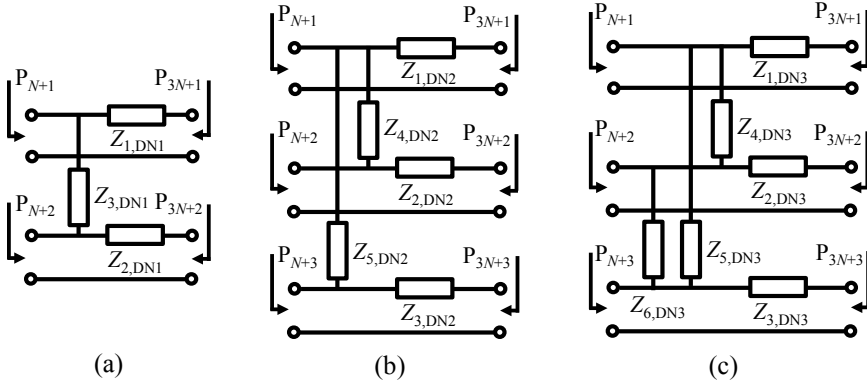
Fig. 6-1   Structure of basic decoupling networks for multi-element antenna systems with
$K = 2$ (DN1 (a)), $K = 3$ (DN2 (b) and DN3 (c)). $Z_{p,DNq}$ with $p = 1, …, 6$ are the pas-
sive decoupling components of DNq with $q = 1, 2, 3$. Reproduced with permission
from © 2017 *IEEE* [Che17].

As an evaluation using these basic decoupling structures, the decoupling for
example 2 in Table 2-1 in the lossless case is performed. According to the in-
itial estimate shown in Table 2-2, the decoupling for $S_{A,23}$ might be unneces-
sary. Therefore, DN2 is implemented. The component value of the network
DN2 and the resulting $|\mathbf{S}^{AD}|$ are shown in Table 6-1. For simultaneous conju-
gate complex matching, the reference impedances for the renormalization of
$\mathbf{S}^{AD}$ and the resultant $|\mathbf{S}^{ADM}|$ are then calculated and listed in Table 6-2. Due
to the fact that the (2,3) and (3,2) element of $|\mathbf{S}^{ADM}|$ are above -10 dB, the de-
coupling for $S_{A,23}$ and $S_{A,32}$ is needed. Therefore, instead of DN2, DN3 is cho-
sen to compensate all the antenna couplings of example 2. In this case, one
set of the component values as well as the decoupling and matching results,
which are able to reach the threshold values, are shown in Table 6-1 and Ta-
ble 6-2.

TABLE 6-1
IMPLEMENTATION OF DECOUPLING NETWORKS FOR TWO EXEMPLARY ANTENNA MATRICES RE-
PRODUCED WITH PERMISSION FROM © 2017 *IEEE* [CHE17].

example	used basic decoupling networks and one set of the corresponding component values [Ω]	$\left\|\mathbf{S}^{\mathrm{AD}}\right\|$ [dB]
2	DN2: $X_{1,\mathrm{DN2}} = -789$, $X_{2,\mathrm{DN2}} = 117$, $X_{4,\mathrm{DN2}} = -3871$, $X_{5,\mathrm{DN2}} = 3225$.	$\begin{bmatrix} -0.1 & -57.5 & -58.4 \\ -57.5 & -0.7 & -25.0 \\ -58.4 & -25.0 & -0.8 \end{bmatrix}$
2	DN3: $X_{1,\mathrm{DN3}} = -317$, $X_{2,\mathrm{DN3}} = 29$, $X_{3,\mathrm{DN3}} = 79$, $X_{4,\mathrm{DN3}} = -894$, $X_{5,\mathrm{DN3}} = 1346$, $X_{6,\mathrm{DN3}} = 548$.	$\begin{bmatrix} -0.4 & -59.9 & -61.3 \\ -59.9 & -2.3 & -56.2 \\ -61.3 & -56.2 & -1.1 \end{bmatrix}$
3	DN1: $X_{1,\mathrm{DN1}} = -42$, $X_{3,\mathrm{DN1}} = -140$. DN3: $X_{1,\mathrm{DN3}} = 41$, $X_{2,\mathrm{DN3}} = 213$, $X_{3,\mathrm{DN3}} = 66$, $X_{4,\mathrm{DN3}} = -541$, $X_{5,\mathrm{DN3}} = 62$, $X_{6,\mathrm{DN3}} = 127$.	$\begin{bmatrix} -1.6 & -57.5 & -47.8 & -17.9 \\ -57.5 & -0.5 & -51.4 & -22.5 \\ -47.8 & -51.4 & -1.9 & -53.7 \\ -17.9 & -22.5 & -53.7 & -2.7 \end{bmatrix}$

TABLE 6-2
SIMULTANEOUS CONJUGATE COMPLEX MATCHING AFTER DECOUPLING STAGE REPRODUCED
WITH PERMISSION FROM © 2017 *IEEE* [CHE17].

Example	Used basic decoupling networks	$Z_{\mathrm{R},n}$ with $n = 1,\dots,4$ [Ω]	$\left\|\mathbf{S}^{\mathrm{ADM}}\right\|$ [dB]
2	DN2	$Z_{\mathrm{R},1} = 70 + j885$ $Z_{\mathrm{R},2} = 31 - j168$ $Z_{\mathrm{R},3} = 42 - j183$	$\begin{bmatrix} -53.1 & -31.8 & -32.5 \\ -31.8 & -54.8 & -9.9 \\ -32.5 & -9.9 & -56.4 \end{bmatrix}$
2	DN3	$Z_{\mathrm{R},1} = 52 + j340$ $Z_{\mathrm{R},2} = 22 - j75$ $Z_{\mathrm{R},3} = 20 - j117$	$\begin{bmatrix} -51.8 & -45.4 & -43.8 \\ -45.4 & -56.5 & -45.7 \\ -43.8 & -45.7 & -50.4 \end{bmatrix}$
3	DN1 & DN3	$Z_{\mathrm{R},1} = 13 - j59$ $Z_{\mathrm{R},2} = 11 - j121$ $Z_{\mathrm{R},3} = 9 + j38$ $Z_{\mathrm{R},4} = 12 + j23$	$\begin{bmatrix} -64.6 & -24.2 & -39.2 & -10.3 \\ -24.2 & -50.3 & -38.3 & -10.4 \\ -39.2 & -38.3 & -53.0 & -41.9 \\ -10.3 & -10.4 & -41.9 & -52.1 \end{bmatrix}$

To achieve the decoupling for antenna arrays with $K > 3$, the number of de-
coupling components might not be sufficient using similar structures as the

basic ones. Hence, the proposed decoupling networks are composed of some basic decoupling networks (DN1, DN2 and DN3) in form of a cascade connection. As shown in Table 2-2, the couplings between element 1 and element 4 as well as between element 2 and element 4 of example 3 as an antenna matrix with $K = 4$ might be weak enough to avoid the decoupling according to the initial estimate. A suitable decoupling structure as a combination of DN1 and DN3 is therefore shown in Fig. 6-2. In this decoupling structure, DN3 is implemented to compensate all the couplings between antenna element n, with $n = 1, \ldots, 3$, while DN1 is used for eliminating the coupling between element 3 and element 4 ($S_{A,34}$ and $S_{A,43}$).
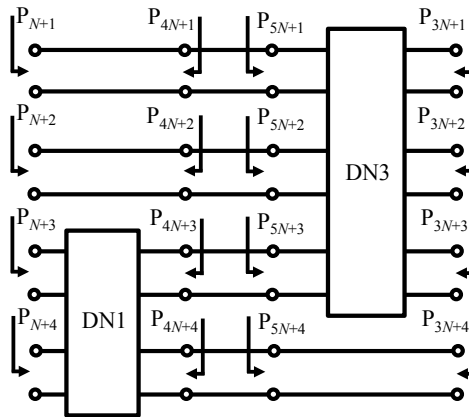
Fig. 6-2 Structure of decoupling networks for example 3 shown in Table 2-1. Reproduced with permission from © 2017 *IEEE* [Che17].

The calculation of the decoupling structure can be realized by multiplying the T-matrices of the decoupling steps [Fre08, Dob10]. The S-matrix of the decoupling step containing DN1 between P_n, with $n = N+1, \cdots, N+4$, and P_n, with $n = 4N+1, \cdots, 4N+4$, shown in Fig. 6-2, called $\mathbf{S^{DN1}}$ is defined as

$$\mathbf{S}^{\mathbf{DN1}} = \begin{bmatrix} \mathbf{S}_{11,\mathbf{DN1}} & \mathbf{S}_{12,\mathbf{DN1}} \\ \mathbf{S}_{21,\mathbf{DN1}} & \mathbf{S}_{22,\mathbf{DN1}} \end{bmatrix}. \tag{6.1}$$

In (6.1), $\mathbf{S}_{11,\mathbf{DN1}}$, $\mathbf{S}_{12,\mathbf{DN1}}$, $\mathbf{S}_{21,\mathbf{DN1}}$, $\mathbf{S}_{22,\mathbf{DN1}}$ are submatrices of $\mathbf{S}^{\mathbf{DN1}}$. Based on the calculated $\mathbf{S}^{\mathbf{DN1}}$, its corresponding transmission (T)-matrix $\mathbf{T}^{\mathbf{DN1}}$ is given by [Fre08, Dob10]

$$\mathbf{T}^{\mathbf{DN1}} = \begin{bmatrix} \mathbf{S}_{12,\mathbf{DN1}} - \mathbf{S}_{11,\mathbf{DN1}}\left(\mathbf{S}_{21,\mathbf{DN1}}\right)^{-1}\mathbf{S}_{22,\mathbf{DN1}} & \mathbf{S}_{11,\mathbf{DN1}}\left(\mathbf{S}_{21,\mathbf{DN1}}\right)^{-1} \\ -\left(\mathbf{S}_{21,\mathbf{DN1}}\right)^{-1}\mathbf{S}_{22,\mathbf{DN1}} & \left(\mathbf{S}_{21,\mathbf{DN1}}\right)^{-1} \end{bmatrix}. \tag{6.2}$$

Similarly, the T-matrix $\mathbf{T}^{\mathbf{DN3}}$ can also be converted from its corresponding S-matrix $\mathbf{S}^{\mathbf{DN3}}$, which represents the S-matrix of the decoupling step containing DN3 between P_n, with $n = 3N+1$, $\cdots$, $3N+4$, and P_n, with $n = 5N+1$, $\cdots$, $5N+4$. The T-matrix $\mathbf{T}^{\mathbf{DN}}$ for the whole decoupling structure between P_n, with $n = N+1$, $\cdots$, $N+4$, and P_n, with $n = 3N+1$, $\cdots$, $3N+4$, is then calculated as a product of $\mathbf{T}^{\mathbf{DN1}}$ and $\mathbf{T}^{\mathbf{DN3}}$, which is given by

$$\mathbf{T}^{\mathbf{DN}} = \begin{bmatrix} \mathbf{T}_{11,\mathbf{DN}} & \mathbf{T}_{12,\mathbf{DN}} \\ \mathbf{T}_{21,\mathbf{DN}} & \mathbf{T}_{22,\mathbf{DN}} \end{bmatrix} = \mathbf{T}^{\mathbf{DN1}} \cdot \mathbf{T}^{\mathbf{DN3}}. \tag{6.3}$$

$\mathbf{T}_{11,\mathbf{DN}}$, $\mathbf{T}_{12,\mathbf{DN}}$, $\mathbf{T}_{21,\mathbf{DN}}$, $\mathbf{T}_{22,\mathbf{DN}}$ are submatrices of $\mathbf{T}^{\mathbf{DN}}$. The conversion of corresponding S-matrix of the whole decoupling structure $\mathbf{S}^{\mathbf{DN}}$ from $\mathbf{T}^{\mathbf{DN}}$ is given by [Fre08, Dob10]

$$\mathbf{S}^{\mathbf{DN}} = \begin{bmatrix} \mathbf{T}_{12,\mathbf{DN}}\left(\mathbf{T}_{22,\mathbf{DN}}\right)^{-1} & \mathbf{T}_{11,\mathbf{DN}} - \mathbf{T}_{12,\mathbf{DN}}\left(\mathbf{T}_{22,\mathbf{DN}}\right)^{-1}\mathbf{T}_{21,\mathbf{DN}} \\ \left(\mathbf{T}_{22,\mathbf{DN}}\right)^{-1} & -\left(\mathbf{T}_{22,\mathbf{DN}}\right)^{-1}\mathbf{T}_{21,\mathbf{DN}} \end{bmatrix}. \tag{6.4}$$

Using (2.3) and (2.4), the values for decoupling and matching for example 3 are shown in Table 6-1 and Table 6-2. Although not all the antenna couplings are compensated, all the off-diagonal elements of $|\mathbf{S}^{\mathbf{ADM}}|$ are lower than

$|S_{\text{dc,thres}}|$. As a result, the presented decoupling network is sufficient to fulfill the predefined requirements.

Another possible structure of DN for example 3 would be two cascade connected DN2. They compensate two of the couplings between antenna element n, with $n = 1, 2, 3$ and that between antenna element n, with $n = 2, 3, 4$, respectively. For the other multi-element antennas with $K > 3$, the suitable decoupling structure can also be built as a cascade connection of the basic decoupling structures, and the value of the network components is calculated by multiplying the corresponding T-matrices.

6.2   Study of the Achievable Bandwidth

To make the band of operation reconfigurable over the investigated frequency range, some components of DMNs are made tunable. Because of the frequency-dependent $\mathbf{S}^{\mathbf{A}}$, the achievable bandwidth of each tuning state is limited. Hence, in this section, the design parameters for achieving a wide bandwidth in each tuned state are discussed according to a simulation-based tunable decoupling and matching for a compact three-element mobile terminal antenna in the lossless case.

The entire drawing of the three-element antenna and the exploded view of its excitation parts (structure demarcated by dashed line) are depicted in Fig. 6-3. The prototype of the presented antenna is realized using a 1.5 mm thick FR4 PCB enclosed by a plastic housing with 1 mm thickness. Nylon ($\varepsilon_r = 2.82$, $\tan(\delta) = 0.015$) with the outer dimensions $133 \times 68 \times 8$ mm^3 is used as the material of the housing.
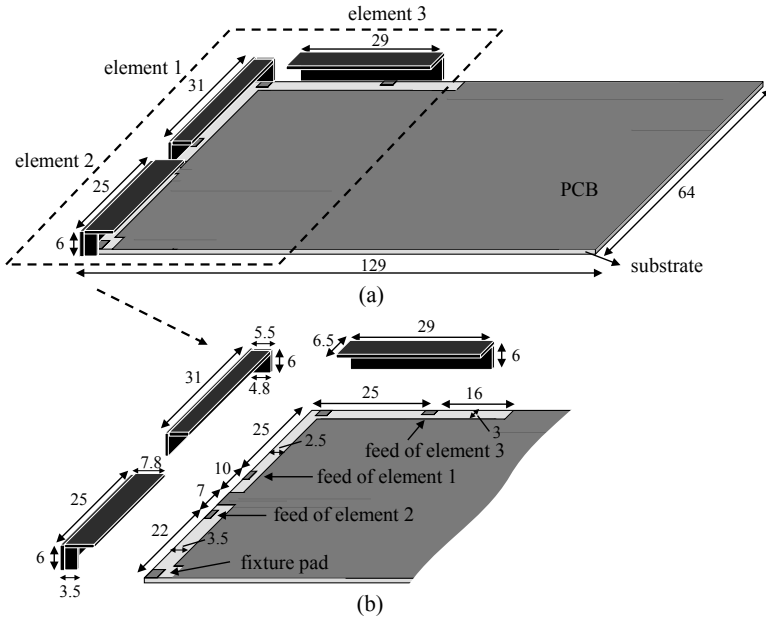
Fig. 6-3 The entire prototype (a) and the exploded excitation parts (b) of an inherently un-matched three-element antenna. Dimensions are in mm. Reproduced with permission from © 2017 *IEEE* [Che17].

The small-sized antenna coupling elements, which are designed to be inherently unmatched over the whole frequency range, are placed next to each other. The reflection coefficients of $\mathbf{S^A}$ ($S_{A,11}$, $S_{A,22}$ and $S_{A,33}$), obtained by numerical simulations in Empire [Emp] are plotted on the Smith-charts in Fig. 6-4, while the black dashed circles denote the $|S_{\text{ma,thres}}| = -6$ dB matching criterion. The simulated amplitude of the mutual couplings ($|S_{A,21}|$, $|S_{A,31}|$ and $|S_{A,32}|$) is seen in Fig. 6-5. For single-band communication, sufficient isolation and matching have to be satisfied simultaneously in the band of operation within the low- and the high-bands. All these requirements shall be fulfilled by DMNs. To study the achievable bandwidth, the DMN is tuned at the mid-frequency of each band of operation.
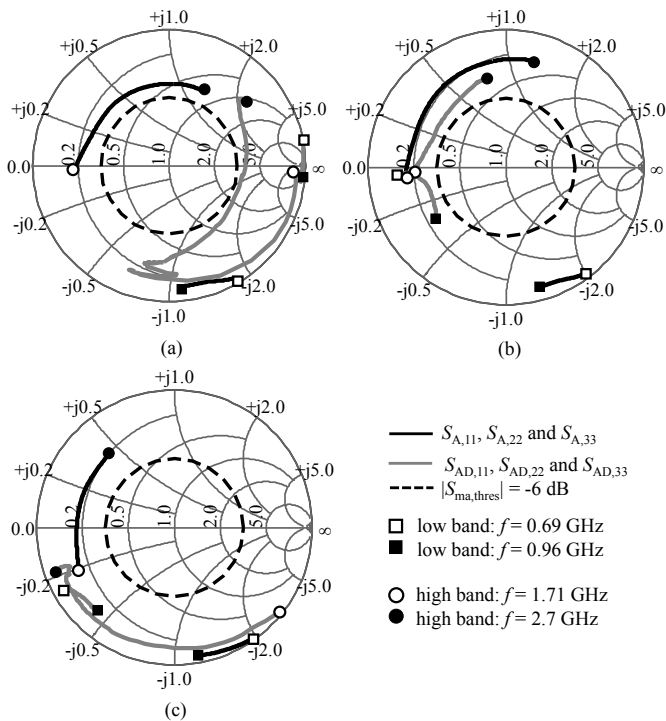
Fig. 6-4 Reflection coefficients of $\mathbf{S^A}$ ($S_{A,11}$, $S_{A,22}$ and $S_{A,33}$) as well as that of $\mathbf{S^{AD}}$ ($S_{AD,11}$ $S_{AD,22}$, and $S_{AD,33}$). (a) element 1, (b) element 2, (c) element 3. Reproduced with permission from © 2017 *IEEE* [Che17].
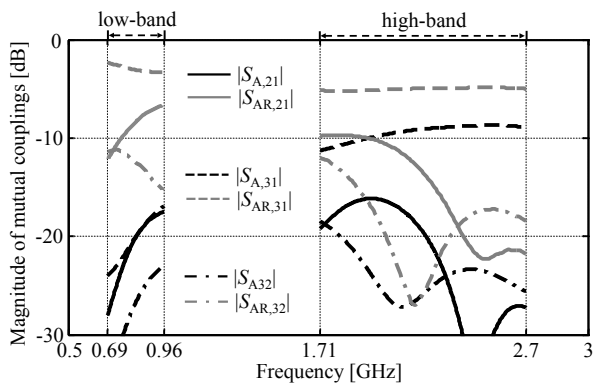
Fig. 6-5 The magnitude of the couplings coefficients of $\mathbf{S^A}$ and $\mathbf{S^{AR}}$. Reproduced with permission from © 2017 *IEEE* [Che17].

To make an initial estimate to determine the necessity and the structure of the decoupling network, $|S_{AR,21}|$, $|S_{AR,31}|$ and $|S_{AR,32}|$ of the renormalized S-matrix $\mathbf{S}^{AR}$ at each frequency point are calculated and are shown in Fig. 6-5 as well. The results indicate that $|S_{AR,32}|$ always reaches the $|S_{dc,thres}|$ = -10 dB threshold. Therefore, a decoupling network having the structure DN2 for only compensating $S_{A,21}$ and $S_{A,31}$ might be sufficient. However, $|S_{ADM,32}|$ cannot always be lower than $|S_{dc,thres}|$ over the whole frequency range. As a result, instead of DN2, DN3 is implemented in this case to compensate all the antenna couplings.

According to (2.3) and (2.4), the reactance value of the decoupling components of DN3 at each frequency point is calculated. To represent the required reactances, the values of inductors and capacitors in the network components as a function of frequency are shown in Fig. 6-6(a). It is seen that the value of most of the RF components is weakly dependent on frequency, especially those at frequencies above 1.9 GHz. In this case, the required component values at other frequencies within an operating band typically don't have a large deviation relative to that at the mid-frequency. This property would be useful to enhance the bandwidth of each tuning. Although $X_{2,DN3}$ and $X_{3,DN3}$ shown in Fig. 6-6(b) between 1.71 GHz and 1.8 GHz show a large frequency variation, the corresponding capacitance values are so small that they can be omitted.

By implementing DN3 for decoupling at each frequency point, the resulting reflection coefficients of $\mathbf{S}^{AD}$ are shown on the Smith-charts in Fig. 6-4. To reach the matching threshold after decoupling, three tunable two-element matching networks are implemented separately. According to $S_{AD,11}$ in the low-band shown in Fig. 6-4, the variation of the corresponding input impedance at P_4 over the frequency is quite high. As studied in Chapter 5, this fact

107

would limit the achievable bandwidth of the matching for element 1 in each tuned state.
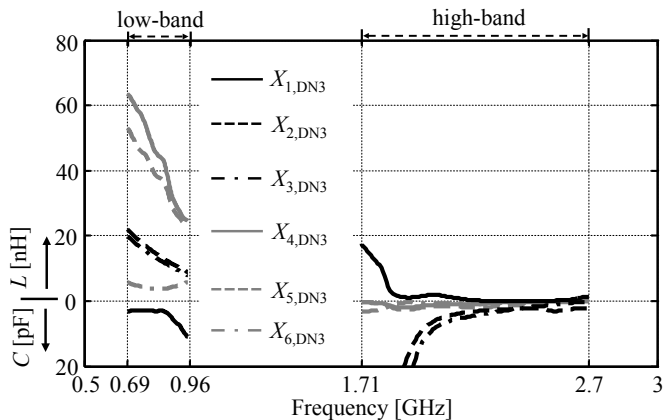
(a)
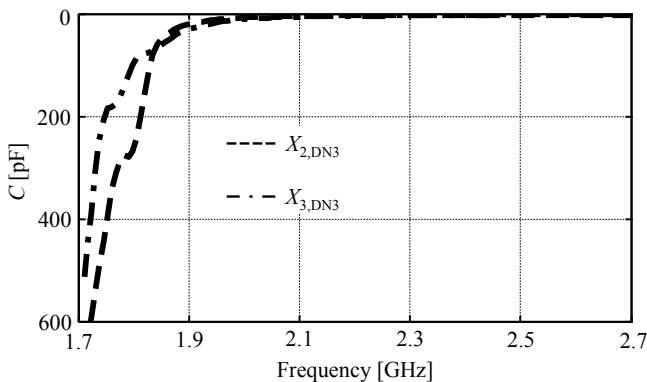
(b)

Fig. 6-6 Required value of inductors and capacitors to compensate the couplings in low- and high-bands (a) and required value of capacitors for representing $X_{2,DN3}$ and $X_{3,DN3}$ in high-band (b) at each frequency point. Reproduced with permission from © 2017 *IEEE* [Che17].

As an evaluation, the uplink or the downlink of 6 E-UTRA operating bands are chosen, which are located at the lower edge, upper edge or in the middle

of the low- or the high band. The parameter values of $\mathbf{S^{ADM}}$ are plotted in Fig. 6-7.

(a)

(b)
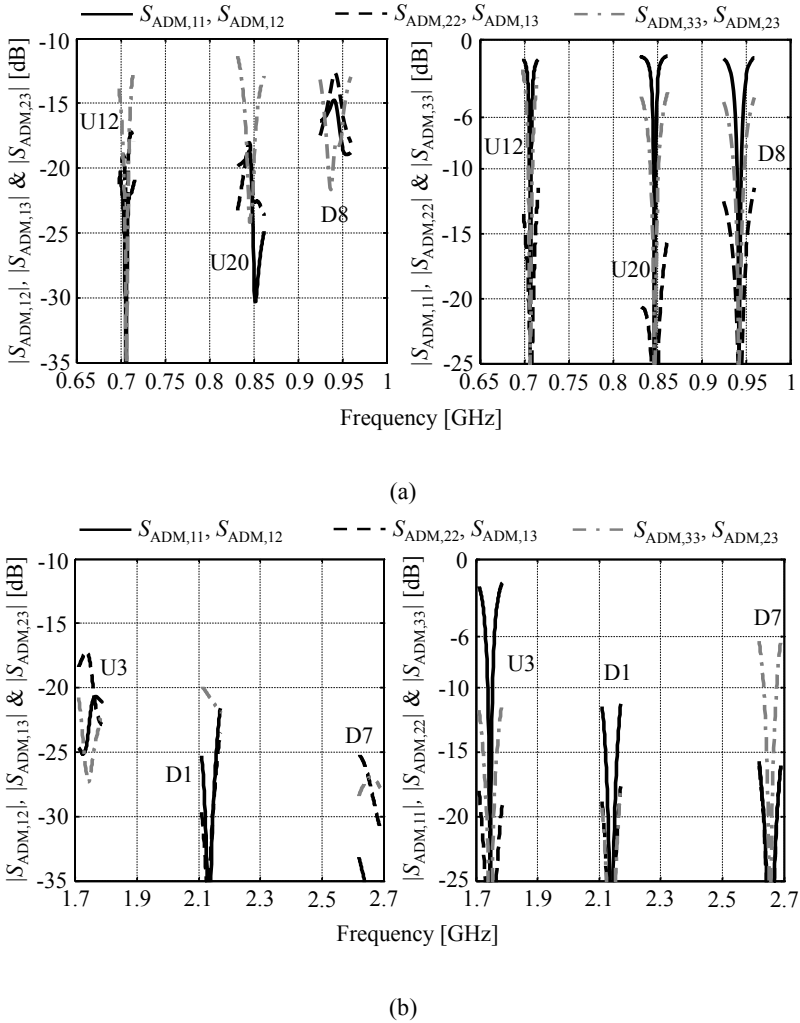
Fig. 6-7 Parameter values of $\mathbf{S^{ADM}}$ of each band in low-band (a) and high-band (b). U*n*, D*n*: uplink or downlink of the E-UTRA operating band *n*. Reproduced with permission from © 2017 *IEEE* [Che17].

The bandwidth in the low-band might only cover one channel of the band of operation, whose bandwidth is between 1.4 MHz and 20 MHz, at a time.

Compared to that in the low-band, the bandwidth in the high-band in each tuned state is significantly larger. As a result, it is desired that the required value of the decoupling components and the reflection coefficients of $\mathbf{S^{AD}}$ have a low frequency-dependence for achieving a wide bandwidth in each tuned state.

The DMN design concept shown in this chapter is studied theoretically. The investigation and evaluation of the concept to reach the decoupling and matching thresholds for the realistic cases are presented in the next chapter.

Chapter 7

Investigation of Practical Decoupling and Matching Networks for Two-Element Antennas

[5]Due to the limitation of the available values and losses using realistic components, the ability of the tunable decoupling and matching concept should be investigated and evaluated. To study the concept intuitively as well as to limit the difficulty of the realization, the investigation and evaluation for the realistic cases presented in this chapter only focus on the decoupling and matching for compact two-element mobile terminal antennas.

The chapter is organized as follows. In Section 7.1, the calculation of the component value and the decoupling ability of DN1 for compensating the couplings between two antenna elements in the lossless and realistic cases are studied. In Section 7.2, the required tunability of the decoupling components is revealed, which allows the utilization of DN1 over a wide frequency range. In Section 7.3, as a practical evaluation, a mock-up system including an in-

---

[5] The following chapter uses textual materials and figures from [Che17] ©
    2017 *IEEE*.

herently broadband unmatched two-element antenna combined with tunable decoupling and matching networks is designed and measured.

7.1 Study of the Realistic Decoupling Ability

If the compensation of the couplings between two-element antennas is necessary, the basic decoupling structure DN1 shown in Fig. 6-1(a) is selected. The topology of the decoupling and matching system for this case is therefore presented in Fig. 7-1.
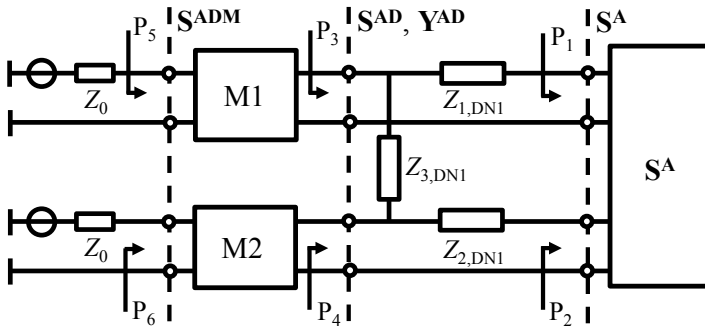
Fig. 7-1 Topology of a two-element antenna decoupling and matching system.

Besides using (2.3) and (2.4), the component values of DN1 can also be simply calculated based on the admittance (Y) and ABCD-matrix transformation. The antenna matrix $\mathbf{S^A}$ can be converted to an ABCD-matrix $\mathbf{ABCD^A}$, where A_A, B_A, C_A and D_A are the components of $\mathbf{ABCD^A}$. Instead of using $\mathbf{S^{AD}}$, the electrical behavior between the decoupled ports (P_3 and P_4) is characterized by a Y-matrix $\mathbf{Y^{AD}}$, which is given by

$$\mathbf{Y^{AD}} = \begin{bmatrix} Y_{AD,11} & Y_{AD,12} \\ Y_{AD,21} & Y_{AD,22} \end{bmatrix}$$

$$= \begin{bmatrix} \dfrac{C_A Z_{2,DN1} + D_A}{B} + \dfrac{1}{Z_{3,DN1}} & \dfrac{BC_A - A}{B} - \dfrac{1}{Z_{3,DN1}} \\ -\dfrac{1}{B} - \dfrac{1}{Z_{3,DN1}} & \dfrac{A_A + C_A Z_{1,DN1}}{B} + \dfrac{1}{Z_{3,DN1}} \end{bmatrix}. \tag{7.1}$$

The expressions for A and B are given by

$$A = \left(A_A + C_A Z_{1,DN1} \right)\left(D_A + C_A Z_{2,DN1} \right). \tag{7.2}$$

$$B = \left(A_A + C_A Z_{1,DN1} \right) Z_{2,DN1} + B_A + D_A Z_{1,DN1}. \tag{7.3}$$

$Y_{AD,mn}$ with m, $n = 1, 2$ are the parameters of $\mathbf{Y^{AD}}$. The coupling coefficients $Y_{AD,12}$ and $Y_{AD,21}$ should be set to zero, leading to a perfect decoupling at the target frequency. Hence, the following two simultaneous equations obtained from (7.1) should be fulfilled

$$B = \left(BC_A - D \right) Z_{3,DN1}, \tag{7.4}$$

and

$$B = -Z_{3,DN1}. \tag{7.5}$$

Due to the fact that $Z_{3,DN1} \neq 0$, (7.4) can be simplified according to (7.5), which is given by

$$B_A C_A - A_A D_A = -1. \tag{7.6}$$

Equation (7.6) is always valid whenever $S_{A,21} \neq 0$. Therefore, only (7.5) needs to be kept, and it can be transformed as a function containing the parameters of $\mathbf{S^A}$ as coefficients, which is expressed as

$$
\left(\left(1-S_{A,11}\right)\left(1-S_{A,22}\right)-S_{A,21}^2\right)Z_{1,DN1}Z_{2,DN1}
$$
$$
+\left(\left(1-S_{A,11}\right)\left(1+S_{A,22}\right)+S_{A,21}^2\right)Z_0Z_{1,DN1}
$$
$$
+\left(\left(1+S_{A,11}\right)\left(1-S_{A,22}\right)+S_{A,21}^2\right)Z_0Z_{2,DN1} \tag{7.7}
$$
$$
+\left(\left(1+S_{A,11}\right)\left(1+S_{A,22}\right)-S_{A,21}^2\right)Z_0^2+2S_{A,21}Z_0Z_{3,DN1}=0.
$$

As discussed in the last chapter, $Z_{1,DN1} = Z_{2,DN1}$ in order to limit the number of solutions to two. In this case, the value of $Z_{1,DN1}$ and $Z_{3,DN1}$ can be calculated by simplifying (7.7), which is given by

$$
\underbrace{\left(1-S_{A,11}-S_{A,22}+S_{A,11}S_{A,22}-S_{A,21}^2\right)Z_{1,DN1}^2}_{a_t}
$$
$$
+\underbrace{2\left(1-S_{A,11}S_{A,22}+S_{A,21}^2\right)Z_0Z_{1,DN1}}_{b_t} \tag{7.8}
$$
$$
+\underbrace{\left(1+S_{A,11}+S_{A,22}+S_{A,11}S_{A,22}-S_{A,21}^2\right)Z_0^2}_{c_t}+\underbrace{2S_{A,21}Z_0}_{d_c}Z_{3,DN1}=0.
$$

a_t, b_t, c_t are the first three terms of the equation while d_c is the coefficient of $Z_{3,DN1}$. According to (7.8), the calculation of $Z_{1,DN1}$ and $Z_{3,DN1}$ using inductors and capacitors as network components in the lossless and realistic cases is shown in the Appendix.

Due to the losses of the realistic components, the calculated value of $X_{1,DN1}$ and $X_{3,DN1}$ might be unrealistic, which would limit the decoupling ability in the realistic case. In this case, the realistic decoupling ability of DN1 is investigated. The study employs a Monte Carlo simulation using different samples of $\mathbf{S^A}$. The total number of these possible samples is defined as N_r. The number of antenna S-matrices (N_d), with which the implementation of the proposed decoupling network is successful, is calculated. The success rate for

the decoupling is then defined as the ratio of N_d to N_r. To perform an accurate study, N_r is set to be approximately 5 billion. Although the decoupling network suffers from component losses, it still indicates a greater than 99.9% success rate, which guarantee the decoupling ability in the realistic case (inductors having a $Q = 50$ and capacitors with a constant resistance of 0.3 Ω).

7.2 Calculation of the Reconfigurable Bandwidth

Due to the limited variation range of the realistic tuning components, the capability of adapting the antenna operating band over a wide frequency range is expected besides the large bandwidth of each tuning state studied in the last chapter. Thus, the frequency dependence of the component value ($Z_{1,DN1}$ and $Z_{3,DN1}$) is studied in this section.

According to (7.8), $Z_{1,DN1}$ and $Z_{3,DN1}$ are calculated based on the parameters of $\mathbf{S^A}$ ($S_{A,11}$, $S_{A,22}$ and $S_{A,21}$) of the inherently broadband unmatched antennas having a low frequency-dependent impedance behavior. The frequency variation of both reflections for such antennas is weak and has usually an initial impact on the phase ($\varphi_{A,11}$ and $\varphi_{A,22}$) [Val13b]. As a result, the frequency variation of $S_{A,11}$ and $S_{A,22}$ can be mimicked by modifying $\varphi_{A,11}$ and $\varphi_{A,22}$ while fixing the value of $|S_{A,11}|$ and $|S_{A,22}|$. The frequency variation of $S_{A,21}$ is represented by varying its value.

To calculate the frequency dependence of $X_{1,DN1}$ and $X_{3,DN1}$ for a two-element antenna with a given value of $|S_{A,11}|$ and $|S_{A,22}|$, the required reactance values derived by varying $\varphi_{A,11}$, $\varphi_{A,22}$ and $S_{A,21}$ are calculated in the realistic case. The standard deviations of $X_{1,DN1}$ and $X_{3,DN1}$ defined as $\sigma(X_{1,DN1})$ and $\sigma(X_{3,DN1})$ are then used to quantify the amount of the variations. The extreme values of $X_{1,DN1}$ and $X_{3,DN1}$ (the 10% lowest and the 10% highest values) are not included in the calculation to make a fair statistical investigation. Based on this ap-

proach, $\sigma(X_{1,DN1})$ and $\sigma(X_{3,DN1})$ for the antennas having different $|S_{A,11}|$ and $|S_{A,22}|$ are calculated. Because of the freedom to name the ports, $|S_{A,11}| \geq |S_{A,22}| \geq |S_{ma,thres}|$ is chosen. The results are shown in Fig. 7-2.

(a)   (b)
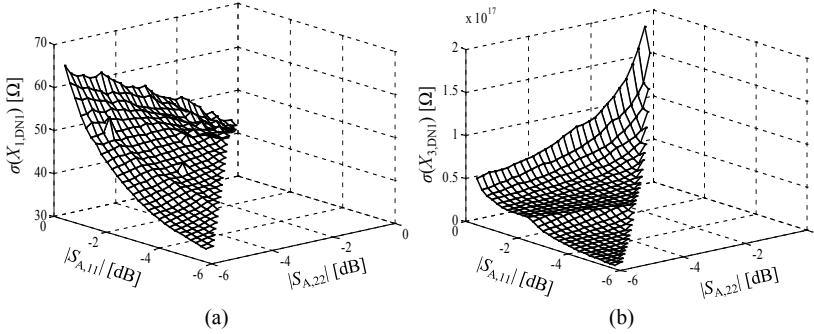
Fig. 7-2 Standard deviation of the decoupling reactance $X_{1,DN1}$ and $X_{3,DN1}$ ($\sigma(X_{1,DN1})$ and $\sigma(X_{3,DN1})$) according to the phase variation of $S_{A,11}$ and $S_{A,22}$. a): $\sigma(X_{1,DN1})$. b): $\sigma(X_{3,DN1})$.

A low $\sigma(X_{1,DN1})$ and $\sigma(X_{3,DN1})$ represent a weak deviation of values, which would be useful for the utilization of tuning components over a broad frequency range. It can be seen from Fig. 7-2 that $X_{1,DN1}$ is quite insensitive to frequency variation. Unlike $X_{1,DN1}$, a low frequency-dependent $X_{3,DN1}$ is not guaranteed.

A possible explanation for Fig. 7-2 can be given according to (7.8). For inherently unmatched antenna elements, the antenna coupling $S_{A,21}$ is correspondingly small. The first three terms shown in (7.8) (a_t, b_t and c_t) containing $S_{A,21}^2$ are thus weakly dependent on the variation of the couplings. On the other hand, the coefficient of $Z_{3,DN1}$ (d_c) is directly proportional to $S_{A,21}$. Therefore, the variation of $S_{A,21}$ might have a stronger impact on $Z_{3,DN1}$ compared to that on $Z_{1,DN1}$, if $S_{A,11}$ and $S_{A,22}$ show a low frequency variation. As a result, only a wide tuning range for $Z_{3,DN1}$ is probably needed in order to

make decoupling reconfigurable over a large frequency range for the antennas having weakly frequency-dependent reflections.

7.3 Practical Evaluation of the Tunable Decoupling and Matching Concept

In the last two sections, the calculation and the requirements of the component value of DN1 for the implementation over a wide frequency range in the realistic case are presented. To evaluate this decoupling and matching concept in a practical example, an inherently broadband unmatched two-element antenna is presented. Its structure is identical to that of the three-element antenna shown in Fig. 6-3, except that it lacks element 3. The measured reflection coefficients ($S_{A,11}$ and $S_{A,22}$) are plotted on the Smith-chart in Fig. 7-3, and the measured amplitude of the antenna coupling ($|S_{A,21}|$) is as seen in Fig. 7-4.
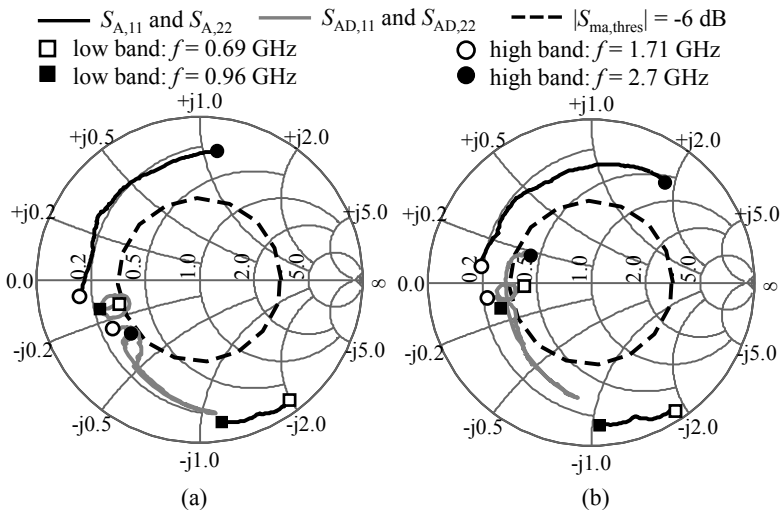
Fig. 7-3 The free-space antenna impedances of the inherently unmatched two-element antenna. (a) element 1, (b) element 2. Reproduced with permission from © 2017 *IEEE* [Che17].
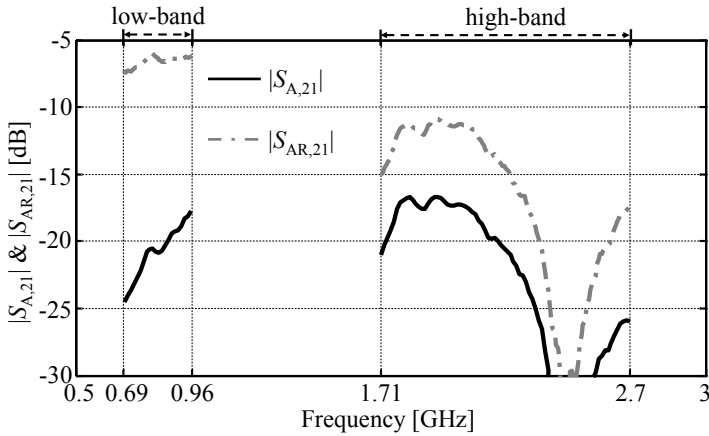
Fig. 7-4   The measured amplitude of the antenna coupling ($|S_{A,21}|$) and the amplitude of the calculated coupling coefficient of renormalized antenna matrix ($|S_{AR,21}|$) at each frequency point for estimating the necessity of decoupling. Reproduced with permission from © 2017 *IEEE* [Che17].

To make the initial estimate regarding the necessity of decoupling, the amplitude of the calculated coupling coefficient of renormalized antenna matrix ($|S_{AR,21}|$) at each frequency point in the lossless case is calculated and shown in Fig. 7-4. Since the worst case value in the whole high-band is less than $|S_{dc,thres}|$, $|S_{ADM,12}|$ and $|S_{ADM,21}|$ would still be smaller than $|S_{dc,thres}|$ = -10 dB only by implementing matching networks. Hence, the need for a decoupling network for the high-band is avoidable.

7.3.1   *Decoupling and Matching in Low-Band*

The results shown in Fig. 7-4 indicate that a complete DMN is required in the low-band. The calculated reactance values $X_{1,DN1}$ and $X_{3,DN1}$ for compensating the coupling at each frequency point in the lossless and the realistic cases are shown in Fig. 7-5. The sum of a_t, b_t and c_t in (7.8) is small and provides a similar frequency-dependent curve as d_c. Hence, although $S_{A,21}$ shows a large frequency-dependence in the low-band, $X_{3,DN1}$ is substantially constant.

118
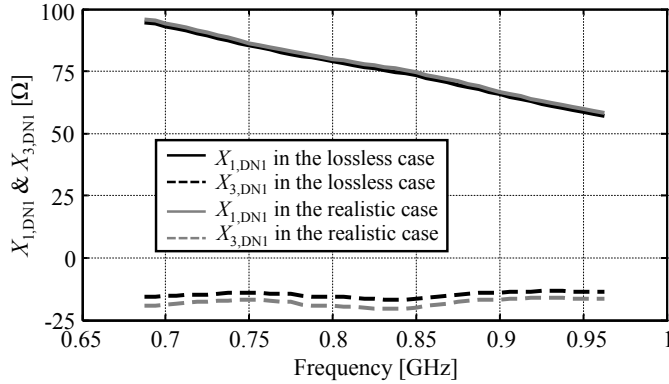
Fig. 7-5   Required reactance values $X_{1,DN1}$ and $X_{3,DN1}$ for decoupling at each frequency point in the low-band in the lossless and the realistic cases. Reproduced with permission from © 2017 *IEEE* [Che17].

The variations of the reactance values in the lossless and realistic cases are quite similar and can be realized through the combination of fixed and tunable components, e.g. series connection of a fixed inductor to a tunable capacitor. Thus, to compensate the coupling in the low-band, a practical realization of DN1 is presented in Fig. 7-6.
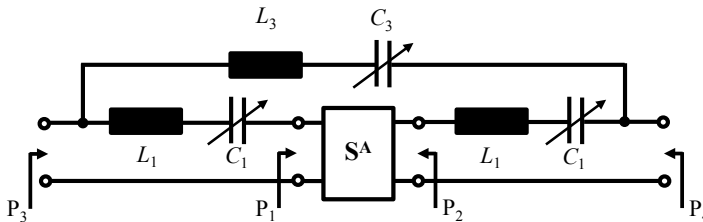
Fig. 7-6   Schematic of the decoupling circuit for the low-band. L_n with $n = 1, 3$: fixed inductors. C_n with $n = 1, 3$: tunable capacitors. Reproduced with permission from © 2017 *IEEE* [Che17].

The varactor SMV1235 is used to represent the tunable capacitor C_1 while the tunable capacitor C_3 is implemented by the varactors SMV1234. However, these combinations may cause undesirable resonances, which degrade the

power transfer from the RF front-end to the antenna elements. One possible solution is keeping the resonances far away from the target frequencies. Due to the limited availability of the RF components, two different fixed inductors are selected to implement L_1 for different frequencies. The value of L_1 is $L_1 = 30$ nH up to 750 MHz. From 750 MHz to 960 MHz, the value of L_1 is set to be $L_1 = 20$ nH. The component value of L_3 is $L_3 = 1.5$ nH. In a practical realization, this requires an additional switch to select the operation band. For evaluating the proposed concept, this switch is omitted and 3 E-UTRA operating bands located within the low-band are chosen. The values of the varactors are tuned across the uplink or downlink of each band for both antenna elements.

By implementing the DN at each frequency point, the resultant reflection coefficients of $\mathbf{S}^{\mathbf{AD}}$ ($S_{AD,11}$ and $S_{AD,22}$), which are shown in Fig. 7-3, can be used as a reference. Based on this knowledge, two additional matching networks are consequently designed, so that not only the decoupling criterion $|S_{dc,thres}|$, but also the predefined matching criterion $|S_{ma,thres}|$ can be achieved. The circuits are shown in Fig. 7-7. The values of the fixed inductors as matching components are $L_4 = 6.2$ nH and $L_5 = 5.6$ nH. C_4 and C_5 represent the fixed capacitors with values $C_4 = 4.7$ pF and $C_5 = 4.3$ pF.
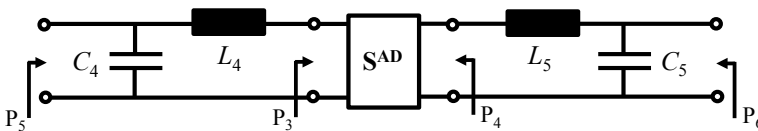
Fig. 7-7   Schematic of the matching circuits for the decoupled two-element antenna in the low-band. C_n, L_n with $n = 4, 5$: fixed capacitors and inductors. Reproduced with permission from © 2017 *IEEE* [Che17].

A picture of the fabricated prototype with an enlarged view of the presented DMN for the low-band (the area demarcated by the dashed line) is presented

120

in Fig. 7-8. The measured parameters of $|\mathbf{S}^{\mathbf{ADM}}|$ can be seen in Fig. 7-9, and the results of the total efficiency measurements are shown in Fig. 7-10. Due to the low frequency-dependent reactance value of $X_{1,\mathrm{DN1}}$ and $X_{3,\mathrm{DN1}}$ shown in Fig. 7-5 as well as the reflection coefficients of $\mathbf{S}^{\mathbf{AD}}$ ($S_{\mathrm{AD,11}}$ and $S_{\mathrm{AD,22}}$) presented in Fig. 7-3, the bandwidth for decoupling and matching in each tuned state can at least cover the uplink or downlink of each E-UTRA band.
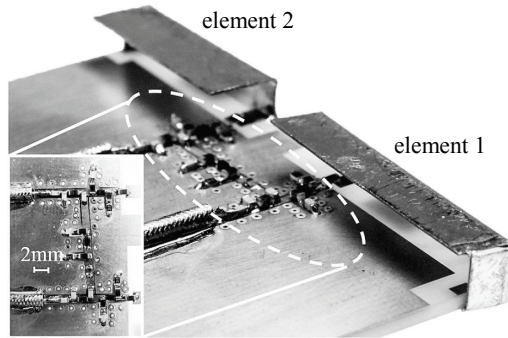
Fig. 7-8 Picture of the fabricated prototype with an enlarged view of the presented DMN for the low-band. Reproduced with permission from © 2017 *IEEE* [Che17].
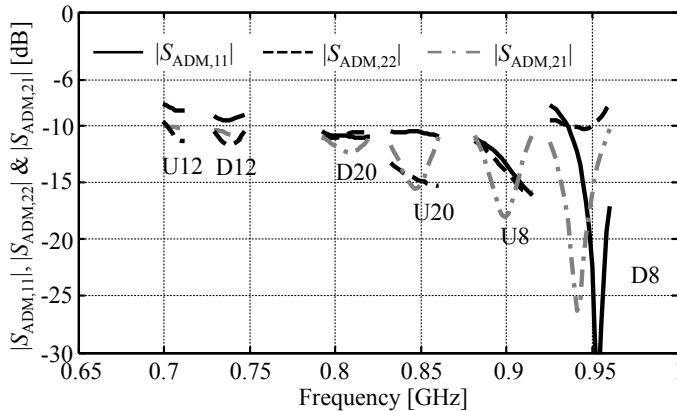
Fig. 7-9 Measured scattering parameters of the uplink and downlink of each band. Un with n = 8, 12, 20: uplink of the E-UTRA operating band n. Dn with n = 8, 12, 20: downlink of the E-UTRA operating band n. Reproduced with permission from © 2017 *IEEE* [Che17].
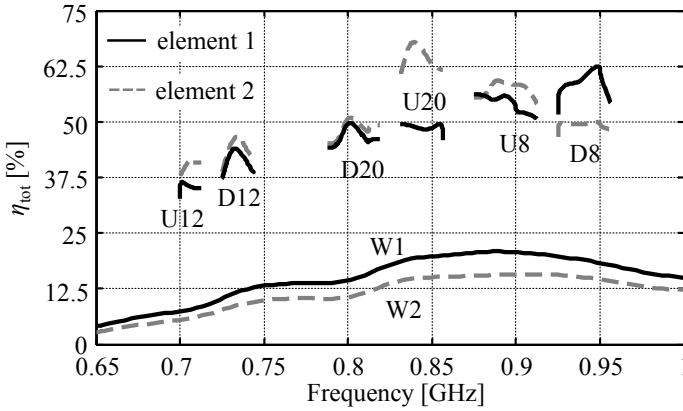
Fig. 7-10 Measured total efficiency (η_{tot}) of the uplink and downlink of each band in linear scale. Un with $n = 8$, 12, 20: uplink of the E-UTRA operating band n. Dn with $n = 8$, 12, 20: downlink of the E-UTRA operating band n. Wn with $n = 1$, 2: element n with $n = 1$, 2 without utilization of the DMNs. Reproduced with permission from © 2017 *IEEE* [Che17].

7.3.2 *Decoupling and Matching in High-Band*

The required reactance values $X_{1,DN1}$ and $X_{3,DN1}$ at each frequency point for the lossless and realistic cases would be as shown in Fig. 7-11, if the decoupling is implemented for the high-band. Compared to the value of $X_{1,DN1}$, the value of $X_{3,DN1}$ shows a much larger deviation at the place, where $S_{A,21}$ is strongly frequency-dependent, while the sum of a_t, b_t and c_t in (7.7) has a large and relative constant value.

Fig. 7-4 reveals that only a matching network for each antenna element is necessary in the high-band. Due to the low frequency-dependent antenna impedance behavior, the circuits for the whole high-band can be simply designed, and their structures are found in Fig. 7-12. Both inductors have the same value $L_7 = L_8 = 2.9$ nH, and the tunable capacitors C_9 and C_{10} are realized by the varactor SMV1231. A picture of the fabricated prototype, with an enlarged view of the matching circuits (the area demarcated by the dashed

122

line) is presented in Fig. 7-13.
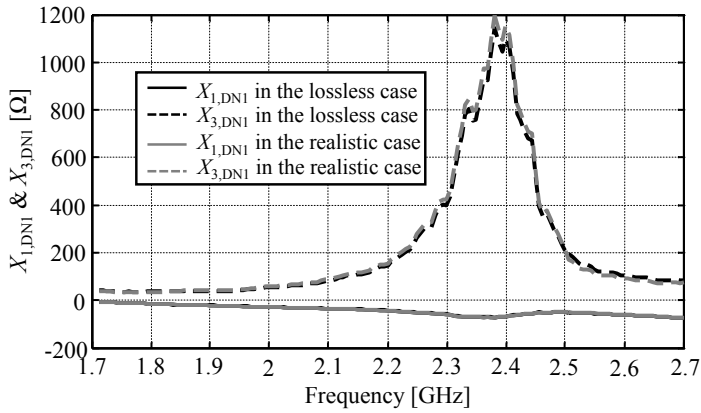
Fig. 7-11 Required reactance values $X_{1,DN1}$ and $X_{3,DN1}$ for decoupling at each frequency points in the high-band with different losses.
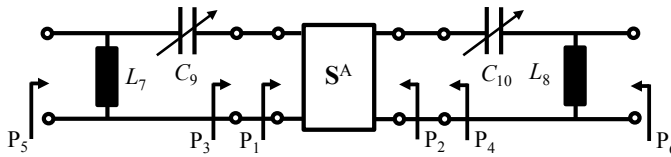
Fig. 7-12 Schematic of the two-element antenna matching circuit for the high-band. C_n, L_n with $n = 7, 8$: fixed matching components. C_n with $n = 9, 10$: tunable matching components. Reproduced with permission from © 2017 *IEEE* [Che17].
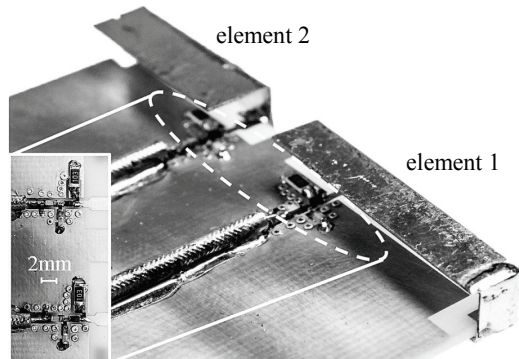
Fig. 7-13 A picture of fabricated prototype with an enlarged view of the presented matching circuit for high-band. Reproduced with permission from © 2017 *IEEE* [Che17].

To evaluate the concept in the high-band, 6 communication bands containing 5 E-UTRA operating bands and the 2.45 GHz WLAN band are selected. The values of both varactors are optimized for each band so that both antenna elements would work in the same band during the measurements. The measured scattering parameters and the total efficiency are shown in Fig. 7-14 and Fig. 7-15, respectively. It is seen that satisfactory results can be achieved without the need for decoupling networks.

In the practical evaluation presented herein, the simple matching networks utilized are designed and operated separately, thus affording a great deal of simplification. Greater values of η_{tot} would be obtained, if the matching stage is optimized by considering all the losses within the antenna system [Rah13]. It should also be mentioned that some other frequency-reconfigurable two-element antenna systems working only in the low-band or in both bands have been published [Kre14, Kuo10, Ilv14b]. However, the radiation elements, which they employed, are quite large in size without providing a better overall total efficiency.
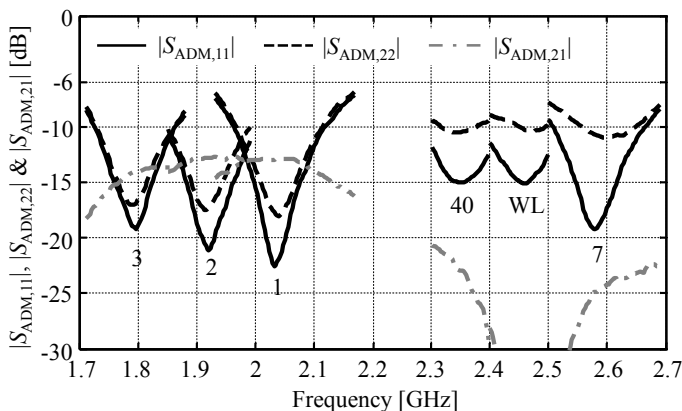
Fig. 7-14 Measured scattering parameters of each band. n with n = 1, 2, 3, …: E-UTRA operating band n. WL: WLAN. Reproduced with permission from © 2017 *IEEE* [Che17].
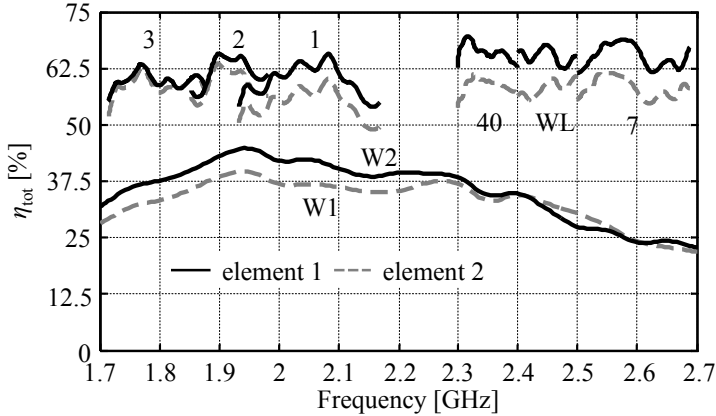
Fig. 7-15 Measured total efficiency (η_{tot}) of each band in linear scale. n with $n = 1, 2, 3, \ldots$: E-UTRA operating band n. WL: WLAN. Wn with $n = 1, 2$: element n with $n = 1, 2$ without implementing the DMN. Reproduced with permission from © 2017 *IEEE* [Che17].

7.3.3 *Analysis of the Power Dissipation Distribution*

The measurement results show the antenna operating band is able to be frequency configurable by employing DMNs over the frequency range $0.69 \leq f\,[\text{GHz}] \leq 2.7$. To gain a deeper insight into the antenna system, the power dissipation distribution is studied. As examples, the power dissipations of the element 2 over the downlink of the E-UTRA operating band 20 and the whole E-UTRA operating band 2 are analyzed. Each dissipated power is calculated as a ratio to the input power. The radiated power of the element 2 is estimated through the measurement of the total efficiency. Some of the dissipated power is either reflected due to the impedance mismatch at P_6 (mismatch losses) or absorbed because of the material losses of the housing and the substrate, etc (material losses). Some other power is dissipated by reason of the losses of the DMN for element 2 (DMN losses). Because of the losses caused by the mutual coupling (coupling losses), the other parts are absorbed by the DMN for element 1 and the load impedance at P_5. The mismatch loss-

es are calculated through the measurement of $S_{\text{ADM},22}$, whereas the analysis of the other losses is performed using ADS simulator. The calculated dissipated power in percentage form is shown in Table 7-1.

TABLE 7-1
THE POWER DISSIPATION OF ELEMENT 2 OVER THE DOWNLINK OF THE BAND E-UTRA 10 AND THE BAND E-UTRA 2

power dissipation	downlink of E-UTRA band 20	E-UTRA band 2
radiated power	46% - 51%	55% - 65%
mismatch losses	7% - 10%	2% - 9%
material losses	15% - 17%	12% - 20%
DMN losses	12% - 16%	17% - 18%
coupling losses	8% - 13%	5% - 7%

As can be seen in Table 7-1, a larger portion of losses is caused by the material losses of the substrate, housing, DMNs, etc. Similar to the matching network presented in Chapter 4, some other tuning devices having lower losses can be utilized instead of varactor diodes in order to improve η_{cd} and consequently the η_{tot} shown in (2.2).

Moreover, a technique called carrier aggregation has been introduced in order to enhance the data throughput, which allows the communication in two or more bands simultaneously [Gpp12]. A fixed dual-band communication using a DMN containing a series or parallel *LC* circuit as each network component is shown in [Coe11] as an example. The goal of adapting several antenna operating bands simultaneously requires the independent tunability of the network components at multiple frequencies. One possible solution is to utilize a set of RF components including several tunable ones, as the network

components of the DMN in order to increase the degrees of freedom for frequency reconfigurability.

Although the adaptive decoupling and matching for the closely spaced multi-element antennas in usage scenarios is out of the scope of this work, the investigations obtained with compact single-element antennas combined with adaptive matching circuits in the presence of user interaction would have valuable contributions to further work.

Chapter 8

Conclusions & Discussions

8.1 Conclusions

Communications over a large frequency range in compact mobile terminals demand that single- and multi-element antennas, with a small form factor, be integrated on a finite-size chassis. However, this gives rise to increased mutual coupling and impedance mismatch. Furthermore, the presence of user interaction also detunes the antenna impedance and modifies the mutual coupling unpredictably. All of these factors result in degradation of the antenna's total efficiency. To mitigate these effects, besides optimization of the antenna structure, a promising option is to adaptively tune a limited operating band of the single- and multi-element antennas.

To achieve this purpose, this thesis contributes design concepts for tunable decoupling and matching networks as an important part of adaptive decoupling and matching systems to provide a reconfigurable band of operation over the frequencies of interest, of small-sized and generic antenna elements, which are close to each other, on a compact mobile terminal. Evaluation of these concepts is effected in this work in the $0.69 \leq f\,[\mathrm{GHz}] \leq 2.7$ frequency

range.

The approach is based on implementation of tunable decoupling and matching networks in different steps to simplify the network design. For multi-element antennas, the necessity of the decoupling branches is initially estimated by assessing the resulting coupling between the RF front-ends, which are simultaneously conjugate complex matched using lossless circuits. This initial estimate is then assessed through the comparison of the resultant coupling coefficients of the renormalized antenna matrix to the decoupling threshold.

For the single-element as well as the multi-element antennas, that require no decoupling, a tunable Π-section matching network providing a wide highly matchable impedance area is studied. The equivalent reactance of the *LC* configuration and the suitable components values within the investigated frequency range should be firstly studied. In addition to the Π-section structure, some boundary conditions of antenna adaptive systems such as impedance detector and ESD protection are also taken into account. Based on this knowledge, the topology of the matching network is optimized for maximizing its tunability for the possible antenna impedance mismatch caused by user interaction.

For achieving a high success rate for impedance matching of the generic antenna elements having small antenna form factor, they are designed to be inherently broadband unmatched, and their antenna impedances need to be located within the highly matchable impedance area of the networks. It is found that such an antenna has a robust impedance against typical usage scenarios. This fact guarantees that the impedance of the antenna remains within the matchable region. Furthermore, the variation of the impedance over the

whole investigated frequency range should be weak, so that the reconfigurability of the band of operation can be realized in a simple fashion. A mock-up-system (an inherently unmatched antenna combined with the varactor-based tunable matching circuitry) shows its benefit in terms of antenna form factor and total efficiency compared to that of antenna systems containing some typical inherently matched antennas.

For the case in which the decoupling for closely spaced multi-element antennas is unavoidable, a tunable decoupling and matching concept as an extension of the tunable matching concept is presented. The decoupling network consisting of basic decoupling structures connected in cascade can be designed based on the initial estimate. For the cases in which not all the coupling coefficients are below the threshold, the network should be redesigned to compensate more couplings. To enhance the bandwidth of each tuning, it is quite useful if the required value of the decoupling components and that of the consequent reflections to be matched have a weak frequency-dependence. Several antenna matrices at one single frequency point and a typical three-element antenna operating over a large frequency range as theoretical and simulation-based examples, can be decoupled and matched following the proposed concept.

A quite high success rate can still be guaranteed, although realistic decoupling networks for two-element antennas suffer from nonzero component losses. Only one of the decoupling components might need to have a large tuning range, which is beneficial for adapting the operation band over a wide frequency range. The operation of a mock-up system including a two-element antenna combined with tunable DMNs evaluates the proposed concept practically.

In conclusion, design concepts for compact single- and multi-element antennas combined with tunable decoupling and matching networks have been presented. These enable small and generic antenna elements on a compact mobile terminal to exhibit a frequency-reconfigurable band of operation over a broad frequency range.

8.2   Discussions

The design of small-sized single- and multi-element antennas for obtaining good total efficiency over a broadband frequency range, while experiencing user interaction, is quite challenging. In this work, instead of optimizing the antenna geometry for broadband decoupling and matching, this purpose is achieved using adaptive antenna systems to adaptively tune the band of operation of antenna elements over a large frequency range. The main contribution of this work is the design concepts of tunable decoupling and matching networks for compact mobile terminal antennas.

According to the proposed decoupling and matching concept, the compact antennas are designed to be inherently broadband unmatched with a frequency-insensitive impedance behavior, and the antenna elements are allowed to be placed next to each other and close to RF front-ends. The size of such antenna elements is more compact compared to the inherently broadband decoupled and matched ones. This simple structure would also be quite advantageous for antenna designs in which one wishes to decrease the impact of the user interaction.

On the other hand, the main difficulty and effort of the design are shifted from the antenna structure to the corresponding tunable decoupling and matching networks. The circuits would still be quite complex, for some antenna systems with a large number of antenna elements, although some de-

coupling branches might be omitted. Besides the DMN, many other components should also be implemented within the antenna adaptive system, such as a microcontroller, driver and impedance detector, which would increase the cost and the complexity. By implementing DMNs, decoupling and matching can only be achieved within a band of operation having limited bandwidth in each tuned state. Hence, this bandwidth might not able to cover the entire desired band.

For practical implementations, some power is dissipated in the realistic components of the networks due to inherent losses. This fact may provide a low value of reflection and coupling coefficients at the RF front-end while reducing the value of the total efficiency. Moreover, due to the limited availability and tunability of realistic RF components, the reconfigurability of the band of operation might not be realized over the whole frequency range of interest.

Several research topics could be further investigated based on this work. One example would be the decoupling and matching simultaneously in two or more bands of operation for implementing the carrier aggregation technique. Another research topic would be the design of tunable DMNs for closely spaced multi-element antennas by including the parasitic effects of other system components in usage scenarios. The practical integration and realizability of the circuits in view of the whole antenna adaptive system should also be considered in future work.

Appendix

Calculation of the Decoupling Network for Two-Element Antennas

The function for calculating the value of the decoupling components is given by

$$
\left(1 - S_{A,11} - S_{A,22} + S_{A,11}S_{A,22} - S_{A,21}^2\right)Z_{1,DN1}^2
$$
$$
+2\left(1 - S_{A,11}S_{A,22} + S_{A,21}^2\right)Z_0 Z_{1,DN1} \tag{A.1}
$$
$$
+\left(1 + S_{A,11} + S_{A,22} + S_{A,11}S_{A,22} - S_{A,21}^2\right)Z_0^2 + 2S_{A,21}Z_0 Z_{3,DN1} = 0.
$$

Because the real and the imagery parts of (A.1) are required to be zero, two simultaneous equations are therefore derived, namely,

$$
A_1\left(R_{1,DN1}^2 - X_{1,DN1}^2 + Z_0^2 - 2Z_0 R_{1,DN1}\right)
$$
$$
+\left(R_{1,DN1}^2 - X_{1,DN1}^2 + Z_0^2 + 2Z_0 R_{1,DN1}\right)
$$
$$
-\left(\mathrm{Re}\{S_{A,11}\} + \mathrm{Re}\{S_{A,22}\}\right)\left(R_{1,DN1}^2 - X_{1,DN1}^2 - Z_0^2\right) + 2A_2 R_{1,DN1}X_{1,DN1} \tag{A.2}
$$
$$
+2A_3 Z_0 X_{1,DN1} - 2\,\mathrm{Im}\{S_{A,21}\}Z_0 X_{3,DN1} + 2\,\mathrm{Re}\{S_{A,21}\}Z_0 R_{3,DN1} = 0,
$$

and

$$B_1 \left(R_{1,DN1}^2 - X_{1,DN1}^2 + Z_0^2 - 2Z_0 R_{1,DN1} \right)$$
$$+2B_2 \left(R_{1,DN1} X_{1,DN1} - Z_0 X_{1,DN1} \right) + 2\operatorname{Re}\{S_{A,21}\} Z_0 X_{3,DN1}$$
$$+2Z_0 X_{1,DN1} + 2B_3 R_{1,DN1} X_{1,DN1} + 2\operatorname{Im}\{S_{A,21}\} Z_0 R_{3,DN1}$$
$$-\left(\operatorname{Im}\{S_{A,11}\} + \operatorname{Im}\{S_{A,22}\} \right)\left(R_{1,DN1}^2 - X_{1,DN1}^2 - Z_0^2 \right) = 0. \tag{A.3}$$

The coefficients A_n and B_n, with $n = 1, 2, 3$ are given by

$$A_1 = \operatorname{Re}\{S_{A,11}\}\operatorname{Re}\{S_{A,22}\} - \operatorname{Im}\{S_{A,11}\}\operatorname{Im}\{S_{A,22}\}$$
$$-\left(\operatorname{Re}\{S_{A,21}\} \right)^2 + \left(\operatorname{Im}\{S_{A,21}\} \right)^2, \tag{A.4}$$

$$A_2 = \operatorname{Im}\{S_{A,11}\}\left(1 - \operatorname{Re}\{S_{A,22}\} \right) + \operatorname{Im}\{S_{A,22}\}\left(1 - \operatorname{Re}\{S_{A,11}\} \right)$$
$$+2\operatorname{Re}\{S_{A,21}\}\operatorname{Im}\{S_{A,21}\}, \tag{A.5}$$

$$A_3 = \operatorname{Re}\{S_{A,11}\}\operatorname{Im}\{S_{A,22}\} + \operatorname{Re}\{S_{A,22}\}\operatorname{Im}\{S_{A,11}\}$$
$$-2\operatorname{Re}\{S_{A,21}\}\operatorname{Im}\{S_{A,21}\}, \tag{A.6}$$

$$B_1 = \operatorname{Re}\{S_{A,11}\}\operatorname{Im}\{S_{A,22}\} + \operatorname{Re}\{S_{A,22}\}\operatorname{Im}\{S_{A,11}\}$$
$$-2\operatorname{Re}\{S_{A,21}\}\operatorname{Im}\{S_{A,21}\}, \tag{A.7}$$

$$B_2 = \operatorname{Re}\{S_{A,11}\}\operatorname{Re}\{S_{A,22}\} - \operatorname{Im}\{S_{A,11}\}\operatorname{Im}\{S_{A,22}\}$$
$$-\left(\operatorname{Re}\{S_{A,21}\} \right)^2 + \left(\operatorname{Im}\{S_{A,21}\} \right)^2, \tag{A.8}$$

$$B_3 = 1 - \operatorname{Re}\{S_{A,11}\} - \operatorname{Re}\{S_{A,22}\}. \tag{A.9}$$

If the components of the decoupling network are lossless, $Z_{1,DN1}$ and $Z_{3,DN1}$ are purely imaginary. Then, substituting (A.2) into (A.3) gives a quadratic equation only containing $X_{1,DN1}$

$$C_1 X_{1,DN1}^2 + C_2 X_{1,DN1} + C_3 = 0. \tag{A.10}$$

The coefficients C_n with n = 1, 2, 3 are given by

$$C_1 = \begin{pmatrix} \mathrm{Re}\{S_{A,11}\} + \mathrm{Re}\{S_{A,22}\} - 1 - \mathrm{Re}\{S_{A,11}\}\mathrm{Re}\{S_{A,22}\} \\ + \mathrm{Im}\{S_{A,11}\}\mathrm{Im}\{S_{A,22}\} + \left(\mathrm{Re}\{S_{A,21}\}\right)^2 \end{pmatrix} \mathrm{Re}\{S_{A,21}\}$$
$$+ \begin{pmatrix} \mathrm{Im}\{S_{A,11}\} + \mathrm{Im}\{S_{A,22}\} - \mathrm{Re}\{S_{A,11}\}\mathrm{Im}\{S_{A,22}\} \\ - \mathrm{Re}\{S_{A,22}\}\mathrm{Im}\{S_{A,11}\} + \mathrm{Re}\{S_{A,21}\}\mathrm{Im}\{S_{A,21}\} \end{pmatrix} \mathrm{Im}\{S_{A,21}\}, \quad (A.11)$$

$$C_2 = 2\begin{bmatrix} \begin{pmatrix} 1 - \mathrm{Re}\{S_{A,11}\}\mathrm{Re}\{S_{A,22}\} \\ + \mathrm{Im}\{S_{A,11}\}\mathrm{Im}\{S_{A,22}\} - \left(\mathrm{Im}\{S_{A,21}\}\right)^2 \end{pmatrix} \mathrm{Im}\{S_{A,21}\} \\ - \begin{pmatrix} -\mathrm{Re}\{S_{A,11}\}\mathrm{Im}\{S_{A,22}\} - \mathrm{Re}\{S_{A,22}\}\mathrm{Im}\{S_{A,11}\} \\ + \mathrm{Re}\{S_{A,21}\}\mathrm{Im}\{S_{A,21}\} \end{pmatrix} \mathrm{Re}\{S_{A,21}\} \end{bmatrix} Z_0, \quad (A.12)$$

$$C_3 = \begin{bmatrix} \begin{pmatrix} 1 + \mathrm{Re}\{S_{A,11}\} + \mathrm{Re}\{S_{A,22}\} + \mathrm{Re}\{S_{A,11}\}\mathrm{Re}\{S_{A,22}\} \\ - \mathrm{Im}\{S_{A,11}\}\mathrm{Im}\{S_{A,22}\} - \left(\mathrm{Re}\{S_{A,21}\}\right)^2 \end{pmatrix} \mathrm{Re}\{S_{A,21}\} \\ + \begin{pmatrix} \mathrm{Im}\{S_{A,11}\} + \mathrm{Im}\{S_{A,22}\} + \mathrm{Re}\{S_{A,11}\}\mathrm{Im}\{S_{A,22}\} \\ + \mathrm{Re}\{S_{A,22}\}\mathrm{Im}\{S_{A,11}\} - \left(\mathrm{Im}\{S_{A,21}\}\right)^2 \end{pmatrix} \mathrm{Im}\{S_{A,21}\} \end{bmatrix} Z_0^2. \quad (A.13)$$

Substituting the calculated $Z_{1,\mathrm{DN1}}$ from (A.10) into (A.2) or (A.3), the value of $Z_{3,\mathrm{DN1}}$ also can be computed.

The inductors and capacitors are commonly used in lumped-element networks. Each decoupling component can be simply represented by a single RF component namely an inductor or a capacitor. Therefore, according to the value of $X_{1,\mathrm{DN1}}$ and $X_{3,\mathrm{DN1}}$, four different cases are studied for the lossless and realistic cases.

Assume that the realistic capacitors C have a constant resistance value ($R_{n,\mathrm{DN1}}$ with n = 1, 3) while the realistic inductors L have a constant Q, whose recip-

rocal value of Q factor is defined as q. Then, for the lossless case, $q = 0$. In this case, the relationship between $R_{n,\text{DN1}}$ and $X_{n,\text{DN1}}$, with $n = 1, 3$ of these inductors is given by

$$\frac{X_{n,\text{DN1}}}{R_{n,\text{DN1}}} = Q = \frac{1}{q}. \tag{A.14}$$

If both decoupling components are represented by inductors ($X_{1,\text{DN1}} > 0$ and $X_{3,\text{DN1}} > 0$), (A.1) becomes

$$
\begin{aligned}
&\left(D_1 + jD_2\right)\left(q^2 - 1 + 2jq\right)X_{1,\text{DN1}}^2 + 2\left(D_3 - jD_4\right)(q + j)Z_0 X_{1,\text{DN1}} \\
&+\left(D_5 + jD_6\right)Z_0^2 + 2\left(\text{Re}\{S_{A,21}\} + j\,\text{Im}\{S_{A,21}\}\right)(q + j)Z_0 X_{3,\text{DN1}} = 0,
\end{aligned} \tag{A.15}
$$

where

$$
\begin{aligned}
D_1 = \;&1 - \text{Re}\{S_{A,11}\} - \text{Re}\{S_{A,22}\} + \text{Re}\{S_{A,11}\}\,\text{Re}\{S_{A,22}\} \\
&- \text{Im}\{S_{A,11}\}\,\text{Im}\{S_{A,22}\} - \left(\text{Re}\{S_{A,21}\}\right)^2 + \left(\text{Im}\{S_{A,21}\}\right)^2,
\end{aligned} \tag{A.16}
$$

$$
\begin{aligned}
D_2 = \;&-\text{Im}\{S_{A,11}\} - \text{Im}\{S_{A,22}\} + \text{Re}\{S_{A,11}\}\,\text{Im}\{S_{A,22}\} \\
&+ \text{Re}\{S_{A,22}\}\,\text{Im}\{S_{A,11}\} - 2\,\text{Re}\{S_{A,21}\}\,\text{Im}\{S_{A,21}\},
\end{aligned} \tag{A.17}
$$

$$
\begin{aligned}
D_3 = \;&1 - \text{Re}\{S_{A,11}\}\,\text{Re}\{S_{A,22}\} + \text{Im}\{S_{A,11}\}\,\text{Im}\{S_{A,22}\} \\
&+ \left(\text{Re}\{S_{A,21}\}\right)^2 - \left(\text{Im}\{S_{A,21}\}\right)^2,
\end{aligned} \tag{A.18}
$$

$$
\begin{aligned}
D_4 = \;&\text{Re}\{S_{A,11}\}\,\text{Im}\{S_{A,22}\} + \text{Re}\{S_{A,22}\}\,\text{Im}\{S_{A,11}\} \\
&- 2\,\text{Re}\{S_{A,21}\}\,\text{Im}\{S_{A,21}\},
\end{aligned} \tag{A.19}
$$

$$
\begin{aligned}
D_5 = \;&1 + \text{Re}\{S_{A,11}\} + \text{Re}\{S_{A,22}\} + \text{Re}\{S_{A,11}\}\,\text{Re}\{S_{A,22}\} \\
&- \text{Im}\{S_{A,11}\}\,\text{Im}\{S_{A,22}\} - \left(\text{Re}\{S_{A,21}\}\right)^2 + \left(\text{Im}\{S_{A,21}\}\right)^2,
\end{aligned} \tag{A.20}
$$

$$D_6 = \text{Im}\{S_{A,11}\} + \text{Im}\{S_{A,22}\} + \text{Re}\{S_{A,11}\}\,\text{Im}\{S_{A,22}\}$$
$$+ \text{Re}\{S_{A,22}\}\,\text{Im}\{S_{A,11}\} - 2\,\text{Re}\{S_{A,21}\}\,\text{Im}\{S_{A,21}\}. \tag{A.21}$$

The quadratic equation only containing $X_{1,\text{DN1}}$, derived from (A.15), is then given by

$$
\left(
\begin{array}{l}
D_1 \left(
\begin{array}{l}
\left(\text{Im}\{S_{A,21}\}q + \text{Re}\{S_{A,21}\}\right)\left(q^2 - 1\right) \\
-2\left(\text{Re}\{S_{A,21}\}q - \text{Im}\{S_{A,21}\}\right)q
\end{array}
\right) \\
-D_2 \left(
\begin{array}{l}
2\left(\text{Im}\{S_{A,21}\}q + \text{Re}\{S_{A,21}\}\right)q \\
+\left(\text{Re}\{S_{A,21}\}q - \text{Im}\{S_{A,21}\}\right)\left(q^2 - 1\right)
\end{array}
\right)
\end{array}
\right) X_{1,\text{DN1}}^2
$$
$$
+2\left(
\begin{array}{l}
D_3 \left(
\begin{array}{l}
\left(\text{Im}\{S_{A,21}\}q + \text{Re}\{S_{A,21}\}\right)q \\
-\left(\text{Re}\{S_{A,21}\}q - \text{Im}\{S_{A,21}\}\right)
\end{array}
\right) \\
+D_4 \left(
\begin{array}{l}
\left(\text{Im}\{S_{A,21}\}q + \text{Re}\{S_{A,21}\}\right) \\
+\left(\text{Re}\{S_{A,21}\}q - \text{Im}\{S_{A,21}\}\right)q
\end{array}
\right)
\end{array}
\right) Z_0 X_{1,\text{DN1}}
$$
$$
+D_5 \left(\text{Im}\{S_{A,21}\}q + \text{Re}\{S_{A,21}\}\right) Z_0^2
$$
$$
-D_6 \left(\text{Re}\{S_{A,21}\}q - \text{Im}\{S_{A,21}\}\right) Z_0^2 = 0. \tag{A.22}
$$

If $Z_{1,\text{DN1}}$ is presented by an inductor while a capacitor is used as $Z_{3,\text{DN1}}$ ($X_{1,\text{DN1}} > 0$ and $X_{3,\text{DN1}} < 0$), (A.1) becomes

$$\left(D_1 + jD_2\right)\left(q^2 - 1 + 2jq\right) X_{1,\text{DN1}}^2$$
$$+2\left(D_3 - jD_4\right)(q + j)Z_0 X_{1,\text{DN1}} + \left(D_5 + jD_6\right)Z_0^2 \tag{A.23}$$
$$+2\left(\text{Re}\{S_{A,21}\} + j\,\text{Im}\{S_{A,21}\}\right)\left(R_{3,\text{DN1}} + jX_{3,\text{DN1}}\right)Z_0 = 0,$$

The quadratic equation for $X_{1,\text{DN1}}$ is then expressed as

$$
\begin{aligned}
&\left(\begin{array}{l} D_1\left(\mathrm{Re}\{S_{A,21}\}\left(q^2-1\right)+2\,\mathrm{Im}\{S_{21}\}q\right) \\ +D_2\left(\mathrm{Im}\{S_{A,21}\}\left(q^2-1\right)-2\,\mathrm{Re}\{S_{21}\}q\right) \end{array}\right)X_{1,\mathrm{DN1}}^2 \\
&+2\left(\begin{array}{l} D_3\left(\mathrm{Re}\{S_{A,21}\}q+\mathrm{Im}\{S_{A,21}\}\right) \\ +D_4\left(\mathrm{Re}\{S_{A,21}\}-\mathrm{Im}\{S_{A,21}\}q\right) \end{array}\right)Z_0 X_{1,\mathrm{DN1}} \\
&+\left(D_5\,\mathrm{Re}\{S_{A,21}\}+D_6\,\mathrm{Im}\{S_{A,21}\}\right)Z_0^2 \\
&+2\left(\left(\mathrm{Re}\{S_{A,21}\}\right)^2+\left(\mathrm{Im}\{S_{A,21}\}\right)^2\right)R_{3,\mathrm{DN1}}Z_0=0.
\end{aligned}
\tag{A.24}
$$

If $Z_{1,\mathrm{DN1}}$ is presented by a capacitor while an inductor is implemented as $Z_{3,\mathrm{DN1}}$ ($X_{1,\mathrm{DN1}}<0$ and $X_{3,\mathrm{DN1}}>0$), the transformation of (A.1) is given by

$$
\begin{aligned}
&\left(D_1+jD_2\right)\left(R_{1,\mathrm{DN1}}^2-X_{1,\mathrm{DN1}}^2+2jR_{1,\mathrm{DN1}}X_{1,\mathrm{DN1}}\right) \\
&+2\left(D_3-jD_4\right)\left(R_{1,\mathrm{DN1}}+jX_{1,\mathrm{DN1}}\right)Z_0+\left(D_5+jD_6\right)Z_0^2 \\
&+2\left(\mathrm{Re}\{S_{A,21}\}+j\,\mathrm{Im}\{S_{A,21}\}\right)(q+j)Z_0 X_{3,\mathrm{DN1}}=0.
\end{aligned}
\tag{A.25}
$$

In this case, the quadratic equation for $X_{1,\mathrm{DN1}}$ is expressed as

$$
\begin{aligned}
&\left(-D_1\left(\mathrm{Re}\{S_{A,21}\}+\mathrm{Im}\{S_{A,21}\}q\right)+D_2\left(\mathrm{Re}\{S_{A,21}\}q-\mathrm{Im}\{S_{A,21}\}\right)\right)X_{1,\mathrm{DN1}}^2 \\
&-2\left(\begin{array}{l} \left(\mathrm{Re}\{S_{A,21}\}q-\mathrm{Im}\{S_{A,21}\}\right)\left(D_1 R_{1,\mathrm{DC1}}+D_3 Z_0\right) \\ \left(\mathrm{Re}\{S_{A,21}\}+\mathrm{Im}\{S_{A,21}\}q\right)\left(D_2 R_{1,\mathrm{DC1}}-D_4 Z_0\right) \end{array}\right)X_{1,\mathrm{DN1}} \\
&+\left(D_1\left(\mathrm{Re}\{S_{A,21}\}+\mathrm{Im}\{S_{A,21}\}q\right)-D_2\left(\mathrm{Re}\{S_{A,21}\}q-\mathrm{Im}\{S_{A,21}\}\right)\right)R_{1,\mathrm{DN1}}^2 \\
&+2\left(\begin{array}{l} D_3\left(\mathrm{Re}\{S_{A,21}\}+\mathrm{Im}\{S_{A,21}\}q\right) \\ +D_4\left(\mathrm{Re}\{S_{A,21}\}q-\mathrm{Im}\{S_{A,21}\}\right) \end{array}\right)Z_0 R_{1,\mathrm{DN1}} \\
&+D_5\left(\mathrm{Re}\{S_{A,21}\}+\mathrm{Im}\{S_{A,21}\}q\right)Z_0^2 \\
&-D_6\left(\mathrm{Re}\{S_{A,21}\}q-\mathrm{Im}\{S_{A,21}\}\right)Z_0^2=0.
\end{aligned}
\tag{A.26}
$$

If $Z_{1,\mathrm{DN1}}$ and $Z_{3,\mathrm{DN1}}$ are represented by capacitors ($X_{1,\mathrm{DN1}}<0$ and $X_{3,\mathrm{DN1}}<0$), (A.1) is transformed to

$$\left(D_1 + jD_2 \right)\left(R_{1,\mathrm{DN1}}^2 - X_{1,\mathrm{DN1}}^2 + 2jR_{1,\mathrm{DN1}}X_{1,\mathrm{DN1}} \right)$$
$$+2\left(D_3 - jD_4 \right)Z_0\left(R_{1,\mathrm{DN1}} + jX_{1,\mathrm{DN1}} \right) + \left(D_5 + jD_6 \right)Z_0^2 \qquad\qquad (\mathrm{A.27})$$
$$+2\left(\mathrm{Re}\{S_{\mathrm{A},21}\} + j\,\mathrm{Im}\{S_{\mathrm{A},21}\} \right)\left(R_{3,\mathrm{DN1}} + jX_{3,\mathrm{DN1}} \right)Z_0 = 0,$$

According to (A.27), the quadratic equation for $X_{1,\mathrm{DN1}}$ is given by

$$-\left(D_1\,\mathrm{Re}\{S_{\mathrm{A},21}\} + D_2\,\mathrm{Im}\{S_{\mathrm{A},21}\} \right)X_{1,\mathrm{DN1}}^2$$
$$+2\left(\begin{matrix} \left(-D_2 R_{1,\mathrm{DN1}} + D_4 Z_0 \right)\mathrm{Re}\{S_{\mathrm{A},21}\} \\ +\left(D_1 R_{1,\mathrm{DN1}} + D_3 Z_0 \right)\mathrm{Im}\{S_{\mathrm{A},21}\} \end{matrix} \right)X_{1,\mathrm{DN1}}$$
$$+\left(D_1\,\mathrm{Re}\{S_{\mathrm{A},21}\} + D_2\,\mathrm{Im}\{S_{\mathrm{A},21}\} \right)R_{1,\mathrm{DN1}}^2 \qquad\qquad (\mathrm{A.28})$$
$$+2\left(D_3\,\mathrm{Re}\{S_{\mathrm{A},21}\} - D_4\,\mathrm{Im}\{S_{\mathrm{A},21}\} \right)Z_0 R_{1,\mathrm{DN1}}$$
$$+\left(D_5\,\mathrm{Re}\{S_{\mathrm{A},21}\} + D_6\,\mathrm{Im}\{S_{\mathrm{A},21}\} \right)Z_0^2$$
$$+2\left(\left(\mathrm{Re}\{S_{\mathrm{A},21}\} \right)^2 + \left(\mathrm{Im}\{S_{\mathrm{A},21}\} \right)^2 \right)R_{3,\mathrm{DN1}}Z_0 = 0.$$

The value of $X_{3,\mathrm{DN1}}$ can be calculated by substituting the value of $X_{1,\mathrm{DN1}}$ into (A.22), (A.24), (A.26) or (A.28) for the four different cases. Usually, two different solutions of $X_{1,\mathrm{DN1}}$ and $X_{3,\mathrm{DN1}}$ can be obtained. As the tunability of the realistic tunable components is limited, a low frequency variation of their required reactances would be useful for their utilization over a broad frequency range. To reduce this variation, the solution with the lower quadratic sum of $X_{1,\mathrm{DN1}}$ and $X_{3,\mathrm{DN1}}$ is chosen. The decoupling can be realized in the cases, in which the sign of both calculated reactances corresponds to the assumption.

Bibliography

[Abu09]   H. F. AbuTarboush, R. Nilavalan, H. S. Al-Raweshidy, and D. Budimir, "Design of ülanar inverted-F antennas (PIFA) for multiband wireless applications," *International Conference on Electromagnetics in Advanced Applications*, pp. 78-81, Sep. 2009.

[Ads]   Advanced Design System website [Online] Available: http://www.keysight.com/en/pc-1297113/advanced-design-system-ads.

[All11]   W. N. Allen and D. Peroulis, "Bandwidth-optimal single-tunable-element matching network for antenna tuning in mobile handsets," *IEEE MTT-S International Microwave Symposium*, pp. 1-4, Jun. 2011.

[Bah03]   I. Bahr and P. Bhartia, *Microwave solid state circuit design*, Hoboken, New Jersey: John Wiley & Sons, Inc., 2003.

[Bah14]   I. J. Bahl, *Control Components using Si, GaAs, and GaN Technologies*, Artech House, 2014.

[Bar61]   S. H. Barnes and J. E. Mann, *Voltage Sensitive Semiconductor Capacitor*, U.S. Patent 2989671 A, Jun. 1961.

[Bau97]   B. A. Baumert *et al.*, "Characterization of sputtered barium strontium titanate and strontium titanate-thin films," *Journal of Applied Physics*, vol. 82, no. 5, pp. 2558-2566, Jun. 1997.

[Beh06]   N. Behdad and K. Sarabandi, "Dual-band reconfigurable antenna with a very wide tunability range," *IEEE Transactions on Antennas and Propagation*, vol. 54, no. 2, pp. 409-416, Feb. 2006.

[Bez08]   A. v. Bezooijen *et al.*, "A GSM/EDGE/WCDMA adaptive series-LC matching network using RF-MEMS switches," *IEEE Journal of Solid-State Circuits*, vol. 43, no. 10, pp. 2259-2268, Oct. 2008.

[Bez11]   A. v. Bezooijen, R. Mahmoudi, and A. v. Roermund, *Adaptive RF front-ends for hand-held applications*, Springer, 2011.

[Bod45]   H. W. Bode, *Network Analysis and Feedback Amplifier Design*, New York, D. Van Nostrand Co., Inc., 1945.

[Bor03]   R. L. Borwick, P. A. Stupar, J. F. DeNatale, R. Anderson, and R. Erlandson, "Variable MEMS capacitors implemented into RF filter systems," *IEEE Transactions on Microwave Theory and Techniques*, vol. 51, no. 1, pp. 315-319, Jan 2003.

Bibliography

[Boy07] K. R. Boyle, Y. Yuan, L. P. Ligthart, "Analysis of mobile phone antenna impedance variations with user proximity," *IEEE Transactions on Antennas and Propagation*, vol.55, no.2, pp.364-372, Feb. 2007.

[Boy13] K. R. Boyle *et al.*, "Gain statistics for mobile phone antenna tuners," *European Conference on Antennas and Propagation (EUCAP)*, pp. 432-436, Apr. 2013.

[Bra01] J. Brank *et al.*, "RF MEMS-based tunable filters", *International Journal of RF and Microwave Computer-Aided Engineering*, vol. 11, pp. 276–284, Sep. 2001.

[Cai11] Y. Cai, Y. J. Guo, "A reconfigurable decoupling and matching network for a frequency agile compact array," *European Conference on Antennas and Propagation (EUCAP)*, pp.896-899, Apr. 2011.

[Car12] A. H. Cardona, "Tunable BaSrTiO3 applications for the RF front end," *IEEE MTT-S International Microwave Symposium Digest (MTT)*, pp. 1-3, Jun. 2012.

[Car83] H. J. Carlin, B. S. Yarman, "The double matching problem: analytic and real frequency solutions," *IEEE Transactions on Circuits and Systems*, vol.30, no.1, pp.15-28, Jan. 1983.

[Cas12] F. Casado, A. Arriola, J. Parrón, E. Arruti, I. Ortego and J. I. Sancho, "Reconfigurable matching network for 2.45 GHz printed IFA on metallic environments," *Loughborough Antennas and Propagation Conference (LAPC)*, pp. 1-4, Nov. 2012.

[Cha05] D. R. Chase, Lee-Yin Chen, and R. A. York, "Modeling the capacitive nonlinearity in thin-film BST varactors," *IEEE Transactions on Microwave Theory and Techniques*, vol. 53, no. 10, pp. 3215-3220, Oct. 2005.

[Cha11] C. C. Chang *et al.*, "Design of millimeter-wave MEMS-based reconfigurable front-end circuits using the standard CMOS technology," *Journal of Micromechanics and Microengineering*, vol. 21, no. 12, Nov. 2011.

[Che04] L. Y. Vicki Chen, R. Forse, D. Chase, and R. A. York, "Analog tunable matching network using integrated thin-film BST capacitors," *IEEE MTT-S International Microwave Symposium Digest*, pp. 261-264 vol.1, Jun. 2004.

[Che08] S.-C. Chen, Y.-S. Wang, and S.-J. Chung, "A decoupling technique for increasing the port isolation between two strongly coupled antennas," *IEEE Transactions on Antennas and Propagation*, vol. 56, no. 12, pp. 3650–3658, Dec. 2008.

[Che12] Y. Chen, and D. Manteuffel, "Distributed MEMS impedance matching network using a SW-DGS technique," *Loughborough Antennas and Propagation Conference (LAPC)*, pp. 1-4, Nov. 2012.

[Che13] Y. Chen, and D. Manteuffel, "Miniaturizing the distributed MEMS impedance matching networks for wireless communications," *International Workshop of Antenna Technology (IWAT)*, pp. 303-306, Mar. 2013.

[Che14]   Y. Chen, R. Martens, R. Valkonen, and D. Manteuffel, "A varactor-based tunable matching network for a non-resonant mobile terminal antenna," *European Conference on Antennas and Propagation (EUCAP)*, pp. 2225-2229, Apr. 2014.

[Che15]   Y. Chen, R. Martens, R. Valkonen, and D. Manteuffel, "Evaluation of adaptive impedance tuning for reducing the form factor of handset antennas," *IEEE Transactions on Antennas and Propagation*, vol. 63, pp. 703-710, Feb. 2015.

[Che17]   Y. Chen, and D. Manteuffel, "A tunable decoupling and matching concept for compact mobile terminal antennas," *IEEE Transactions on Antennas and Propagation*, vol. 65, pp. 1570-1578, Apr. 2017.

[Che88]   W. K. Chen, *Broadband Matching: Theory and Implementations*, second edition, IEEE Press Series on Electromagnetic Wave Theory, Singapore, World Scientific Publishing Co. Pte. Ltd., 1988.

[Chi07]   C. Y. Chiu, C. H. Cheng, R. D. Murch, , and C. R. Rowell, "Reduction of mutual coupling between closely-packed antenna elements," *IEEE Transactions on Antennas and Propagation*, vol. 55, no. 6, pp. 1732–1738, Jun. 2007.

[Chi16]   T. Chiu, C. Hung, and K. Hsu, "Reconfigurable resonant module for multi-band antenna design," *IET Microwaves, Antennas & Propagation*, vol. 10, no. 3, pp. 326-332, Feb. 2016.

[Coe11]   J. C. Coetzee, "Dual-frequency decoupling networks for compact antenna arrays," *International Journal Microwave Science Technology*, pp. 1-3, Jan. 2011.

[Cor12]   G. Cornetta, D. J. Santos, and J. M. Vazquez, *Wireless Radio-Frequency Standards and System Design: Advanced Techniques*, Engineering Science Reference, 2012.

[Cox02]   J. Cox, *Fundamentals of Linear Electronics: Integrated and Discrete*, Albany, NY: Delmar, 2002.

[Cti]   *CTIA Test Plan for Mobile Station over the Air Performance*, Rev. 3.1, Dec. 2010, (Draft), www.ctia.org.

[Cut99]   T. R. Cuthbert, *Broadband direct-coupled and matching RF networks*, Greenwood, AR.: TRCPEP Publications, 1999.

[Dar39]   S. Darlington, "Synthesis of reactance 4-poles which produce prescribed insertion loss characteristics: including special applications to filter design," *Journal of Mathematics and Physics*, vol. 18, pp. 257–353, Apr. 1939.

[Dia08]   A. Diallo, C. Luxey, P. L. Thuc, R. Staraj, and G. Kossiavas, "Enhanced two-antenna structures for universal mobile telecommunications system diversity terminals," *IET Microwaves, Antennas & Propagation*, vol. 2, no. 1, pp. 93–101, Feb. 2008.

[Dob10]   J. A. Dobrowolski, *Microwave Network Design using the Scattering Matrix*, Norwood, MA: Artech House, 2010.

Bibliography

[Dos04]   S. Dossche, S. Blanch, and J. Romeu, "Optimum antenna matching to mini-mise signal correlation on a two-port antenna diversity system," *Electronics Letters*, vol. 40, no. 19, pp. 1164–1165, Sep. 2004.

[Egg11]   D. L. Eggleston, *Basic Electronics for Scientists and Engineers*, Cambridge, UK: Cambridge University Press, 2011.

[Ela13]   N. I. M. Elamin, T. A. Rahman, A. Y. Abdulrahman, "New adjustable slot meander patch antenna for 4G handheld devices," *IEEE Antennas and Wireless Propagation Letters*, vol.12, pp.1077-1080, Sep. 2013.

[Elf12]   I. T. E. Elfergani *et al*., "Reconfigurable antenna design for mobile handsets including harmonic radiation measurements," *IET Microwaves, Antennas & Propagation*, vol. 6, no. 9, pp. 990-999, Jun. 2012.

[Emp]   Empire XPU (2015) website [Online] Available: htttp://www.empire.de

[Epc]   Epcos AG, Munich, Germany.

[Epc08]   *Application Note SAW-Components, ESD Protection for SAW Filters Application Note #17*, EPCOS AG, Munich, Germany, 2008.

[Fab07]   M. C. Fabrés, *Systematic Design of Antennas using the Theory of Characteristic Modes*, Ph.D. dissertation, School of Telecommunications Engineering, Polytechnic University of Valencia, Valencia, Spain, 2007.

[Far07]   E. A. Fardin, *Barium Strontium Titanate Thin Films for Tunable Applications*, Ph. D. dissertation, School of Electrical and Computer Engineering Science, RMIT University, Melbourne, Australia, 2007.

[Fos98]   G. J. Foschini and M. J. Gans, "On limits of wireless communications in a fading environment when using multiple antennas," *Wireless Personal Communications*, vol. 6, pp. 311–335, Mar. 1998.

[Fre08]   J. Frei, X. D. Cai, and S. Muller, "Multiport *S*-parameter and *T*-parameter conversion with symmetry extension," *IEEE Transactions on Microwave Theory and Techniques*, vol. 56, no. 11, pp. 2493-2504, Nov. 2008.

[Fuj08]   K. Fujimoto, *Mobile Antenna Systems Handbook*, Norwood, MA: Artech House, 2008.

[Ful10]   P. Fulay, *Electronic, Magnetic and Optical Materials*, CRC press, 2010.

[Gar13]   J. L. T. Garzon, A. A. de Salles, A. C. O. Pedra, and S. Severo, "T-slot PIFA with excitation of the ground plane resonant modes and considerations of the interaction between antenna, mobile handset and user's head," *SBMO/IEEE MTT-S Interactional Microwave and Optoelectronics Conference (IMOC)*, pp. 1-5, Aug. 2013.

[Gil03]   R. Gilmore and L. Besser, *Practical RF Circuit Design for Modern Wireless Systems: Active Circuits and Systems*, Norwood, MA: Artech House, 2003.

[Glo05]   I. A. Glover, S. R. Pennock, and P. R. Shepherd, *Microwave Devices, Circuits and Subsystems for Communications Engineering*, Chichester, England: John Wiley & Sons Ltd, Inc., 2005.

[Gev09]   S. Gevorgian, *Ferroelectrics in Microwave Devices, Circuits and Systems: Physics, Modeling, Fabrication and Measurements*, Springer, 2009.

[Gpp12]   3GPP technical specification 36.101, "E-UTRA user equipment (UE) radio transmission and reception (release 10)", V10.8.0, Sep. 2012.

[Gu11]   Q. Gu, J. R. De Luis, A. S. Morris, and J. Hilbert, "An analytical algorithm for pi-network impedance tuners," *IEEE Transactions on Circuits and Systems*, vol. 58, pp. 2894-2905, Dec. 2011.

[Gu13]   Q. Gu, A. S. Morris, "A new method for matching network adaptive control," *IEEE Transactions on Microwave Theory and Techniques*, vol.61, no.1, pp.587-595, Jan. 2013.

[Gu15]   Q. Gu, *RF Tunable Devices and Subsystems: Methods of Modeling, Analysis and Applications*, Springer, 2015.

[Guo13]   Q. Guo *et al.*, "Interaction between internal antenna and external antenna of mobile phone and hand effect," *IEEE Transactions on Antennas and Propagation*, vol. 61, pp. 862-870, Feb. 2013.

[Gup13]   P. Gupta, P. Singh, R. K. Chaudhry, and P. Srivastava, "Design and analysis of RF MEMS varactor for extended tuning range," *International Conference on Control, Computing, Communication & Materials (ICCCCM)*, pp. 1-4, Aug. 2013.

[Gup83]   I. J. Gupta, A. A. Ksienski, "Effect of mutual coupling on the performance of adaptive arrays," *IEEE Transactions on Antennas and Propagation*, vol.31, no.5, pp.785-791, Sep. 1983.

[Hil16]   J. L. Hilbert, *Tunable RF Components and Circuits: Applications in Mobile Handsets*, Boca Raton, FL, CRC Press.

[Hol10a]   J. Holopainen, R. Valkonen, R. Kivekas, J. Ilvonen, P. Vainikainen, "Broadband equivalent circuit model for capacitive coupling element-based mobile terminal antenna," *IEEE Antennas and Wireless Propagation Letters*, vol.9, pp.716-719, Jul. 2010.

[Hol10b]   J. Holopainen *et al.*, "Equivalent circuit model-based approach on the user body effect of a mobile terminal antenna," *Loughborough Antennas and Propagation Conference (LAPC)*, pp. 217-220, Nov. 2010.

[Hua07]   T. Huang, K. R. Boyle, "User interaction studies on handset antennas," *European Conference on Antennas and Propagation (EUCAP)*, pp. 1-6, Nov. 2007.

[Hua08]   Y. Huang, K. Boyle, *Antennas From Theory to Practice*, Chichester, UK: John Wiley & Sons Ltd, 2008.

[Hua10]   C. Huang *et al.*, "Low distortion tunable RF components, a compound semiconductor opportunity", *CS ManTech Conference*, pp. 13-17, May 2010.

[Hui07]   H. T. Hui, "Decoupling methods for the mutual coupling effect in antenna arrays: a review", *Recent Patens on Engineering*, vol. 1, no. 2, pp. 187-193, Apr. 2007.

147

Bibliography

[Ian13]   Jacopo Iannacci, *Practical Guide to RF-MEMS*, Weinheim, Germany: Wiley-VCH GmbH & Co., 2006.

[Ida04]   I. Ida, J.-I. Takada, T. Toda, and Y. Oishi, "An adaptive impedance matching system and its application to mobile antennas," *IEEE Region 10 Conference*, pp. 543-546, Nov. 2004.

[Ilv11]   J. Ilvonen, O. Kivekas, J. Holopainen, R. Valkonen, K. Rasilainen, and P. Vainikainen, "Mobile terminal antenna performance with the user's hand: effect of antenna dimensioning and location," *IEEE Antennas and Wireless Propagation Letters*, vol. 10, no. , pp. 772-775, Aug. 2011.

[Ilv12]   J. Ilvonen, R. Valkonen, J. Holopainen, O. Kivekas, P. Vainikainen, "Reducing the interaction between user and mobile terminal antenna based on antenna shielding," *European Conference on Antennas and Propagation (EUCAP)*, pp.1889-1893, Mar. 2012.

[Ilv14a]   J. Ilvonen, R. Valkonen, J. Holopainen and V. Viikari, "Design strategy for 4G handset antennas and a multiband hybrid antenna," *IEEE Transactions on Antennas and Propagation*, vol. 62, no. 4, pp. 1918-1927, Apr. 2014.

[Ilv14b]   J. Ilvonen, *Multiband and Environment Insensitive Handset Antennas*, Ph. D. dissertation, Department of Radio Science and Engineering, Aalto University, Espoo, Finland, 2014.

[Ima91]   Y. Imamura, "Variable capacitance capacitor array," US5117206, June 1991.

[Inf04]   *Application Note No. 086 Silicon Discretes,* Infineon Technologies AG, Germany, 2004.

[Ion02]   G. V. Ionis, A. Dec, and K. Suyama, "Differential multi-finger MEMS tunable capacitors for RF integrated circuits," *IEEE MTT-S International Microwave Symposium Digest*, vol. 1, pp. 345-348, Jun. 2002.

[Jai10]   R. P. Jain, *Modern Digital Electronics*, New Delhi: Tata McGraw-Hill Publishing Company Limited, 2010.

[Jak04]   R. Jakoby, P. Scheele, S. Muller, and C. Weil, "Nonlinear dielectrics for tunable microwave components," *International Conference on Microwaves, Radar and Wireless Communications*, pp. 369-378, vol.2, May 2004.

[Jam04]   A. Jamil, T. S. Kalkur, and N. Cramer, "Verilog-A modeling of ferroelectric high-K capacitors for tunable circuit applications," *Integrated Ferroelectrics*, vol. 66, pp. 163-170, May 2004.

[Kab01]   A. K. Kabir, *Voltage Controlled Oscillators Tuned with BST Ferroelectric Capacitors*, Ph. D. dissertation, Department of Electrical and Computer Engineering, University of Colorado, 2001.

[Khi15]   A. Khidre, F. Yang and A. Z. Elsherbeni, "A patch antenna with a varactor-loaded slot for reconfigurable dual-band operation," *IEEE Transactions on Antennas and Propagation*, vol. 63, no. 2, pp. 755-760, Feb. 2015.

[Kim12]   B.-N. Kim, and J.-H. Jung, *Broadband Antenna using Coupling Matching with Short-Circuited End of Radiator*, U.S. Patent 13/264 680, Feb. 2012.

148

[Kor98]   V. Korenivski and R. B. van Dover, "Design of high frequency inductors based on magnetic films," *IEEE Transactions on Magnetics*, vol. 34, no. 4, pp. 1375-1377, Jul. 1998.

[Kre14]   A. Krewski, A. Schroeder, "Electrically switchable multiport matching network for 2-port MIMO antennas," *European Conference on Antennas and Propagation (EuCAP)*, pp. 2827-2828, Apr. 2014.

[Kuo10]   R. Kuonanoja, "Low correlation handset antenna configuration for LTE MIMO applications," *IEEE Antennas and Propagation Society International Symposium (APSURSI)*, pp.1-4, Jul. 2010.

[Kur65]   K. Kurokawa, "Power waves and the scattering matrix", *IEEE Trans. Microwave Theory Techniques*, vol. 13, no. 2, pp. 194-202, Mar. 1965.

[Kiv05]   O. Kivekas, *Design of High Efficiency Antenna for Mobile Communications Devices*, Ph. D. dissertation, Department of Radio Science and Engineering, Aalto University, Espoo, Finland, 2005.

[Lar91]   L. E. Larson, R. H. Hackett, M. A. Melendes, and R. F. Lohr, "Micromachined microwave actuator (MIMAC) technology – a new tuning approach for microwave integrated circuits," *Microwave Millimeter-Wave Monolithic Circuits Symposium*, pp. 27-30, Jun. 1991.

[Lau03]   M. A. Laughton, D. J. Warne, *Electrical Engineer's Reference Book*, Burlington, MA: Elsevier Science, 2003.

[Lau06a]   B. K. Lau, J. B. Andersen, A. F. Molisch, G. Kristensson, "Antenna matching for capacity maximization in compact MIMO systems," *International Symposium on Wireless Communication Systems (ISWCS)*, pp.253-257, Sep. 2006.

[Lau06b]   B. K. Lau, J. B. Andersen, G. Kristensson, and A. F. Molisch, "Impact of matching network on bandwidth of compact antenna arrays," *IEEE Transactions on Antennas and Propagation*, vol. 54, no. 11, pp. 3225-3238, Nov. 2006.

[Lau12]   B. Lau and J. Andersen, "Simple and efficient decoupling of compact arrays with parasitic scatterers," *IEEE Transactions on Antennas and Propagation*, vol. 60, no. 2, pp. 464-472, Feb. 2012.

[Li08]   Y. Li, C. Luxey, B. Derat, D. Pasquet, and J.-C. Bolomey, "Comparison between matching circuits and parasitic patches to enlarge the bandwidth of a mobile phone," *International Symposium Antennas and Propagation (ISAP)*, vol. 60, no. 2, pp. 464-472, Oct. 2008.

[Li09]   C.-H. Li, E. Ofli, N. Chavannes, and N. Kuster, "Effects of hand phantom on mobile phone antenna performance," *IEEE Transactions on Antennas and Propagation*, vol. 57, no. 9, pp. 2763-2770, Sep. 2009.

[Lim10]   J. H. Lim, G. T. Back, Y. I. Ko, C. W. Song and T. Y. Yun, "A reconfigurable PIFA using a switchable PIN-diode and a fine-tuning varactor for USPCS/WCDMA/m-WiMAX/WLAN," *IEEE Transactions on Antennas and Propagation*, vol. 58, no. 7, pp. 2404-2411, July 2010.

Bibliography

[Lin08]   P. Lindberg, A. Kaikkonen, and B. Kochali, "Body loss measurements of internal terminal antennas in talk position using real human operator," *International Workshop on Antenna Technology (IWAT)*, pp. 358-361, Mar. 2008.

[Liu06]   C. Liu, *Foundations of MEMS*, Upper Saddle River, New Jersey: Pearson Education, Inc., 2006.

[Liu09]   D. Liu, B. Gaucher, U. Pfeiffer, and J. Grzyb, *Advanced Millimeter-wave Technologies: Antennas, Packaging and Circuits*, ISBN 9780470996171, John Wiley & Sons, 2009.

[Liu10]   C. L. Liu, Y. F. Lin, C. M. Liang, S. C. Pan, and H. M. Chen, "Miniature internal penta-band monopole antenna for mobile phones," *IEEE Transactions on Antennas and Propagation*, vol. 58, no. 3, pp. 1008-1011, Mar. 2010

[Liu14]   C.-C. Liu, and Y.-H. Lin, *Broadband Antenna Element*, U.S. Patent 13/689 782, Feb. 2014.

[Luc10]   S. Lucyszyn, *Advanced RF MEMS*, New York: Cambridge University Press, 2010.

[Lud76]   A. C. Ludwig, "Mutual coupling, gain, and directivity of an array of two identical antennas," *IEEE Transaction on Antenna and Propagation*, vol. 24, no. 6, pp. 837-841, Nov. 1976.

[Mad07]   M. Maddela, R. Ramadoss and R. Lempkowski, "PCB MEMS-based tunable coplanar patch antenna," *IEEE International Symposium on Industrial Electronics*, pp. 3255-3260, Jun. 2007.

[Mal12]   L. G. Maloratsky, *Integrated Microwave Front-Ends with Avionics Applications*, Artech House, 2012.

[Mar13]   R. Martens, J. Holopainen, E. Safin, J. Ilvonen, and D. Manteuffel, "Optimal dual-antenna design in a small terminal multiantenna system," *IEEE Antennas and Wireless Propagation Letter*, vol. 12, pp. 1700-1703, Dec. 2013.

[Mar14]   R. Martens, Y. Chen, and D. Manteuffel, "Tunability comparison of a capacitive coupling element and a planar inverted-F antenna," *Loughborough Antennas and Propagation Conference (LAPC)*, pp. 667-668, Nov. 2014.

[Mar15]   F. Martin, *Artificial Transmission Lines for RF and Microwave Applications*, John Wiley & Sons. Inc., New Jersey, US, 2015.

[MAT]   MATLAB (R2015a) website [Online] Available: http://www.mathworks.de

[Mav96]   R. Mavaddat, *Network Scattering Parameters*, World Scientific, Singapore, 1996.

[Mcl96]   J. S. McLean, "A re-examination of the fundamental limits on the radiation Q of electrically small antennas," *IEEE Transactions on Antennas and Propagation*, vol. 44, pp. 672-675, May 1996.

[Mor11]   A. S. Morris, Q. Gu, M. Ozkar, and S. P. Natarajan, "High performance tuners for handsets," *IEEE MTT-S International Microwave Symposium Digest (MTT)*, pp. 1-4, Jun. 2011.

[Mot73]   *Application Note AN-551 Tuning Diodes Design Techniques*, Motorola Semi-conductor Products Inc., 1973.

[Mul00]   J. B. Muldavin and G. M. Rebeiz, "High isolation CPW MEMS shunt switches part 1: modeling," *IEEE Transaction on Microwave Theory and Techniques*, vol. 48, pp. 1045-1052, Jun. 2000.

[Mur]   Murata Manufacturing Co., Ltd.. Nagaokakyo, Kyoto, Japan.

[Mur11]   N. Murtaza, M. A. Hein, E. Zameshaeva, "Reconfigurable decoupling and matching network for a cognitive antenna," *European Microwave Conference (EuMC)*, pp.874-877, Oct. 2011.

[Nat06]   J. Nath, *Design and Characterization of Frequency Agile RF and Microwave Devices using Ferroelectrics*, Ph. D. dissertation, North Carolina State University, North Carolina, USA, 2006.

[Nat11]   S. P. Natarajan, S. J. Cunningham, A. S. Morris, and D. R. Dereus, "CMOS integrated digital RF MEMS capacitors," *IEEE 11th Topical Meeting on Silicon Monolithic Integrated Circuits in RF Systems (SiRF)*, pp. 173-176, Jan. 2011.

[Ngu08]   V. A. Nguyen, R. A. Bhatti, and S. O. Park, "A simple PIFA-based tunable internal antenna for personal communication handsets," *IEEE Antennas and Wireless Propagation Letters*, vol. 7, pp. 130-133, May 2008.

[Ngu12]   V. H. Nguyen *et al.*, "Miniaturized and reconfigurable notch antennas using a BST thin film varactor," *Proceedings of the 2012 IEEE International Symposium on Antennas and Propagation*, pp. 1-2, Jul. 2012.

[Nin06]   N. Ning *et al.*, "A tunable magnetic inductor," *IEEE Transactions on Magnetics*, vol. 42, no. 5, pp. 1585-1590, May 2006.

[Obe04]   J. Oberhammer, *Novel RF MEMS Switch and Packaging Concepts*, Ph.D. dissertation, Department of Signals, Sensors and Systems, Royal Institute of Technology, Stockholm, Sweden, 2004.

[Oh07]   S. K. Oh, H. S. Yoon, and S. O. Park, "A PIFA-type varactor-tunable slim antenna with a PIL patch feed for multiband applications," *IEEE Antennas and Wireless Propagation Letters*, vol. 6, pp. 103-105, Apr. 2007.

[Pag15]   J. Pagazani *et al.*, "A RF tunable agile filter: from component to system design," *Symposium on Design, Test, Integration and Packaging of MEMS/MOEMS (DTIP)*, pp. 1-6, Apr. 2015.

[Rah07]   J. Rahola, J. Ollikainen, "Analysis of isolation of two-port antenna systems using simultaneous matching," *European Conference on Antennas and Propagation (EuCAP)*, pp. 1-5, Nov. 2007.

[Rah13]   J. Rahola, "Simultaneous multiport matching circuit optimization for multi-antenna systems," *European Conference on Antennas and Propagation (EuCAP)*, pp. 2778-2781, Apr. 2013.

Bibliography

[Ram16]   M. Rammal *et al.*, "BST thin film capacitors integrated within a frequency tunable antenna," *International Workshop on Antenna Technology (iWAT)*, pp. 44-47, Mar. 2016.

[Pap03]   J. Papapolymerou, K. L. Lange, C. L. Goldsmith, A. Malczewski and J. Kleber, "Reconfigurable double-stub tuners using MEMS switches for intelligent RF front-ends," *IEEE Transaction on Microwave Theory and Techniques*, vol. 51, pp. 271-278, Jan. 2003.

[Pat08]   D. R. Patrick and S. W. Fardo, *Electricity and Electronics Fundamentals*, CRC Press, 2008.

[Pat12]   C. D. Patel, *High Performance RF MEMS Metal-Contact Switches and Switching Networks*, Ph. D. dissertation, University of California, San Diego, US, 2012.

[Pay13]   K. Payandehjoo and R. Abhari, "Compact multi-band PIFAs on a semi-populated mobile handset with tunable isolation," *IEEE Transactions on Antennas and Propagation*, vol. 61, no. 9, pp. 4814-4819, Sep. 2013.

[Pet14]   A. Petoa, *Frequency-Agile Antennas for Wireless Communications*, Norwood, MA: Artech House, 2014.

[Poi12]   R. A. Poisel, *Antenna Systems and Electronic Warfare Applications*, Norwood, MA: Artech House, 2012.

[Pol09]   M. Pelosi, O. Franek, M. B. Knudsen, and G. F. Pedersen, "User's proximity effects in mobile phones," *European Conference on Antennas and Propagation (EuCAP)*, pp.1022-1024, Mar. 2009.

[Poz11]   D. M. Pozar, *Microwave Engineering*, ISBN 978-0470631553, John Wiley & Sons, 2011.

[Qia05]   D. Qiao *et al.*, "Antenna impedance mismatch measurement and correction for adaptive CDMA transceivers," *IEEE MTT-S International Microwave Symposium Digest,* pp. 783-786, Jun. 2005.

[Rad]   RadantMEMS, Littleton, MA, US.

[Ram12]   P. Ramachandran, Z. Milosavljevic, and C. Beckman, "Adaptive penta-band handset Antenna with hand effect compensation," *IET Microwaves Antennas & Propagation*, vol. 6, pp. 79-86, Jan. 2012.

[Reb03a]   G. M. Rebeiz, *RF MEMS Theory, Design, and Technology*, Hoboken, New Jersey: John Wiley & Sons, Inc., 2003.

[Reb03b]   G. M. Rebeiz, "RF MEMS switches: status of the technology," *International Conference on Solid-State Sensors, Actuators and Microsystems*, vol.2, pp. 1726-1729, June 2003.

[Reb09]   G. M. Rebeiz *et al.*, "Tuning in to RF MEMS," *IEEE Microwave Magazine*, vol.10, no.6, pp.55-72, Oct. 2009.

[Rei04]   E. D. Reilly, *Concise Encyclopedia of Computer Science*, Hoboken, NJ, USA: Wiley, 2004.

[Riz02]   J. B. Rizk, and G. M. Rebeiz, "Digital-type RF MEMS switched capacitors," *IEEE MTT-S International Microwave Symposium Digest*, vol.2, pp. 1217-1220, June 2002.

[Rob01]   I. D. Robertson and S. Lucyszyn, *RFIC and MMIC Design and Technology*, London: The Institution of Engineering and Technology, 2001.

[Row12]   C. Rowell and E. Y. Lam, "Mobile-phone antenna design," *IEEE Antennas and Propagation Magazine*, vol. 54, pp. 14-34, Aug. 2012.

[Saa08]   J. Saal, J. Andelm, W. D. Nothwang, and M. W. Cole, "The impact of acceptor dopent magnesium and oxygen vacancy defects on the lattice of barium strontium titanate," *Integrated Ferroelectrics*, vol.101, pp.142-151, 2008.

[Sal16]   S. Salivahanan, N. Suresh Kumar, and A. Vallavaraj, *Electronic Devices and Circuits*, New Delhi: Tata McGraw-Hill Publishing Company Limited, 2016.

[Sal78]   N. Saleh, "Variable microelectronic inductors," *IEEE Transactions on Components, Hybrids, and Manufacturing Technology*, vol. 1, no. 1, pp. 118-124, Mar. 1978.

[Sch04]   D. F. Schwartz, J. C. Allen, "Wide-band impedance matching: H^∞ performance bounds," *IEEE Transactions on Circuits and Systems II: Express Briefs*, vol.51, no.7, pp.364-368, Jul. 2004.

[Sha03]   M. V. Shakhrai, "Microelectromechanical (MEMS) varactors for mobile communications," *Siberian Russian Workshop on Electron Devices and Material*, pp. 3-9, Jul. 2003.

[Sin11]   M. Singh, T. Ohji, R. Asthana, and S. Mathur, *Ceramic Integration and Joining Technologies: From Macro to Nanoscale*, Hoboken, New Jersey: John Wiley & Sons, Inc., 2011.

[Sky12]   Skyworks Solutions, *SMV123x Series: Hyperabrupt Junction Tuning Varactors*, datasheet, Jun. 2012.

[Smi93]   B. L. Smith and M.-H. Carpentier, *The Microwave Engineering Handbook*, Chapman & Hall, 1993.

[Smi13]   N. J. Smith, C. Chen, J. L. Volakis, "An improved topology for adaptive agile impedance tuners," *IEEE Antennas and Wireless Propagation Letters*, vol.12, pp.92-95, Jan. 2013.

[Spe]   SPEAG, Schmid & Partner Engineering AG. Zürich, Switzerland.

[Swe07]   A. A. Sweet, *Designing Bipolar Transistor Radio Frequency Integrated Circuits*, Artechhouse, 2007.

[Tan12]   X. Tang, K. Mouthaan, J. C. Coetzee, "Tunable decoupling and matching network for diversity enhancement of Closely Spaced Antennas," *IEEE Antennas and Wireless Propagation Letters*, vol.11, pp.268-271, Feb. 2012.

[Tan82]   Aram A. Tanielian, Joan M. Crishal, *Pin diode switchable capacitance arrays*, Semetex Corporation, Defense Technical Information Center, Dec. 1982.

Bibliography

[Tom02]   A. Tombak *et al.*, "Tunable barium strontium titanate thin film capacitors for RF and microwave applications," *IEEE Microwave and Wireless Components Letters*, vol. 12, no. 1, pp. 3-5, Jan. 2002.

[Vai02]   P. Vainikainen, J. Ollikainen, O. Kivekäs, and I. Kelander, "Resonator-based analysis of the combination of mobile handset antenna and chassis," *IEEE Transactions on Antennas and Propagation*, vol. 50, pp. 1433-1444, Oct. 2002.

[Val07]   R. Valkonen, J. Holopainen, C. Icheln, P. Vainikainen, "Broadband tuning of mobile terminal antennas," *European Conference on Antennas and Propagation (EuCAP)*, pp.1-6, Nov. 2007.

[Val10]   R. Valkonen, C. Luxey, J. Holopainen, C. Icheln, P. Vainikainen, "Frequency-reconfigurable mobile terminal antenna with MEMS switches," *European Conference on Antennas and Propagation (EuCAP)*, pp.1-5, Apr. 2010.

[Val11]   R. Valkonen *et al.*, "Avoiding the interaction between hand and capacitive coupling element based mobile terminal antenna," *European Conference on Antennas and Propagation (EuCAP)*, pp.2781-2785, Apr. 2011.

[Val12]   R. Valkonen, J. Ilvonen, and P. Vainikainen, "Naturally non-selective handset antennas with good robustness against impedance mistuning," *European Conference on Antennas and Propagation (EUCAP)*, pp. 796-800, Mar. 2012.

[Val13a] R. Valkonen, M. Kaltiokallio, and C. Icheln, "Capacitive coupling element antennas for multi-standard mobile handsets," *IEEE Transactions on Antennas and Propagation*, vol. 61, pp. 2783-2791, May 2013.

[Val13b] R. Valkonen, *Impedance Matching and Tuning of Non-Resonant Mobile Terminal Antennas*, Ph. D. dissertation, Department of Radio Science and Engineering, Aalto University, Espoo, Finland, 2013.

[Var03]   V. K. Varadan, K. J. Vinoy, and K. A. Jose, *RF MEMS and Their Applications*, Chichester: John Wiley & Sons Ltd, 2003.

[Vau03]   R. Vaughan, J. B. Andersen, *Channels, Propagation and Antennas for Mobile Communications*, IET, 2003.

[Ven05]   G. D. Vendelin, A. M. Pavio, and U. L. Rohde, *Microwave Circuit Design using Linear and Nonlinear Techniques*, Hoboken, New Jersey: John Wiley & Sons, Inc., 2005.

[Ven99]   O. G. Vendik, E.K.Hollmann, A. B. Kozyrev, and A. M. Prudan, "Ferroelectric tuning of planar and bulk microwave devices," *Journal of Superconductivity*, vol. 12, pp. 325-338, Apr. 1999.

[Vil06]   J. Villanen, J. Ollikainen, O. Kivekas, P. Vainikainen , "Coupling element based mobile terminal antenna structures," *IEEE Transactions on Antennas and Propagation*, vol.54, no.7, pp.2142-2153, Jul. 2006.

[Vol]   Voltronics Inc., New York, USA.

[Vol08]   C. Volmer, J. Weber, R. Stephan, K. Blau, and M. A. Hein, "An eigen-analysis of compact antenna arrays and its application to port decoupling," *IEEE Transactions on Antennas and Propagation*, Volume 52, Issue 2, pp. 360-370, Feb. 2008.

[Vol10]   C. Volmer, *Compact Antenna Arrays in Mobile Communications: A Quantitative Analysis of Radiator Coupling*, Ph. D. dissertation, Institute for Information Technology, Ilmenau University of Technology, Ilmenau, Germany, 2010.

[Wal04]   J. W. Wallace and M. A. Jensen, "Mutual coupling in MIMO wireless systems: a rigorous network theory analysis," *IEEE Transactions on Wireless Communications*, vol. 3, no. 4, pp. 1317-1325, Jul. 2004.

[Wan09]   X. Wang, *Tunable Microwave Filters using Ferroelectric Thin Films*, Ph. D. dissertation, Faculty of Engineering, University of Birmingham, Birmingham, UK, 2009.

[Wan12]   G. Wang and B. Pan, *Passive RF Component Technology: Materials, Techniques, and Applications*, ISBN 978-0470510698, Wiley-Blackwell, 2008.

[Wat08]   R. Waterhouse, *Printed Antennas for Wireless Communications*, ISBN 978-0470631553, John Wiley & Sons, 2011.

[Web06]   J. Weber, C. Volmer, K. Blau, R. Stephan, and M. A. Hein, "Miniaturized antenna arrays using decoupling networks with realistic elements," *IEEE Transactions on Microwave Theory and Techniques*, vol. 54, no. 6, pp. 2733-2740, Jun. 2006.

[Wha06]   R. B. Whatley, Z. Zhou, and K. L. Melde, "Reconfigurable RF impedance tuner for match control in broadband wireless devices," *IEEE Transactions on Antennas and Propagation*, vol. 54, no. 2, pp. 470–478, Feb. 2006.

[Wha10]   R. Whatley, T. Ranta and D. Kelly, "RF front-end tunability for LTE handset applications," *IEEE Compound Semiconductor Integrated Circuit Symposium (CSICS)*, pp. 1-4, Oct. 2010.

[Wis]   WiSpry Inc, Irvine, CA, USA.

[Xie14]   J. Xie, Y. Yu, H. Zhang, "A compact multiband internal antenna for 4G mobile terminals on a support," *International Conference on Computational Intelligence and Communication Networks (CICN)*, pp.10-12, Nov. 2014.

[Yar06]   B. S. Yarman, M. Sengul, P. Lindberg, and A. Rydberg, "A single matching network design for a double band PIFA antenna via simplified real frequency technique," *Asia-Pacific Microwave Conference (APMC)*, pp. 1325-1328, Dec. 2006.

[Yar08]   B. S. Yarman, *Design of Ultra Wideband Antenna Matching Networks: via Simplified Real Frequency Technique*, Springer Science + Business Media B.V., 2008.

[Yok93]   I. Yokoshima, "RF impedance measurements by voltage-current detection," *IEEE Transactions on Instrumentation and Measurement*, vol.42, no.2, pp.524-527, Apr. 1993.

Bibliography

[Yor00]   R. York *et al*., "Microwave integrated circuits using thin-film BST," *IEEE International Symposium on the Applications of Ferroelectrics*, pp. 195-200 vol. 1, Jul. 2000.

[You64]   D. C. Youla , "A new theory of broad-band matching," *IEEE Transactions on Circuit Theory*, vol.11, no.1, pp.30-50, Mar. 1964.

[Zha13]   K. Zhao, S. Zhang, Z. Ying, T. Bolin, and S. He, "Reduce the hand-effect body loss for the LTE mobile antenna in CTIA talking and data modes," *Progress in Electromagnetic Research*, vol. 137, pp.73-85, Jun. 2013.

[Zhu09a]   F.-G. Zhu, J.-D. Xu, and Q. Xu, "Reduction of mutual coupling between closely-packed antenna elements using defected ground structure," *Electronics Letters*, vol. 45, no. 12, pp. 601–602, Jun. 2009.

[Zhu09b]   X. Zhu, *Switchable and Tunable Ferroelectric Thin Film Radio Frequency Components*, Ph. D. dissertation, Electrical Engineering, University of Michigan, US, 2009.

[Zin03]   I. Zine-El-Abidine, M. Okoniewski, and J. G. McRory, "A new class of tunable RF MEMS inductors," *Proceedings International Conference on MEMS, NANO and Smart Systems*, 2003, pp. 114-115.

Curriculum Vitae

Personal Details

Name: Yi Chen

Date of Birth: 10th October 1982

Nationality: Chinese

Education

2004 – 2011   Diploma in Electrical Engineering and Information Technology, Karlsruhe Institute of Technology, Germany

2011 – 2016   Ph.D. candidate in the University of Kiel, Germany

2016-2017   Ph.D. candidate in the University of Hannover, Germany

Additional Qualifications

2012   Participate the ESoA (European School of Antennas) course (RF MEMS based Antennas), Ankara, Turkey, 25-29 June.